

**DOCTORAL THESIS**

**PREPARATION AND APPLICATIONS OF  
ORGANOFLUORINE COMPOUNDS/CALCIUM  
NANOCOMPOSITES**

**MARCH 2016**

**TOMOYA SAITO**

# **Preparation and Applications of Organofluorine Compounds/Calcium Nanocomposites**

Doctoral Course  
Graduate School of Materials Science and Technology  
Hirosaki University

Doctoral Thesis

March 2016

Tomoya Saito

## Contents

<b>General Introduction</b>	1
1. Organic-inorganic composites	1
2. Properties of fluorine and organofluorine compounds	4
3. Fluorinated organic/inorganic composites	10
4. Calcium compounds	14
5. Organic compounds/calcium composites	14
6. Thesis outline	16
 <b>Chapter 1. Fluoroalkyl End-capped Oligomers Possessing Non-flammable</b>	 28
<b>Characteristic in Calcium Carbonate Nanocomposites</b>	
1.1. Introduction	29
1.2. Experimental	31
1.2.1. Measurements	31
1.2.2. Materials	31
1.2.3. Preparation of fluoroalkyl end-capped ACA oligomer/calcium carbonate nanocomposites	32
1.2.4. Treatment of $R_F-(DMAA)_n-R_F$ /calcium carbonate nanocomposites before and after calcination at 800 °C with 1N hydrochloric acid and 1, 2-dichloroethane	33

1.2.5.	Preparation of modified poly(methyl methacrylate) films treated with fluoroalkyl end-capped oligomers/calcium carbonate nanocomposites before and after calcination at 800 °C	33
1.3.	Results and discussion	35
1.3.1.	Preparation of fluoroalkyl end-capped oligomer/calcium carbonate nanocomposites	35
1.3.2.	Thermal stability of fluoroalkyl end-capped oligomer/calcium carbonate nanocomposites	42
1.3.3.	Application to the surface modification of poly(methyl methacrylate) films by using fluoroalkyl end-capped oligomers/calcium carbonate nanocomposites before and after calcination at 800 °C	49
1.4.	Conclusion	54
<b>Chapter 2.</b>	<b>Low Molecular Weight Aromatic Compounds Possessing Nonflammable and Flammable Characteristics in Calcium Fluoride Nanocomposite Matrices after Calcination at 800 °C</b>	<b>59</b>
2.1.	Introduction	60
2.2.	Experimental	62
2.2.1.	Measurements	62
2.2.2.	Materials	63
2.2.3.	Preparation of calcium fluoride/bisphenol AF nanocomposites	63



2.3.	Results and discussion	65
2.3.1.	Preparation of calcium fluoride/low molecular weight aromatic compound nanocomposites	65
2.3.2.	Thermal stability of calcium fluoride/low molecular weight aromatic compound nanocomposites	69
2.4.	Conclusion	85
<b>Chapter 3.</b>	<b>Reaction of Fluorinated Aliphatic Alcohols with Calcium Chloride:</b>	<b>90</b>
	<b>Formation of the Fluorinated Alcohol/Calcium Fluoride Nanocomposites</b>	
	<b>– Thermal Stability and Application to the Surface Modification of These</b>	
	<b>Nanocomposites</b>	
3.1.	Introduction	91
3.2.	Experimental	94
3.2.1.	Measurements	94
3.2.2.	Materials	95
3.2.3.	Preparation of 1 <i>H</i> , 1 <i>H</i> , 2 <i>H</i> , 2 <i>H</i> , 6 <i>H</i> , 6 <i>H</i> -nonadecafluoro-1-undecanol (DTFA)/calcium fluoride nanocomposites	95
3.2.4.	Preparation of modified poly(methyl methacrylate) films treated with 1 <i>H</i> , 1 <i>H</i> , 2 <i>H</i> , 2 <i>H</i> , 6 <i>H</i> , 6 <i>H</i> -nonadecafluoro-1-undecanol (DTFA)/calcium fluoride nanocomposites before and after calcination at 800 °C	96
3.3.	Results and discussion	97

3.3.1.	Preparation of 1 <i>H</i> , 1 <i>H</i> , 2 <i>H</i> , 2 <i>H</i> , 6 <i>H</i> , 6 <i>H</i> -nonadecafluoro-1-undecanol (DTFA)/calcium fluoride nanocomposites by using calcium chloride	97
3.3.2.	Thermal stability of 1 <i>H</i> , 1 <i>H</i> , 2 <i>H</i> , 2 <i>H</i> , 6 <i>H</i> , 6 <i>H</i> -nonadecafluoro-1-undecanol (DTFA)/calcium fluoride nanocomposites	104
3.3.3.	Surface modification of poly(methyl methacrylate) by using 1 <i>H</i> , 1 <i>H</i> , 2 <i>H</i> , 2 <i>H</i> , 6 <i>H</i> , 6 <i>H</i> -nonadecafluoro-1-undecanol (DTFA)/calcium fluoride nanocomposites before and after calcination at 800 °C	108
3.4.	Conclusion	113
<b>Chapter 4.</b>	<b>Facile Creation of Superoleophobic and Superhydrophilic Surface by Using Fluoroalkyl End-capped Vinyltrimethoxysilane Oligomer/Calcium Silicide Nanocomposites – Development of These Nanocomposites to Environmental Cyclical Type-fluorine Recycle Through Formation of Calcium Fluoride</b>	117
4.1.	Introduction	118
4.2.	Experimental	121
4.2.1.	Measurements	121
4.2.2.	Materials	122
4.2.3.	Preparation of fluoroalkyl end-capped vinyltrimethoxysilane oligomer/calcium silicide nanocomposites $[R_F-(VM-SiO_2)_n-R_F/CaSi_2]$	122
4.2.4.	Preparation of modified glass treated with $R_F-(VM-SiO_2)_n-R_F/CaSi_2$ nanocomposites by dipping method	123

4.3.	Results and discussion	124
4.3.1.	Preparation of fluoroalkyl end-capped vinyltrimethoxysilane oligomer/calcium silicide nanocomposites $[R_F-(VM-SiO_2)_n-R_F/CaSi_2]$	124
4.3.2.	Preparation of modified glass treated with $R_F-(VM-SiO_2)_n-R_F/CaSi_2$ nanocomposites by dipping method	129
4.3.3.	Crystalline structures of $R_F-(VM-SiO_2)_n-R_F/CaSi_2$ nanocomposites before and after calcination at 800 °C	140
4.4.	Conclusion	143
<b>Chapter 5.</b>	<b>Facile Creation of Modified Surface Possessing the Controlled Wettability between Superamphiphobic and Superoleophobic-Superhydrophilic Characteristics by Using Perfluorocarboxamides/Calcium Carbonate/Calcium Fluoride Nanocomposites: Application to the Separation of Oil and Water</b>	149
5.1.	Introduction	150
5.2.	Experimental	153
5.2.1.	Measurements	153
5.2.2.	Materials	154
5.2.3.	Preparation of perfluorocarboxamides/calcium carbonate/calcium fluoride nanocomposites	154
5.2.4.	Preparation of modified glass treated with perfluorocarboxamides/calcium carbonate/calcium fluoride nanocomposites	155
5.2.5.	Preparation of the surfactant-stabilized oil (dodecane)-in-water emulsion	156

5.3.	Results and discussion	157
5.3.1.	Preparation of perfluorocarboxamides/calcium carbonate/calcium fluoride nanocomposites	157
5.3.2.	Preparation of modified glass treated with perfluorocarboxamides/calcium carbonate/calcium fluoride nanocomposites	162
5.3.3.	Application of the perfluorocarboxamides/calcium carbonate/calcium fluoride nanocomposites to the membrane materials for liquid-liquid separation	167
5.4.	Conclusion	173
	<b>Conclusions</b>	177
	<b>Publications</b>	183
	<b>Acknowledgements</b>	187

## General Introduction

### 1. Organic-inorganic composites

Much attractive attention has been paid to advanced hybrid organic-inorganic composites because of exhibiting a large variety of synergistic characteristics deriving from flexibility and multiplicity related to the organic compounds, and thermal stability, high mechanical properties and bioactivity imparted by inorganic compounds.<sup>1 ~ 4)</sup> There have hitherto been numerous studies on the fabrication and properties of organic/inorganic composites.<sup>5 ~ 27)</sup> In general, organic/inorganic composite materials are prepared by using organic polymers<sup>5 ~ 9)</sup>, surfactants<sup>10)</sup>, and alkoxysilanes<sup>11 ~ 13)</sup> as an organic materials and silica gel ( $\text{SiO}_2$ )<sup>14 ~ 20)</sup>, calcium carbonate ( $\text{CaCO}_3$ )<sup>21 ~ 24)</sup>, titanium oxide ( $\text{TiO}_2$ )<sup>25, 26)</sup>, and zinc oxide ( $\text{ZnO}$ )<sup>9, 27)</sup> as a inorganic materials through the chemical bonding<sup>8, 9, 11, 12, 14, 15, 22, 24, 26, 27)</sup>, hydrogen bonding interaction<sup>19, 25)</sup>, ionic interaction<sup>6, 7, 10, 13, 17, 18, 20)</sup> and oleophilic-oleophilic interaction<sup>5, 16, 21, 23)</sup> between organic and inorganic materials. The properties of the obtained composite materials are in general superior to each individual material. In these composite materials, especially, organic polymer/inorganic composites have various applications to a wide variety of fields such as coating, medical materials, catalysts and fuel cells.<sup>28 ~ 33)</sup> Nanometer size-controlled inorganic fine particles are likely to aggregate with the organic polymer due to

their higher surface energy<sup>34)</sup>, decreasing the compatibility between organic polymers and inorganic particles to cause the decline in the functionality.<sup>35 ~ 37)</sup> Therefore, the surface modification of inorganic nanoparticles have been extensively studied in order to improve the compatibility between organic polymers and inorganic particles.<sup>6, 9, 11, 23, 26, 27, 38 ~ 43)</sup> In fact, aliphatic acids<sup>38 ~ 40)</sup>, organic polymers<sup>27, 41)</sup>, organic silane coupling agents<sup>9, 11, 26, 42, 43)</sup> and surfactants<sup>6, 23)</sup>, which possess the reactive functional groups such as carboxyl groups<sup>6, 23, 27, 38 ~ 40)</sup>, amino groups<sup>26, 41, 43)</sup> and vinyl groups<sup>9, 11, 42)</sup> have been widely used in the surface modification of inorganic particles, and these modified inorganic nanoparticle surfaces can interact with the organic polymers to produce the corresponding organic polymers/inorganic composites. As a result, these obtained organic polymers/inorganic composites can exhibit the superior properties to those of the parent organic polymers (see Table 1).<sup>6, 9, 11, 23, 26, 27, 38 ~ 43)</sup>

Table 1 Examples of organic polymer/inorganic composite materials

Inorganic materials	Surface modification	Organic polymer	Properties	Ref.
CaCO <sub>3</sub>	PGP <sup>a)</sup>	PET <sup>b)</sup>	Good thermal stability and dispersibility in PET matrices	5
SiO <sub>2</sub>	Trimethoxymethylsilane	PC <sup>c)</sup>	Good thermal and flame resistance	16
CaCO <sub>3</sub>	Sodium stearate	PP <sup>d)</sup>	Enhancement of thermal stability and tensile strength	23
TiO <sub>2</sub>	γ-aminopropyltriethoxysilane	PANI <sup>e)</sup>	Good thermal stability and high photocatalytic activity	26
ZnO	Polymethacrylic acid	Polymethacrylic acid	Good dispersibility in water	27
ZnO	3-methacryloxypropyltrimethoxysilane	PS <sup>f)</sup>	Good thermal stability and UV-shielding effect	44

a) PGP: Polyethylene glycol phosphate

b) PET: Poly (ethylene terephthalate)

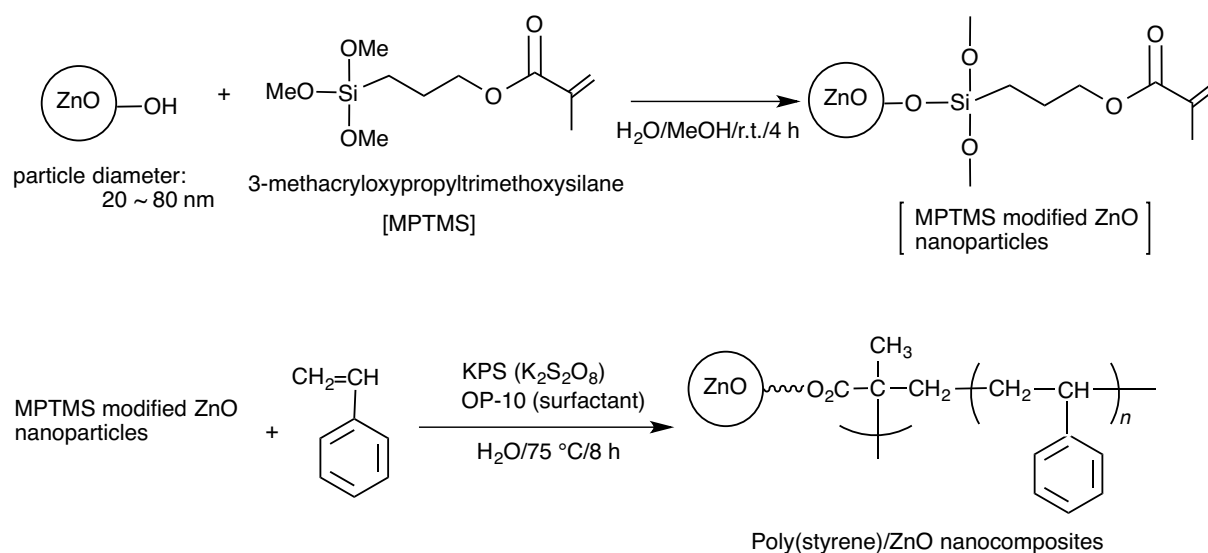
c) PC: Polycarbonate

d) PP: Polypropylene

e) PANI: Polyaniline

f) PS: Poly(styrene)

For example, Tang et al. reported on the fabrication of poly(styrene) (PS)/ZnO nanocomposites by the emulsion polymerization of styrene monomer with the surface modified ZnO nanoparticles treated with 3-methacryloxypropyltrimethoxysilane (MPTMS) in the presence of polyoxyethylene nonylphenyl ether (OP-10) to afford the expected nanocomposites (see Scheme 1).<sup>44)</sup>



Scheme 1 <sup>44)</sup>

The obtained nanocomposites can enhance the thermal stability and UV-shielding properties, compared with those of the parent polymers. <sup>44)</sup>

In this way, the preparation of organic/inorganic composite materials is in particular interest from the developmental viewpoints of new functional materials. However, the thermal stability of organic polymers in the organic/inorganic composites is in general poor, compared with that of the parent inorganic materials. <sup>15, 26, 41)</sup>

## 2. Properties of fluorine and organofluorine compounds

The unique characteristics which fluorinated compounds possess are derived from the fact as follows <sup>45 ~ 55)</sup>:



Table 2 Physical properties of hydrogen, fluorine and chlorine<sup>45-55)</sup>

	H	F	Cl
Electronegativity (Pauling)	2.1	4.0	3.0
Ionization energy (kJ/mol)	1312	1681	1256
Electron affinity (kJ/mol)	75	350	365
A van der Waals radius (Å)	1.20	1.35	1.80
Polarizability (10 <sup>-24</sup> cc)	0.79	1.27	4.61
Bond energies of X-X (kJ/mol)	435	155	243
Bond energies of C-X (kJ/mol)	414	441	329
Bond lengths of C-X (Å)	1.10	1.27	1.77
Polarizability C-X (10 <sup>-24</sup> cc)	0.66	0.68	2.58

(1) Fluorine is the most electronegative of all the elements as shown in Table 2. The high electronegative is conducive to high oxidation potential, high ionization and high electron affinity.<sup>45~47)</sup> Thus, the organic fluorinated compounds can promote the formation of strong hydrogen bonding between the fluorine in organic fluorinated compounds and the hydrogen in organic compounds.<sup>47)</sup> Moreover, the acidity of fluorinated aliphatic alcohols and fluorinated carboxylic acid are higher than the corresponding hydrocarbon aliphatic alcohols and hydrocarbon carboxylic acid (see Table 3).<sup>47, 48, 54, 55)</sup>

Table 3 Acidities of fluorinated (or hydrocarbon) aliphatic alcohols and carboxylic acid<sup>47, 48, 54, 55)</sup>

	pK <sub>a</sub>		pK <sub>a</sub>
CH <sub>3</sub> COOH	4.76	CH <sub>3</sub> CH <sub>2</sub> OH	15.9
CH <sub>2</sub> FCOOH	2.66	CF <sub>3</sub> CH <sub>2</sub> OH	12.4
CHF <sub>2</sub> COOH	1.24	(CF <sub>3</sub> ) <sub>2</sub> CHOH	9.3
CF <sub>3</sub> COOH	0.23	(CF <sub>3</sub> ) <sub>3</sub> COH	5.4

(2) Fluorine has the second smallest atomic radius following hydrogen.<sup>46, 49)</sup> The second smallest atomic radius is conducive to short bond length and low polarizability of carbon-fluorine bond (see Table 2).<sup>46, 47, 50)</sup> Thus, organofluorine compounds have the low reflective indices and surface tensions as shown in Table 4.<sup>47, 51, 52)</sup>

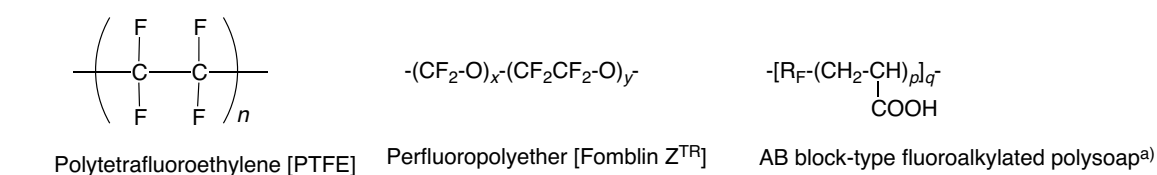
Table 4 Refractive indices and surface tensions of fluorocarbon and hydrocarbon<sup>47, 51, 52)</sup>

Compounds	Refractive index ( $n_D^{20}$ )	Surface components	$\gamma_c$ (mN/m)
C <sub>6</sub> H <sub>6</sub>	1.501	-CH <sub>3</sub>	24
C <sub>6</sub> H <sub>4</sub> F <sub>2</sub>	1.443	-CF <sub>3</sub>	6
C <sub>6</sub> H <sub>2</sub> F <sub>4</sub>	1.408	-CF <sub>2</sub> H	15
C <sub>6</sub> F <sub>6</sub>	1.378	-CH <sub>2</sub> CH <sub>2</sub> -	31
-(CH <sub>2</sub> CH <sub>2</sub> ) <sub>n</sub> -	1.510	-CF <sub>2</sub> CF <sub>2</sub> -	18
-(CF <sub>2</sub> CF <sub>2</sub> ) <sub>n</sub> -	1.380		

(3) F<sub>2</sub> is the most reactive due to the very weak F-F bond (155 kJmol<sup>-1</sup>) and can form the very strong bond with other atoms. For example, the strength of the carbon – fluorine bond (441 kJmol<sup>-1</sup>) is superior to that of carbon – hydrogen bond (414 kJmol<sup>-1</sup>) or the carbon – chlorine

bond ( $329 \text{ kJmol}^{-1}$ ) as shown in Table 2.<sup>45, 46, 53)</sup> Such bond strength related to fluorine gives the extraordinary thermal, light and chemical resistance toward the organofluorine compounds.<sup>45, 46, 53)</sup> Thus, organofluorine compounds such as fluorinated aliphatic alcohols, fluorinated carboxylic acids or sulfonic acids, fluorinated surfactants, fluorosilicones and fluoropolymers have been practically applied to the surface modification, lubricant, catalyst, fuel cells and optical materials.<sup>56 ~ 62)</sup> In these organofluorine compounds, there have been great interest in the fluoropolymers due to exhibiting a variety of unique properties such as high thermal stability, chemical resistance, low refractive indices, low dielectric constant in comparison with the traditional hydrocarbon polymers.<sup>56, 59, 61)</sup> Some of typical fluoropolymers are listed in Fig. 1.<sup>56, 63 ~ 67)</sup>

#### Fluorinated polymers



#### (Meth)acrylate copolymers containing fluoroalkyl groups as side chain

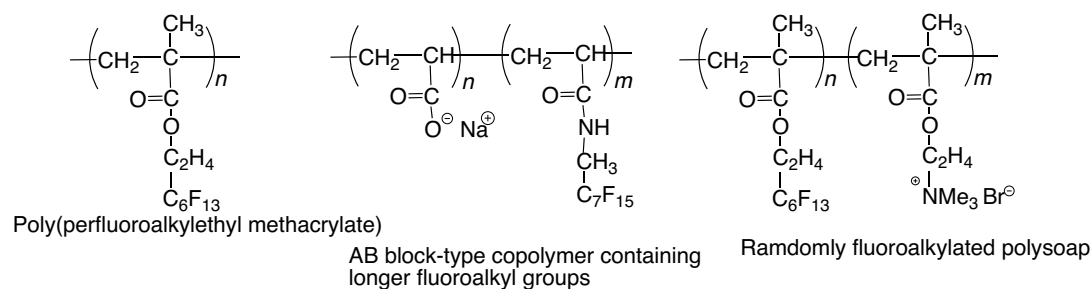
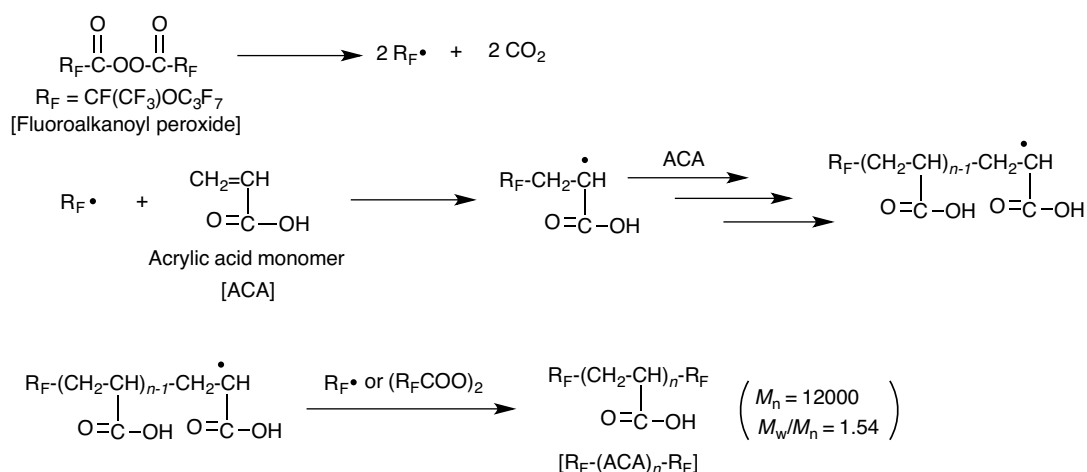


Fig. 1 Chemical structures of fluorinated polymers and (meth)acrylate copolymers containing fluoroalkyl groups as side chain<sup>56, 63-67)</sup>

a)  $\text{R}_\text{F} = -\text{CF}(\text{CF}_3)[\text{OCF}_2\text{CF}(\text{CF}_3)]_n\text{O}(\text{CF}_2)_5\text{O}-[\text{CF}(\text{CF}_3)\text{CF}_2\text{O}]_m\text{CF}(\text{CF}_3)-$ ; ( $n+m=3$ )

As shown in Fig. 1, fluorinated polymers such as polytetrafluoroethylene [PTFE], perfluoropolyether and AB block-type fluoroalkylated polysoap have been applied to the electrical materials, surface modifications and optical materials, because these polymers have high thermal stability, chemical stability, low surface tension, low dielectric constant and low refractive index.<sup>56, 63, 64)</sup> The (meth)acrylate copolymers containing longer fluoroalkyl groups as the side chain have been also applied to the surface modifications, due to their surface activity and higher solubility and adhesion ability toward a variety of substrates than those of the traditional perfluoropolymers.<sup>65 ~ 67)</sup> However, these (meth)acrylate copolymers containing longer fluoroalkyl groups are unstable under acidic or alkaline conditions since the fluoroalkyl groups are introduced into such polymers through the ester or the amide bonds.<sup>68)</sup> In these fluorinated polymers, two fluoroalkyl end-capped oligomers [ $R_F-(M)_n-R_F$ ; fluoroalkyl groups; M = radical polymerizable monomer] can be easily prepared by using fluoroalkanoyl peroxide as a key intermediate.<sup>69 ~ 72)</sup> For example, two fluoroalkyl end-capped acrylic acid oligomer have been already prepared by primary radical termination or radical chain transfer to the peroxide under the oligomeric conditions, in which the concentration of the peroxide was almost the same as that of acrylic acid as shown in Scheme 2.<sup>64, 73)</sup>



Scheme 2 <sup>64, 73)</sup>

These obtained  $\text{R}_\text{F}\text{-(M)}_n\text{-R}_\text{F}$  oligomers are attractive functional materials, because they exhibit various unique properties such as high solubility toward not only water but also traditional organic solvents, surface active properties and nanometer size-controlled molecular aggregates which cannot be achieved by the corresponding non-fluorinated and randomly or block-type fluoroalkylated ones.<sup>69 ~ 72)</sup> In fact, as shown in Fig. 2, two fluoroalkyl end-capped acrylic acid oligomers  $[\text{R}_\text{F}\text{-(ACA)}_n\text{-R}_\text{F}]$  are effective for reducing the surface tension of water, compared with that of block-type fluoroalkylated polysoap illustrated in Fig. 1.<sup>64, 73)</sup>

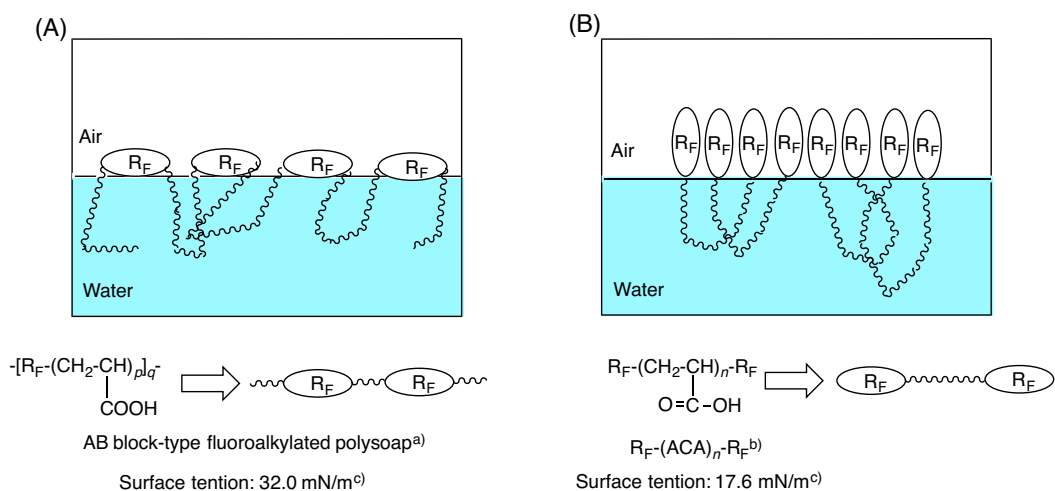


Fig. 2 Surface arrangement of block-type fluoroalkylated polysoap (A) and two fluoroalkyl end-capped oligomers (B) in aqueous solutions<sup>64, 73)</sup>

a)  $R_F = -CF(CF_3)[OCF_2CF(CF_3)]_nO(CF_2)_5O-[CF(CF_3)CF_2O]_mCF(CF_3)-$ ; ( $n+m = 3$ )

b)  $R_F = CF(CF_3)OC_3F_7$

c) Surface tension of water: 72.6 mN/m

In addition, the  $R_F-(M)_n-R_F$  oligomers have been applied to the surface modification of traditional organic polymer such as poly(methyl methacrylate) [PMMA] to exhibit a good oleophobicity imparted by fluorines toward the modified PMMA film surface.<sup>72)</sup> However, the  $R_F-(M)_n-R_F$  oligomers have the poor thermal stability compared with that of perfluoropolymers such as poly(tetrafluoroethylene). Thus, the improvement of thermal stability of these fluorinated oligomers through the nanocomposite reactions with inorganic materials is essential for the fabrication of new fluorinated functional materials.

### 3. Fluorinated organic/inorganic composites

Organic/inorganic composites are interesting materials because these composite materials can combine the unique properties related to both organic and inorganic materials, as

mentioned above.<sup>1 ~ 4)</sup> The fabrication of organofluorine compounds/inorganic composites possessing a variety of unique characteristics related to the fluorines is of particular interest from the developmental viewpoints of new functional materials. In fact, several fluorinated organic/inorganic composites have been already reported, as shown in Table 5.<sup>74 ~ 80)</sup>

Table 5 Examples of organic fluorinated compound/inorganic composite materials

Organic fluorinated compounds	Inorganic materials	Properties	Ref.
PFPE <sup>a)</sup>	SiO <sub>2</sub>	Hydrophobicity and low friction properties	74
Poly(fluoroimide acrylate)	SiO <sub>2</sub>	Good transparency and thermal stability, low moisture permeation	75
Fluorinated aliphatic alcohol	TiO <sub>2</sub>	High thermal stability and photocatalytic activity	76
PTFE <sup>b)</sup>	TiO <sub>2</sub>	Transfer and state changes of fluorine	77
FAS <sup>c)</sup>	ZnO	Superhydrophobicity and Superoleophobicity	78
PVDF-HFP <sup>d)</sup>	MgO	Good thermal stability and electroconductivity	79
PVDF-HFP <sup>d)</sup>	Al <sub>2</sub> O <sub>3</sub>	Low thermal shrinkage	80

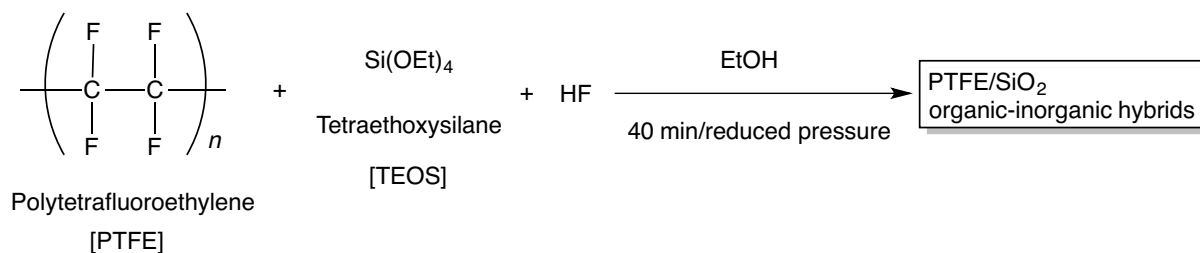
a) PFPE: Perfluoropolyether

b) PTFE: Polytetrafluoroethylene

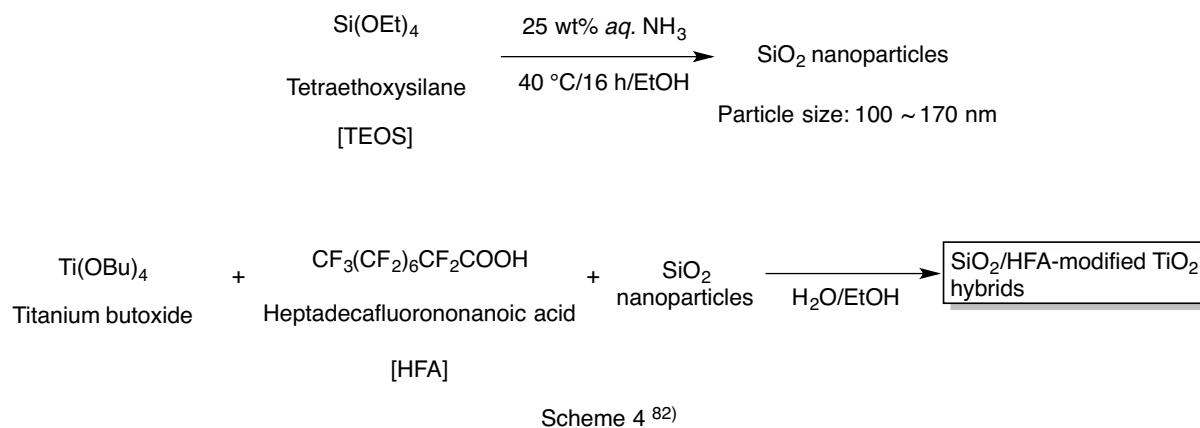
c) (heptadecafluoro-1, 1, 2, 2-tetrahydrodecyl)-trimethoxysilane

d) PVDF-HFP: Poly(vinylidene fluoride-co-hexafluoropropylene)

For example, Chen et al. previously reported that PTFE/SiO<sub>2</sub> hybrids can be prepared by the sol-gel reaction of tetraethoxysilane (TEOS) in the presence of the PTFE under acidic conditions.<sup>81)</sup>



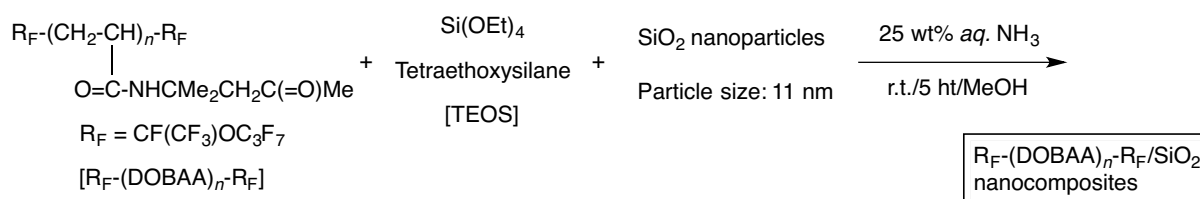
Moreover, Xu et al. have reported that silica/heptadecafluorononanoic acid (HFA)-modified TiO<sub>2</sub> hybrids are prepared by the reaction of titanium tetra-n-butoxide and heptadecafluorononanoic acid (HFA) to afford the corresponding fluorinated hybrids as shown in Scheme 4. <sup>82)</sup>



The obtained silica/HFA-modified TiO<sub>2</sub> hybrids were applied to the surface modification of polyester fabric surfaces, and the obtained modified surfaces can show the superamphiphobic characteristic. <sup>82)</sup>



On the other hand, it is well known that  $R_F-(M)_n-R_F$  oligomers can form the nanometer size-controlled molecular aggregates.<sup>69 ~ 72)</sup> These fluoroalkyl end-capped oligomeric aggregates can interact with numerous guest molecules such as fullerene, carbon nanotube, organic dyes, metal (gold, silver and palladium) nanoparticles and inorganic fine particles such as silica ( $SiO_2$ ), titanium oxide ( $TiO_2$ ), calcium carbonate ( $CaCO_3$ ) and zinc oxide ( $ZnO$ ) to afford the corresponding fluorinated oligomers/guest molecules nanocomposites.<sup>71, 72, 83)</sup> These nanocomposites can also provide a variety of interesting properties imparted by both fluorinated oligomers and inorganic materials.<sup>71, 72, 83)</sup> For example, fluoroalkyl end-capped *N*-(1, 1-dimethyl-3-oxobutyl)acrylamide oligomer  $[R_F-(DOBAA)_n-R_F]/SiO_2$  nanocomposites were prepared by the sol-gel reactions of the corresponding fluorinated oligomer with tetraethoxysilane in the presence of  $SiO_2$  nanoparticles under alkaline conditions (see Scheme 5).<sup>84)</sup>



Scheme 5<sup>84)</sup>

Interestingly, the  $R_F-(DOBAA)_n-R_F$  oligomer in the nanocomposites can exhibit a nonflammable characteristic even after calcination at 800 °C through the formation of

ammonium hexafluorosilicate during the sol-gel reactions, although the PTFE in the silica gel matrices can exhibit a clear weight loss after calcination around at 700 °C, quite similar to that of the parent PTFE.<sup>84)</sup>

#### **4. Calcium compounds**

Calcium compounds such as calcium carbonate ( $\text{CaCO}_3$ ), calcium fluoride ( $\text{CaF}_2$ ), hydroxyapatite [ $\text{Ca}_{10}(\text{PO}_4)_6(\text{OH})_2$ ] and calcium sulfate ( $\text{CaSO}_4$ ) have been widely used in the industrial fields such as inorganic filler, optical materials and biomaterial.<sup>85 ~ 88)</sup> Especially,  $\text{CaCO}_3$  particles have been widely used as the inorganic filler in order to not only the improvement of the mechanical properties but also the cost reduction of the traditional polymer, rubber, paint, cosmetic and paper.<sup>89, 90)</sup>  $\text{CaCO}_3$  particles have also attracted much attention in the biomimetic material field.<sup>7)</sup>

#### **5. Organic compounds/calcium composites**

There have been hitherto numerous studies on the fabrication of organic/inorganic composites by using calcium compounds such as calcium carbonate, because calcium carbonate is commercially available cheap materials.<sup>5 ~ 9, 21 ~ 24, 91)</sup> In general, organic/calcium carbonate composite materials have been prepared by using aliphatic acids, amino acids and

organic polymers possessing carboxyl groups as shown in Table 6, since calcium carbonate can interact effectively with their carboxyl groups.<sup>7, 35, 39, 91, 92)</sup> The modified calcium carbonate particles have been already developed as the polymer filler (see Table 2).<sup>7, 35, 39, 91, 92)</sup>

Table 6 Examples of organic/calcium inorganic composite materials

Surface modified toward CaCO <sub>3</sub>	Organic polymer	Properties	Ref.
Poly(acrylic acid)	Poly(acrylic acid)	Controlled crystalline structure and morphology and layered thin films	7
{ Poly(acrylic acid) PBAA <sup>a)</sup>	PVC <sup>b)</sup>	Good dispersibility and high flexural strength	35
Oleic acid	PMMA <sup>c)</sup>	Good thermal stability and acid resistance	38
Poly(glutamic acid)	Poly(glutamic acid)	Controlled surface morphology and Superhydrophobicity	91
{ Sodium stearate Oleic acid	PMMA <sup>c)</sup>	Good thermal stability	92

a) PBAA: Poly(butadiene-*co*-acrylonitrile-*co*-acrylic acid)

b) PVC: Poly(vinyl chloride)

c) PMMA: Poly(methyl methacrylate)

In this way, organic compounds/calcium composites are mostly prepared by organic compound containing carboxyl groups through the ionic interaction between the cationic calcium moiety in calcium carbonate and the anionic carboxyl groups in organic compounds.<sup>7, 35, 39, 91, 92)</sup> However, studies on the organic compounds/calcium composites possessing fluorines or fluoroalkyl groups have been hitherto very limited.<sup>93, 94)</sup> Therefore, it is of particular interest to develop novel fluorinated organic compounds/calcium composites

possessing unique characteristics imparted by both fluorines and the calcium compounds, from the developmental viewpoints of new fluorinated functional materials.

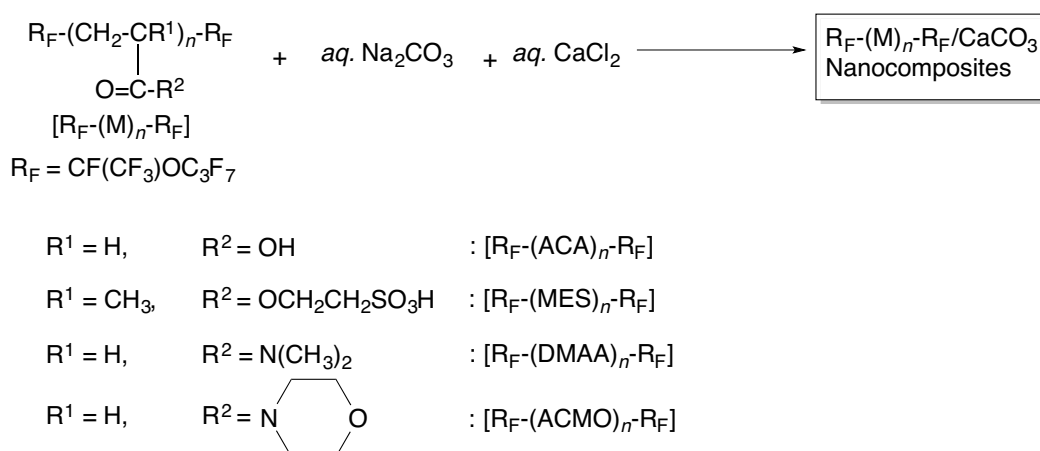
## 6. Thesis outline

$R_F-(DOBAA)_n-R_F/SiO_2$  nanocomposites have been already prepared by the sol-gel reactions of the corresponding fluorinated oligomer with tetraethoxysilane in the presence of  $SiO_2$  nanoparticles under alkaline conditions, and the  $R_F-(DOBAA)_n-R_F$  oligomer in the nanocomposites can exhibit a nonflammable characteristic even after calcination at 800 °C through the formation of ammonium hexafluorosilicate during the sol-gel process.<sup>84)</sup> Effective interactions between ammonium hexafluorosilicate and these fluorinated oligomers in silica gel matrices enable the corresponding oligomers to afford a nonflammable characteristic.<sup>84)</sup> The formation of ammonium hexafluorosilicate during the sol-gel reaction can be attributed to the very strong Si-F bond (129 kcal or 540 kJ/mol).<sup>95)</sup> The bond-strengthening effect of fluorine also appears in Ca-F bond (132 kcal or 552 kJ/mol).<sup>96)</sup> From these findings, the preparation of organofluorine compounds/calcium composites through the nanocomposite reactions of the corresponding fluorinated compounds with calcium compounds, which should be derived from the bond-strengthening effect in Ca-F bond, is of particular interest from the developmental viewpoints of novel fluorinated

functional materials.

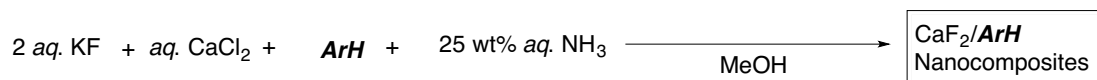
In this study, preparation and applications of a variety of organofluorine compounds/calcium nanocomposites including the calcium fluoride/low molecular weight aromatic compounds nanocomposites will be described.

In chapter 1, preparation and thermal stability of a variety of fluoroalkyl end-capped oligomers/calcium carbonate nanocomposites are described (see Scheme 6), and application to the surface modification of poly(methyl methacrylate) (PMMA) by using these nanocomposites before and after calcination are also described.

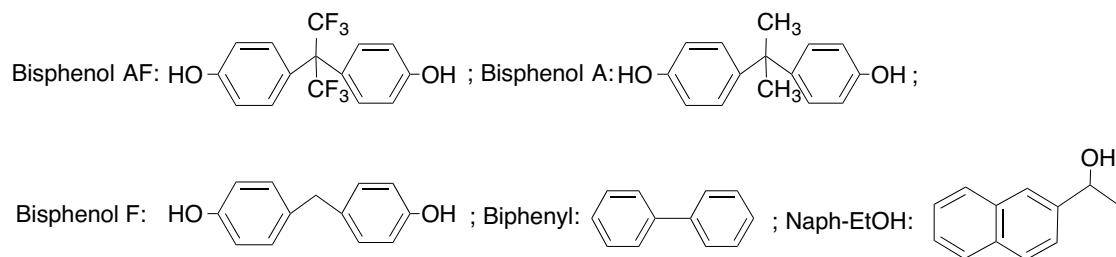


Scheme 6

In chapter 2, preparation and thermal stability of calcium fluoride/low molecular weight aromatic compounds nanocomposites are described (see Scheme 7).

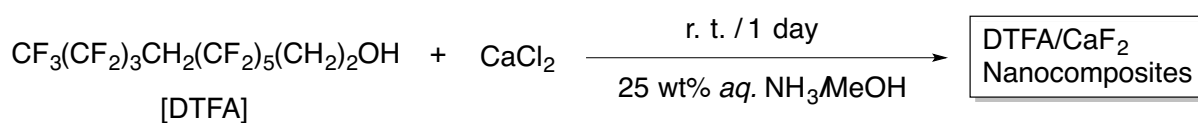


**ArH:** Bisphenol AF, Bisphenol A, Bisphenol F, Biphenyl, Naph-EtOH



Scheme 7

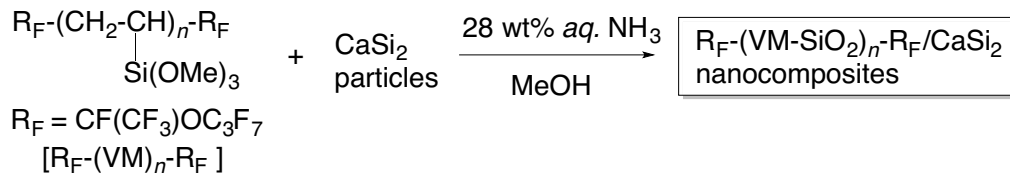
In chapter 3, reactions of fluorinated aliphatic alcohols with calcium chloride to afford the corresponding fluorinated alcohol/calcium fluoride nanocomposites are described (see Scheme 8). Thermal stability and application to the surface modification of these nanocomposites are also described.



Scheme 8

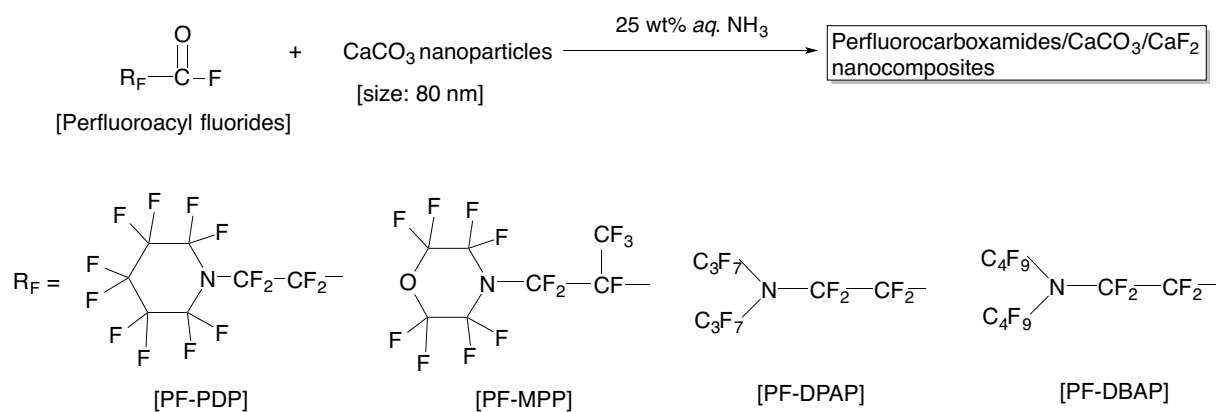
In chapter 4, preparation and surface modification of glass by using fluoroalkyl end-capped vinyltrimethoxysilane oligomer/calcium silicide nanocomposites are described (see Scheme 9). In this chapter, development of these nanocomposites to environmental

cyclical type-fluorine recycle through the formation of calcium fluorides is also described.



Scheme 9

In chapter 5, preparation and surface modification of perfluorocarboxamides/calcium carbonate/calcium fluoride nanocomposites are described (see Scheme 10). Application to the separation of the mixture of oil and water by using these fluorinated nanocomposites will be also described.



Scheme 10

## References

- 1) P. Gomez-Romero and C. Sanchez (Eds), *Functional Hybrid Materials*, Wiley, Weinheim (2004).
- 2) C.J. Brinker and G. W. Scherer, “*Sol-gel Science*” Academic, Boston (1990).
- 3) M. Pedroso, M. Dias, C. Azuma, G. R. San, and C. Mothe, *Colloid Polym. Sci.*, **281**, 19 (2003).
- 4) O. Sel, A. Soules, B. Ameduri, B. Boutevin, C. Laberty-Robert, G. Gebel, and C. Sanchez, *Adv. Funct. Mater.*, **20**, 1090 (2010).
- 5) X. Chen, Y. Zhu, B. Zhou, Y. Guo, W. Gao, Y. Ma, S. Guan, L. Wang, and Z. Wang, *Powder Technol.*, **204**, 21 (2010).
- 6) F. Jiang, Y. Yang, L. Huang, X. Chen, and Z. Shao, *J. Appl. Polym. Sci.*, **114**, 3686 (2009).
- 7) T. Kato, A. Sugawara, and N. Hosoda, *Adv. Mater.*, **14**, 869 (2002).
- 8) D.-M. Qi, Y.-Z. Bao, Z.-X. Weng, and Z.-M. Huang, *Polymer*, **47**, 4622 (2006).
- 9) R. Y. Hong, L. L. Chen, J. H. Li, H. Z. Li, Y. Zheng, and J. Ding, *Polym. Adv. Technol.*, **18**, 901 (2007).
- 10) Y. Qiao, J. Yin, and X. Zhao, *Smart Mater. Struct.*, **16**, 332 (2007).



- 11) C. G. Ma, M. Z. Rong, M. Q. Zhang, and K. Friedrich, *Polym. Eng. Sci.*, **45**, 529 (2005).
- 12) H. Wang, H. Zhou, A. Gestos, J. Fang, and T. Lin, *ACS Appl. Mater. Interfaces*, **5**, 10221 (2013).
- 13) Y. Li, L. Li, and J. Sun, *Angew. Chem.*, **122**, 6265 (2010).
- 14) S. Kim, E. Kim, S. Kim, and W. Kim, *J. Colloid Interface Sci.*, **292**, 93 (2005).
- 15) W. Zhou, J. H. Dong, K. Y. Qiu, and Y. Wei, *J. Polym. Sci. Part A; Polym. Chem.*, **36**, 1607 (1998).
- 16) F. Yang, I. Bogdanova, and G. L. Nelson, *Polym. Adv. Technol.*, **19**, 602 (2008).
- 17) S. Sunny, N. Vogel, C. Howell, T. L. Vu, and J. Aizenberg, *Adv. Funct. Mater.*, **24**, 6658 (2014).
- 18) J. Yang, H. Song, X. Yan, H. Tang, and C. Li, *Cellulose*, **21**, 1851 (2014).
- 19) R. Tamaki, K. Naka, and Y. Chujo, *Polym. J.*, **30**, 60 (1998).
- 20) R. Tamaki and Y. Chujo, *Chem. Mater.*, **11**, 1719 (1999).
- 21) C.-H. Chen, C.-C. Teng, S.-F. Su, W.-C. Wu, and C.-H. Yang, *J. Polym. Sci. Part B; Polym. Phys.*, **44**, 451 (2006).
- 22) J. Yu, J. Yu, Z.-X. Guo, and Y.-F. Gao, *Macromol. Rapid Commun.*, **22**, 1261 (2001).
- 23) T. D. Lam, T. V. Hoang, D. T. Quang, and J. S. Kim, *Mater. Sci. Eng. A*, **501**, 87 (2009).
- 24) M. Avella, M. E. Errico, and G. Gentile, *Macromol. Symp.*, **247**, 140 (2007).

- 25) E. Ukaji, T. Furusawa, M. Sato, and N. Suzuki, *Appl. Surf. Sci.*, **254**, 563 (2007).
- 26) J. Li, L. Zhu, Y. Wu, Y. Harima, A. Zhang, and H. Tang, *Polymer*, **47**, 7361 (2006).
- 27) E. Tang, G. Cheng, X. Ma, X. Pang, and Q. Zhao, *Appl. Surf. Sci.*, **252**, 5227 (2006).
- 28) F. Martinez, G. Morales, A. Martin, and R. Grieken, *Appl. Catal. A: Gen.*, **347**, 169 (2008).
- 29) Z. Jie, T. Haolin, and P. Mu, *J. Membr. Sci.*, **312**, 41 (2008).
- 30) E. Jacquilot, J. Galy, J.-F. Gerard, A. Roche, E. Chevet, E. Fouissac, and D. Verchere, *Prog. Org. Coat.*, **66**, 86 (2009).
- 31) C. S. Gill, B. A. Price, and C. W. Jones, *J. Catal.*, **251**, 145 (2007).
- 32) M. Fujiwara, K. Shiokawa, K. Morigaki, Y. Zhu, and Y. Nakahara, *Chem. Eng. J.*, **137**, 14 (2008).
- 33) S.-H. Hsu, Y.-L. Chang, Y.-C. Tu, C.-M. Tsai, and W.-F. Su, *ACS Appl. Mater. Interfaces*, **5**, 2991 (2013).
- 34) T. Korenaga, *J. Soc. Inorg. Mater. Jpn.*, **9**, 346 (2002).
- 35) I. Bonadies, M. Avella, R. Avolio, C. Carfagna, M. E. Errico, and G. Gentile, *J. Appl. Polym. Sci.*, **122**, 3590 (2011).
- 36) T. Zaharescu, S. Jipa, W. Kappel, and P. Supaphol, *Macromol. Symp.*, **242**, 319 (2006).
- 37) W. Gao, X. Ma, Z. Wang, and Y. Zhu, *Colloids Surf. A*, **389**, 230 (2011).

- 38) B. A. Bhanvase, D. V. Pinjari, P. R. Gogate, S. H. Sonawane, and A. B. Pandit, *Chem. Eng. Process*, **50**, 1160 (2011).
- 39) X. Ma, B. Zhou, Y. Deng, Y. Sheng, C. Wang, Y. Pan, and Z. Wang, *Colloids Surf. A*, **312**, 190 (2008).
- 40) A. R. Mahdavian, M. Ashjari, and A. B. Makoo, *Eur. Polym. J.*, **43**, 336 (2007).
- 41) K. Chrissafis, K. M. Paraskevopoulos, G. Z. Papageorgiou, and D. N. Bikiaris, *J. Appl. Polym. Sci.*, **110**, 1739 (2008).
- 42) T. Tsukagoshi, Y. Kondo, and N. Yoshino, *Colloids Surf. B*, **54**, 101 (2007).
- 43) H. Salmah, A. Faisal, and H. Kamarudin, *Int. J. Polym. Mater. Polym. Biomater.*, **60**, 429 (2011).
- 44) E. Tang, H. Liu, L. Sun, E. Zheng, and G. Cheng, *Eur. Polym. J.*, **43**, 4210 (2007).
- 45) L. Pauling, “*The Nature of the Chemical Bond and the Structure of Molecules and Crystals: An Introduction to Modern Structural Chemistry*”, Cornell University Press, New York (1960).
- 46) P. Atkins, “*Shriver and Atkins’ Inorganic Chemistry 5 th Edition*”, Oxford University Press, Great Britain (2010).
- 47) B. E. Smart, *J. Fluorine Chem.*, **109**, 3 (2001).
- 48) M. R. Shaaban, H. Ishii, and T. Fuchigami, *J. Org. Chem.*, **65**, 8685 (2000).

- 49) A. Bondi, *J. Phys. Chem.*, **68**, 441 (1964).
- 50) K. Takano and Y. Hashimoto, *DIC Technical Review*, **7**, 13 (2001).
- 51) J. D. Dunitz, *Chem. Bio. Chem.*, **5**, 614 (2004).
- 52) E. F. Hare, E. G. Shafrin, and W. A. Zisman, *J. Phys. Chem.*, **58**, 236 (1954).
- 53) W. R. Dolbier Jr., *J. Fluorine Chem.*, **126**, 157 (2005).
- 54) K. Uneyama, “*Organofluorine Chemistry*”, Wiley-Blackwell, New Jersey (2006).
- 55) P. Ballinger and F. A. Long, *J. Am. Chem. Soc.*, **82**, 795 (1960).
- 56) K. Johns and G. Stead, *J. Fluorine Chem.*, **104**, 5 (2000).
- 57) E. T. Kang and Y. Zhang, *Adv. Mater.*, **12**, 1481 (2000).
- 58) Z. Cui, E. Drioli, and Y. M. Lee, *Prog. Polym. Sci.*, **39**, 164 (2014).
- 59) T. Imae, *Curr. Opin. Colloid Interface Sci.*, **8**, 307 (2003).
- 60) J. Yang, Z. Zhang, X. Xu, X. Zhu, X. Men, and X. Zhou, *J. Mater. Chem.*, **22**, 2834 (2012).
- 61) S. Ando, T. Matsuura, and S. Sasaki, *Macromolecules*, **25**, 5858 (1992).
- 62) G. Caporiccio, P. M. Cann, and H. A. Spikes, *Wear*, **193**, 261 (1996).
- 63) G. W. Tyndall and P. B. Leezenberg, *Tribol. Lett.*, **4**, 103 (1998).
- 64) H. Sawada, E. Sumino, M. Oue, M. Baba, T. Kira, S. Shigeta, M. Mitani, H. Nakajima, M. Nishida, and Y. Moriya, *J. Fluorine Chem.*, **74**, 21 (1995).

- 65) I. J. Park, S.-B. Lee, C. K. Choi, and K.-J. Kim, *J. Colloid Interface Sci.*, **181**, 284 (1996).
- 66) F. Petit, I. Iliopoulos, R. Audebert, and S. Szonyi, *Langmuir*, **13**, 4229 (1997).
- 67) D. Cochin, P. Hendlinger, and A. Laschewsky, *Colloid Polym. Sci.*, **273**, 1138 (1995).
- 68) S. Koizumi, A. Ohmori, T. Shimazu, and M. Iwatani, *Hyomen Kagaku*, **13**, 428 (1992).
- 69) H. Sawada, *Chem. Rev.*, **96**, 1779 (1996).
- 70) H. Sawada, *J. Fluorine Chem.*, **101**, 315 (2000).
- 71) H. Sawada, *Polym. J.*, **39**, 637 (2007).
- 72) H. Sawada, *Polym. Chem.*, **3**, 46 (2012).
- 73) H. Sawada, Y. Minoshima, and H. Nakajima, *J. Fluorine Chem.*, **65**, 169 (1993).
- 74) P. Saravanan, N. Satyanarayana, and S. K. Sinha, *Tribol. Lett.*, **49**, 169 (2013).
- 75) C.-C. Lin, S.-H. Hsu, Y.-L. Chang, and W.-F. Su, *J. Mater. Chem.*, **20**, 3084 (2010).
- 76) S. Guo, S. Soma, K. Okuno, T. Saito, T. Nakagawa, K. Sato, and H. Sawada, *Composites: Part B.*, **70**, 80 (2015).
- 77) M. Senna, A. Duvel, V. Sepelak, J. Shi, K. Lucenildo, D. Silva, V. Laporte, S. Lebedkin, C. Kubel, D. Wang, D. Schunemann, K.-D. Becker, and P. Heitjans, *J. Phys. Chem. C*, **117**, 15272 (2013).
- 78) C. Jin, J. Li, S. Han, J. Wang, and Q. Sun, *Appl. Surface. Sci.*, **320**, 322 (2014).

- 79) C.-G. Wu, M.-I. Lu, C.-C. Tsai, and H.-J. Chuang, *J. Powder Sour.*, **159**, 295 (2006).
- 80) H.-S. Jeong, S. C. Hong, and S.-Y. Lee, *J. Membr. Sci.*, **364**, 177 (2010).
- 81) Y.-C. Chen, C.-C. Tsai, and Y.-D. Lee, *J. Polym. Sci. Part A; Polym. Chem.*, **42**, 1789 (2004).
- 82) Z. Xu, Y. Zhao, H. Wang, X. Wang, and T. Lin, *Angew. Chem.*, **127**, 4610 (2015).
- 83) D. W. Smith, S. T. Lacono, and S. S. Lyer (Eds), *Handbook of Fluoropolymer Science and Technology*, Wiley, Weinheim (2014).
- 84) H. Sawada, T. Tashima, H. Kakehi, T. Nishiyama, M. Kikuchi, M. Miura, Y. Sato, and N. Isu, *Polym. J.*, **42**, 167 (2010).
- 85) M. Murariu, L. Bonnaud, P. Yoann, G. Fontaine, S. Bourbigot, and P. Dubois, *Polym. Degrad. Stability*, **95**, 374 (2010).
- 86) J. D. T. Kruschwitz and W. T. Pawlewicz, *Appl. Opt.*, **36**, 2157 (1997).
- 87) H. Takashima, K.-I. Iwaki, R. Furukuwa, K. Takishita, and H. Sawada, *J. Colloid Interface Sci.*, **320**, 436 (2008).
- 88) G. Li, K.-C. Mai, K.-C. Feng, and Y.-P. Huang, *Polym. Int.*, **55**, 891 (2006).
- 89) E. Dalas, P. Klepetsanis, and P. G. Koutsoukos, *Langmuir*, **15**, 8322 (1999).
- 90) M. S. Sobhy, D. E. El-Nashar, and N. A. Maziad, *Egypt. J. Sol.*, **26**, 241 (2003).
- 91) H. Cao, J. Yao, and Z. Shao, *J. Solid State Chem.*, **199**, 338 (2013).

- 92) X. Ma, Y. Liu, Y. Yu, H. Lei, X. Lv, L. Zhao, S. Ren, and Z. Wang, *J. Appl. Polym. Sci.*, **108**, 1421 (2008).
- 93) J. S. C. Campos, A. A. Riberio, and C. X. Cardoso, *Mater. Sci. Eng.*, **136**, 123 (2007).
- 94) F. Morel, V. Bounor-Legare, E. Espuche, O. Persyn, and M. Lacroix, *Eur. Polym. J.*, **48**, 919 (2012).
- 95) R. Walsh, *Acc. Chem. Res.*, **14**, 246 (1981).
- 96) G. D. Blue, J. W. Green, R. G. Bautista, and J. L. Margrave, *J. Phys. Chem.*, **67**, 877 (1963).

## CHAPTER 1

### **Fluoroalkyl End-capped Oligomers Possessing Nonflammable Characteristic in Calcium Carbonate Nanocomposites**



## 1.1. Introduction

It is well-known that traditional organic polymers such as poly(ethylene), poly(styrene) and poly(vinyl chloride) decompose completely at around 400 ~ 500 °C. On the other hand, perfluorinated polymers such as poly(tetrafluoroethylene) decompose at higher temperatures at around 600 °C because of the bond-strengthening effect of fluorine for the C-C and C-F bonds in highly fluorinated compounds.<sup>1 ~ 5)</sup> Hitherto, there has been increasing interest in the material sciences toward the development of fluorinated polymers, especially, partially fluoroalkylated polymers such as fluoroalkyl end-capped oligomers ( $R_F-[M]_n-R_F$ ;  $R_F$  = fluoroalkyl groups;  $M$  = radical polymerizable monomers) are attractive functional materials, because they exhibit various unique properties such as high solubility, surface active properties, biological activities and nanometer size-controlled molecular aggregates which cannot be achieved by the corresponding non-fluorinated, randomly or block-type fluoroalkylated polymers, and low-molecular weight fluorinated surfactants.<sup>6 ~ 10)</sup> However, the molecular weights of fluoroalkyl end-capped oligomers are in general within 10,000, and their thermal stability is extremely poor compared with that of traditional perfluorinated polymers. Thus, from the developmental viewpoints of new fluorinated heat-resistant materials, it is in particular interest to develop fluoroalkyl end-capped oligomers/inorganic

nanocomposites. In fact, it has been already reported that fluoroalkyl end-capped *N*-(1,1-dimethyl-3-oxobutylacrylamide) oligomer/silica nanocomposites can give no weight loss behavior corresponding to the content of fluorinated oligomer in the silica nanocomposite matrices at all even after calcination at 800 °C.<sup>11, 12)</sup> This chapter shows that not only silica nanoparticles but also calcium carbonate nanoparticles can give no weight loss characteristic toward fluoroalkyl end-capped oligomers in the corresponding composite matrices even after calcination at 800 °C.

## **1.2. Experimental**

### **1.2.1 Measurements**

Dynamic light scattering (DLS) measurements were measured by using Otsuka Electronics DLS-7000HL (Tokyo, Japan). Fourier-transform infrared (FT-IR) spectra were measured using Shimadzu FTIR-8400 FT-IR spectrophotometer (Kyoto, Japan). Field emission scanning electron micrographs (FE-SEM) were obtained using JEOL JSM-7000F (Tokyo, Japan). X-ray diffraction (XRD) measurements were performed by the use of Mac Science M18XHF-SRA (Tokyo, Japan). Thermal analyses were recorded on Bruker axS TG-DTA2000SA differential thermobalance (Kanagawa, Japan). The contact angles were measured by the use of Kyowa Interface Science Drop Master 300 (Saitama, Japan).

### **1.2.2. Materials**

Acrylic acid (ACA) and 2-(methacryloyloxy)ethanesulfonic acid (MES) were used as received from Toagosei Co., Ltd (Tokyo, Japan) and Polyscience, Inc. (PA, USA), respectively. *N,N*-dimethylacrylamide (DMAA) and acryloylmorpholine (ACMO) were used

as received from Kohjin Co., Ltd. (Tokyo, Japan). Calcium chloride and sodium carbonate were purchased from Wako Pure Chemical Industries (Osaka, Japan). A variety of fluoroalkyl end-capped oligomers were prepared by reaction of fluoroalkanoyl peroxide with the corresponding monomers according to the previously reported methods.<sup>13 ~ 15)</sup>

### **1.2.3. Preparation of fluoroalkyl end-capped ACA oligomer/calcium carbonate nanocomposites**

To fluoroalkyl end-capped ACA oligomer ( $R_F-[ACA]_n-R_F$ ) (23 mg) was added 0.2 mol/dm<sup>3</sup> aqueous sodium carbonate solution (5 ml) and 0.5 mol/dm<sup>3</sup> aqueous calcium chloride solution (2 ml). The mixture was stirred with a magnetic stirring bar at room temperature for 1 day and then was centrifuged for 30 min. The obtained product was washed with water in several times. The expected fluoroalkyl end-capped ACA oligomer/calcium carbonate nanocomposite powders thus obtained were dried in vacuum at 50 °C for 1 day to afford purified particle powders (82 mg). Other fluoroalkyl end-capped oligomers/calcium carbonate nanocomposites were also prepared under similar conditions.

#### **1.2.4. Treatment of $R_F-(DMAA)_n-R_F$ /calcium carbonate nanocomposites before and after calcination at 800 °C with 1N hydrochloric acid and 1, 2-dichloroethane**

To  $R_F-(DMAA)_n-R_F$ /calcium carbonate nanocomposite powders before and after calcination at 800 °C (50 mg), respectively, was added 1N hydrochloric acid (10 ml) and then were stirred with a magnetic stirring bar at room temperature for 1 day. The obtained well-dispersed solutions were evaporated off under reduced pressure, and 1, 2-dichloroethane (DE) (5 ml) was added to the obtained products. The DE solutions were centrifuged for 30 min, and the obtained supernatant solutions were evaporated off under reduced pressure to measure the FT-IR spectra, respectively.

#### **1.2.5. Preparation of modified poly(methyl methacrylate) films treated with fluoroalkyl end-capped oligomers/calcium carbonate nanocomposites before and after calcination at 800 °C**

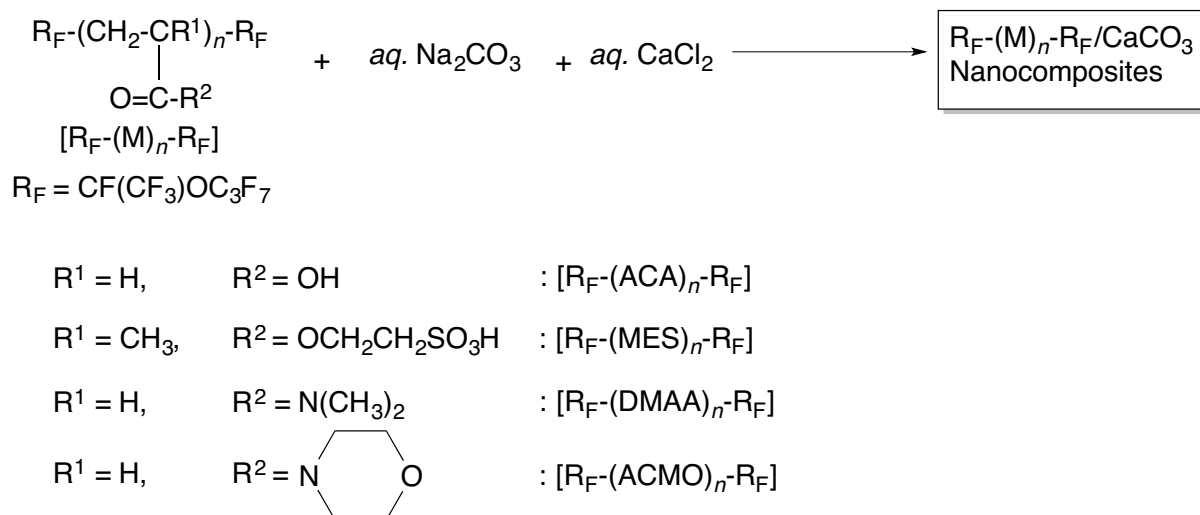
Modified poly(methyl methacrylate) (PMMA) films were prepared by casting tetrahydrofuran (THF) solutions (25 ml) containing PMMA (990 mg) and fluoroalkyl end-capped oligomers/calcium carbonate nanocomposite powders before and after calcinations

at 800 °C (10 mg) on glass plates. The solvents were evaporated at room temperature, and the films formed were peeled off and dried at 50 °C for 24 h under vacuum to afford the modified PMMA films. The contact angles for dodecane on the films were determined at room temperature by the use of goniometer-type contact angle measurements.

### 1.3. Results and discussion

#### 1.3.1. Preparation of fluoroalkyl end-capped oligomer/calcium carbonate nanocomposites

Fluoroalkyl end-capped oligomers possessing amide, carboxyl and sulfo groups are expected to interact with calcium carbonate nanoparticles as a guest molecule in their oligomeric aggregates, which can be formed through the aggregation of the end-capped fluoroalkyl segments.<sup>6 ~ 10)</sup> In fact, it was previously reported that fluoroalkyl end-capped oligomer possessing amide groups has an extraordinarily higher calcium ion binding power compared to traditional organic chelating agents.<sup>16)</sup> Thus, sodium carbonate can react with calcium chloride in the presence of a variety of fluoroalkyl end-capped oligomers ( $R_F-[M]_n-R_F$ ) at room temperature to give the corresponding  $R_F-(M)_n-R_F/CaCO_3$  composites in 14 ~ 72 % isolated yields. These results are shown in Scheme 1-1 and Table 1-1.



Scheme 1-1

Table 1-1 Preparation of  $\text{R}_F-(\text{M})_n-\text{R}_F/\text{CaCO}_3$  nanocomposites using 1.0 mmol for  $\text{Na}_2\text{CO}_3$  and 1.0 mmol for  $\text{CaCl}_2$

Run		$R_F-(M)_n-R_F$ (mg)	Yield <sup>a)</sup> (%)	Size of composites <sup>b)</sup> Before calcination (nm)	After calcination (nm)
1	$R_F-(ACA)_n-R_F$	23	67	$36.7 \pm 12.0$	$25.0 \pm 6.1$
2		56	14	$38.0 \pm 9.4$	$20.0 \pm 4.6$
3		112	27	$40.4 \pm 9.6$	$24.2 \pm 5.7$
4	$R_F-(MES)_n-R_F$	23	62	$113 \pm 21$	$37.6 \pm 7.4$
5		56	52	$24.9 \pm 5.5$	$57.9 \pm 6.8$
6		112	30	$27.6 \pm 6.6$	$81.3 \pm 14.4$
7	$R_F-(DMAA)_n-R_F$	23	72	$104 \pm 19$	$84.7 \pm 14.4$
8		56	58	$29.1 \pm 5.7$	$35.9 \pm 3.2$
9		112	44	$30.6 \pm 6.8$	$26.7 \pm 5.9$
10	$R_F-(ACMO)_n-R_F$	23	70	$114 \pm 27$	$31.2 \pm 7.1$
11		56	58	$33.4 \pm 9.7$	$41.7 \pm 9.7$
12		112	43	$40.4 \pm 9.6$	$49.5 \pm 11.4$
Original $CaCO_3$	-	-	98	$97.0 \pm 18.6$	$65.3 \pm 9.2$

<sup>a)</sup> Yield was based on  $\text{R}_F$ -oligomer and  $\text{CaCO}_3$

<sup>b)</sup> Determined by dynamic light scattering (DLS) measurements in methanol

The composites thus obtained are white-colored powders and were found to exhibit a good dispersibility and stability in not only water but also in traditional organic solvents such as methanol (MeOH), 2-propanol (IPA), THF, dimethyl sulfoxide and *N, N*-dimethylformamide.



Moreover, in the cases of  $R_F-(MES)_n-R_F$ ,  $R_F-(DMAA)_n-R_F$  and  $R_F-(ACMO)_n-R_F$ /calcium carbonate composites, these composites also had a good dispersibility and stability in fluorinated aliphatic solvents (1 : 1 mixed solvents [AK-225<sup>TR</sup>] of 1,1-dichloro-2,2,3,3,3-pentafluoropropane and 1,3-dichloro-1,2,2,3,3-pentafluoropropane). Thus, the size of the composites in Table 1-1 have been measured by the use of DLS measurements at 25 °C, and these results were also shown in Table 1-1. Table 1-1 shows that the size of these obtained composites is nanometer size-controlled fine particles (25 ~ 114 nm) in MeOH solutions.

FE-SEM of MeOH solutions of  $R_F-(DMAA)_n-R_F/CaCO_3$  composites (Run 7 in Table 1-1) before and after calcination at 800 °C have been measured, and the results are shown in Fig. 1-1.

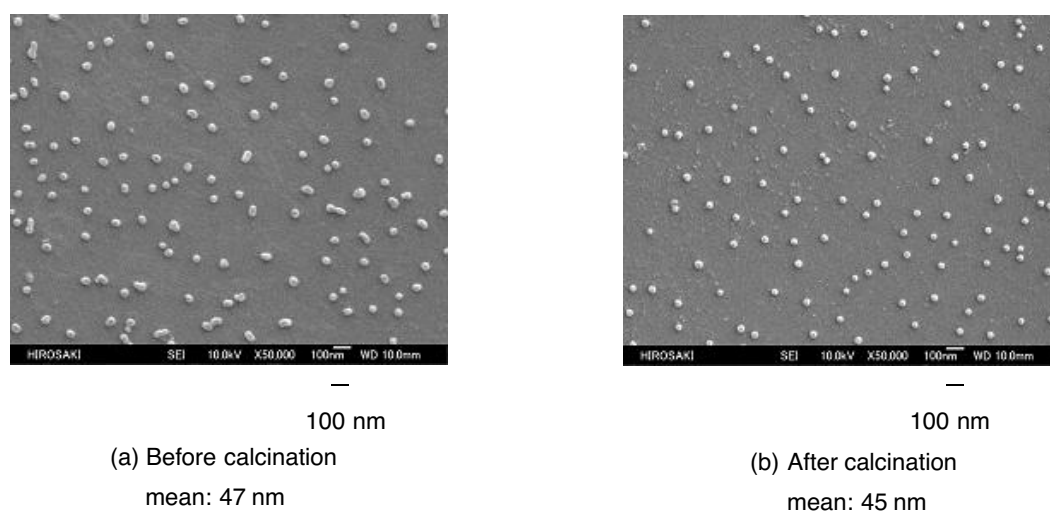


Fig. 1-1 Field emission scanning electron microscopy (FE-SEM) images of well-dispersed methanol solutions of  $R_F-(DMAA)_n-R_F/CaCO_3$  nanocomposites (Run 7 in Table 1-1) before (a) and after (b) calcination at 800 °C

Electron micrographs of the composites before and after calcination at 800 °C showed the formation of composite fine particles with mean diameters of 47 nm and 45 nm, respectively, and it was demonstrated that the appearance of white-colored nanocomposite powders did not change at all before and even after calcination at 800 °C. Sizes of the fluorinated oligomers/calcium carbonate nanocomposites in Table 1-1 after calcination at 800 °C were also measured in MeOH by using DLS measurements. The sizes of the composites were nanometer size controlled (20 ~ 85 nm: see Table 1-1), and the obtained values were almost the same as those before calcination (see Table 1-1). As shown in Fig. 1-1 and Run 7 in Table 1-1, the similar particle sizes for the composites before and after calcination have been obtained in DLS and FE-SEM measurements, respectively.

To verify the crystalline structures of these fluorinated calcium carbonate nanocomposites, the XRD spectra of the nanocomposites in Table 1-1 have been measured. These results are shown in Figs. 1-2 ~ 1-5.

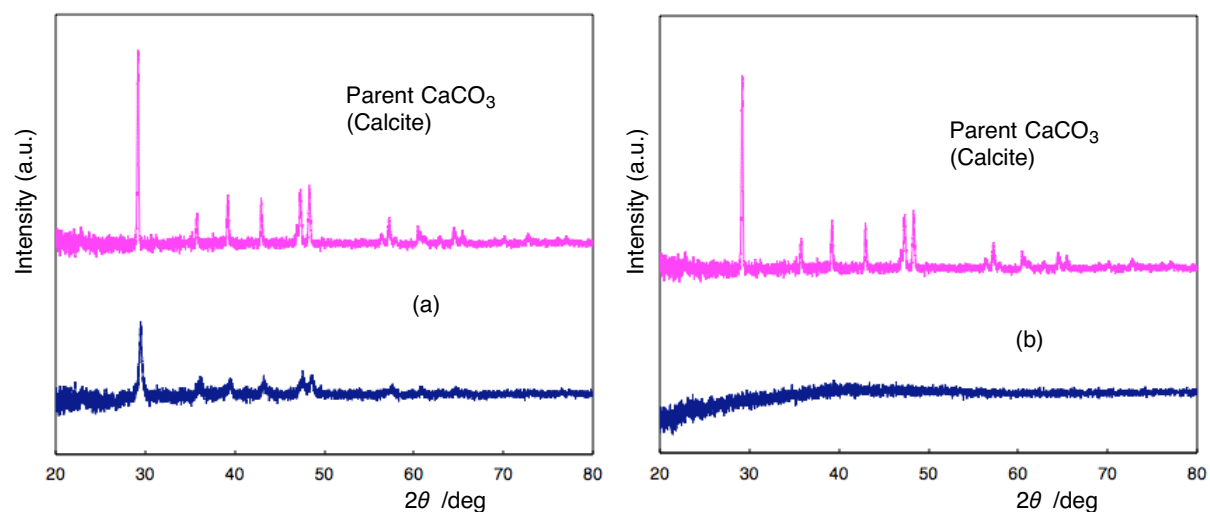


Fig. 1-2 XRD patterns of  $\text{R}_F\text{-(ACA)}_n\text{-R}_F/\text{CaCO}_3$  nanocomposites (Run 1 in Table 1-1) (a), (Run 3 in Table 1-1) (b)

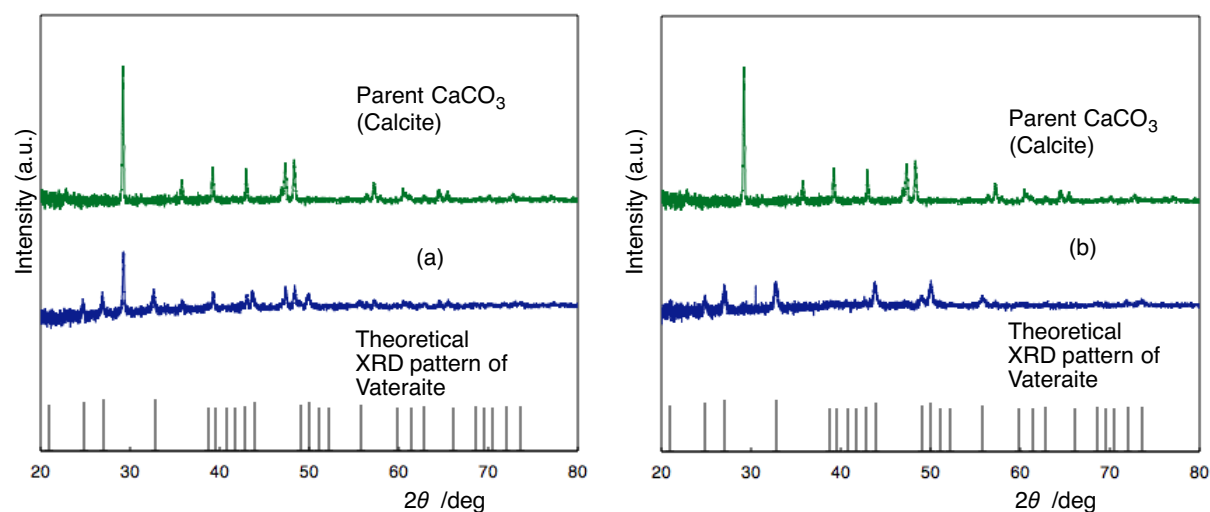


Fig. 1-3 XRD patterns of  $\text{R}_F\text{-(MES)}_n\text{-R}_F/\text{CaCO}_3$  nanocomposites (Run 4 in Table 1-1) (a), (Run 6 in Table 1-1) (b)

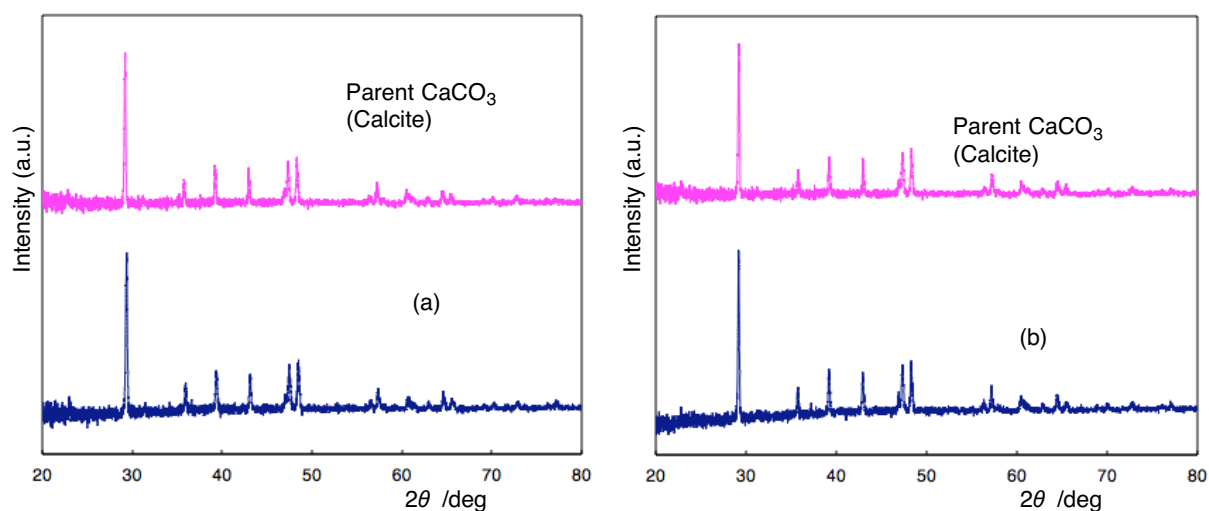


Fig. 1-4 XRD patterns of  $R_F$ -(DMAA) $_n$ - $R_F$ /CaCO<sub>3</sub> nanocomposites (Run 7 in Table 1-1) (a), (Run 9 in Table 1-1) (b)

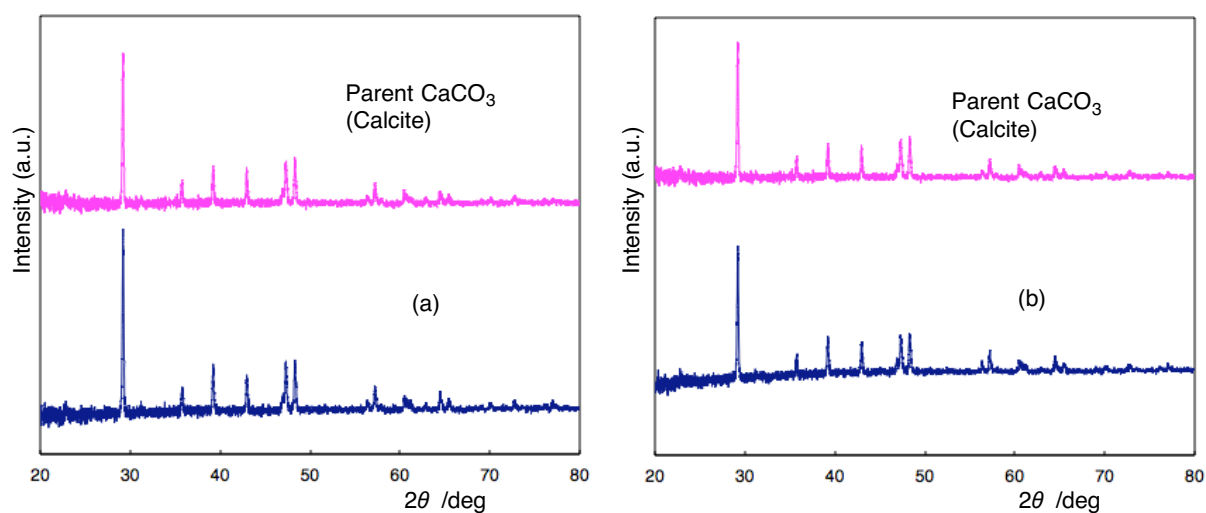


Fig. 1-5 XRD patterns of  $R_F$ -(ACMO) $_n$ - $R_F$ /CaCO<sub>3</sub> nanocomposites (Run 10 in Table 1-1) (a), (Run 12 in Table 1-1) (b)

$R_F$ -(ACA) $_n$ - $R_F$ /CaCO<sub>3</sub> nanocomposites, in which the theoretical oligomer content in the composites is 19 % (Run 1 in Table 1-1), were found to give a clear XRD pattern related to the same calcite structure as that of the original calcium carbonate particles (see Fig. 1-2-[a]).

Very recently, nano-sized silica-coated calcium carbonate fillers have been modified by

fluoroalkyl-alkoxysilane, and this modified fluorinated calcium carbonate filler was applied to the preparation of the nanocomposites with poly(vinylidene fluoride) (PVDF) by using melt blending technique.<sup>17)</sup> XRD spectra of the obtained PVDF/fluorinated calcium carbonate nanocomposites were also reported to exhibit peaks characteristic of calcite type.<sup>17)</sup>

$R_F-(ACA)_n-R_F/CaCO_3$  nanocomposites, in which the theoretical oligomer content in the composites is 53 % (Run 3 in Table 1-1), were unable to give a clear XRD pattern related to the calcite structure (see Fig. 1-2-[b]). This finding would be due to the preferential formation of calcium salts of  $R_F-(ACA)_n-R_F$  oligomer during the composite reaction process. Usually, it is well known that polyacrylamide hydrogels possessing sulfo groups can give the thermodynamically stable calcite modification of calcium carbonate.<sup>18, 19)</sup> However, interestingly, XRD patterns of  $R_F-(MES)_n-R_F/CaCO_3$  nanocomposites, in which the theoretical oligomer content in the composites is 19 % (Run 4 in Table 1-1), were found to give not only calcite but also vaterite structures (see Fig. 1-3-[a]). More interestingly, the vaterite crystal structure's patterns (see Fig. 1-3-[b]) were mainly observed in  $R_F-(MES)_n-R_F/CaCO_3$  nanocomposites possessing a higher theoretical oligomer content in the composites: 53 % (Run 6 in Table 1-1). This finding would be due to the effective interaction between the sulfo groups in oligomer and encapsulated calcium carbonate nanoparticles in the fluorinated oligomeric aggregate cores.

$R_F-(DMAA)_n-R_F/CaCO_3$  nanocomposites (see Fig. 1-4) and  $R_F-(ACMO)_n-R_F/CaCO_3$  nanocomposites (see Fig. 1-5) were found to give the same calcite structure as that of  $R_F-(ACA)_n-R_F/CaCO_3$  nanocomposites (Fig. 1-2-(a)). In this way, it was demonstrated that a higher acidic  $R_F-(MES)_n-R_F$  oligomer than  $R_F-(ACA)_n-R_F$  oligomer can give effectively not calcite but vaterite structure toward calcium carbonate during the nanocomposite reactions. Thus, the present fluorinated oligomers/calcium carbonate nanocomposites are applicable to a novel synthetic approach to the fabrication of composites materials via controlling crystal growth with fluorinated oligomeric aggregate cores as a template.

### **1.3.2. Thermal stability of fluoroalkyl end-capped oligomer/calcium carbonate nanocomposites**

To clarify the presence of fluorinated oligomers in calcium carbonate nanocomposites, thermal stability of these nanocomposites in Table 1-1 have been studied by the thermogravimetric analyses (TGA) measurements, in which the weight loss of these nanocomposites was measured by raising the temperature around 800 °C at a 10 °C/min heating rate under air atmospheric conditions, and the results for the weight loss at 800 °C were shown in Figs. 1-6 ~ 1-9.

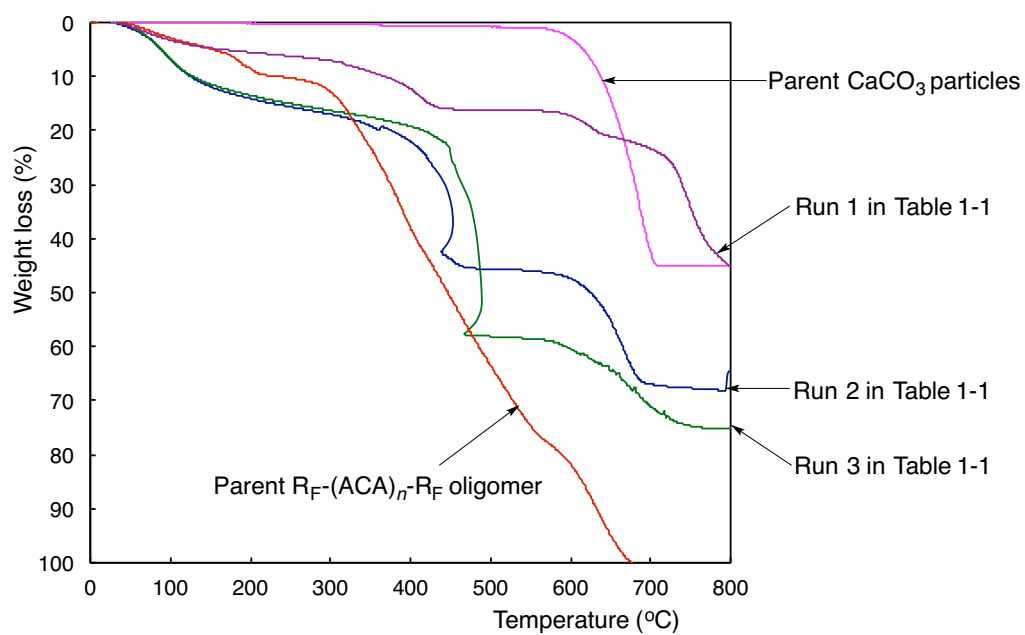


Fig. 1-6 Thermogravimetric analyses of  $\text{R}_\text{F}-(\text{ACA})_n-\text{R}_\text{F}/\text{CaCO}_3$  nanocomposites

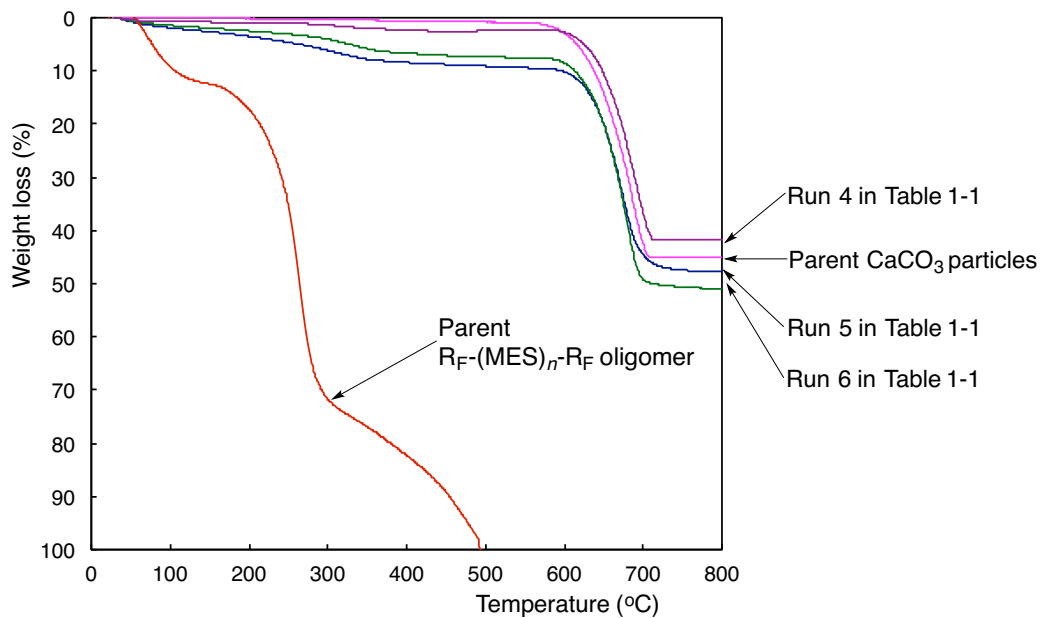


Fig. 1-7 Thermogravimetric analyses of  $\text{R}_\text{F}-(\text{MES})_n-\text{R}_\text{F}/\text{CaCO}_3$  nanocomposites

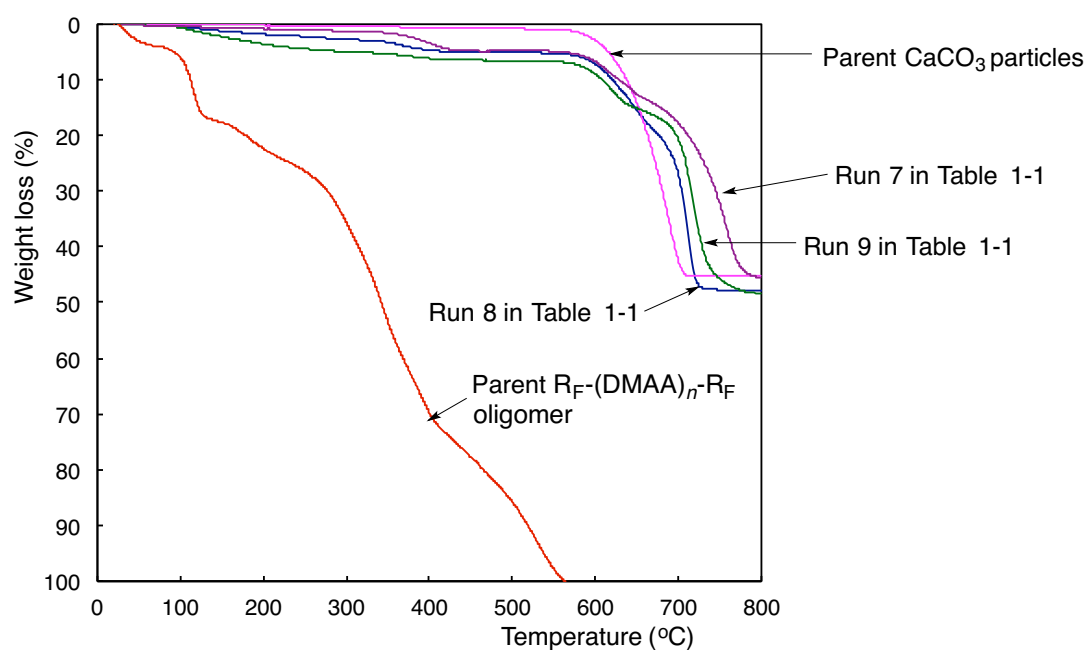


Fig. 1-8 Thermogravimetric analyses of  $\text{R}_\text{F}-(\text{DMAA})_n-\text{R}_\text{F}/\text{CaCO}_3$  nanocomposites

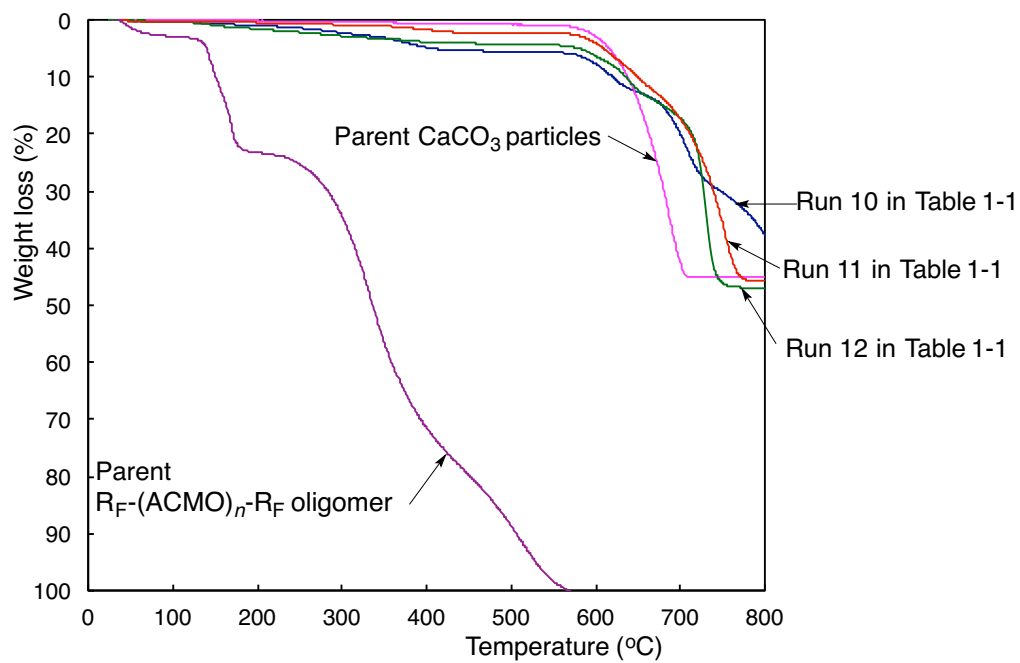


Fig. 1-9 Thermogravimetric analyses of  $\text{R}_\text{F}-(\text{ACMO})_n-\text{R}_\text{F}/\text{CaCO}_3$  nanocomposites



As shown in Figs. 1-6 ~ 1-9, no weight loss corresponding to the fluorinated oligomers in the calcium carbonate nanocomposites, in which each theoretical oligomer content in the composites is 19 % (Runs 1, 4, 7 and 10 in Table 1-1), were observed even after calcination at 800 °C. In these fluorinated oligomers/calcium carbonate nanocomposites, a clear weight loss corresponding to the contents of  $R_F-(ACA)_n-R_F$  oligomer (see Runs 2 and 3 in Table 1-1) can be observed, indicating that  $R_F-(ACA)_n-R_F$  oligomer, of whose feed ratio (56 mg/1.0 mmol or 112 mg/1.0 mmol) based on the used sodium carbonate or calcium chloride is higher than that of Run 1 in Table 1-1, should interact smoothly with calcium ions to give calcium salts derived from  $R_F-(ACA)_n-R_F$  oligomer. The formation of such calcium salts enables calcium carbonate to afford amorphous crystal structures towards the nanocomposites as shown in Fig. 1-2-(b). On the other hand,  $R_F-(MES)_n-R_F/CaCO_3$ ,  $R_F-(DMAA)_n-R_F/CaCO_3$  and  $R_F-(ACMO)_n-R_F/CaCO_3$  nanocomposites were unable to afford a clear weight loss in each feed ratio illustrated in Table 1-1, compared with that of  $R_F-(ACA)_n-R_F/CaCO_3$  nanocomposites. This finding suggests that calcium carbonate composite matrices should enable  $R_F-(MES)_n-R_F$ ,  $R_F-(DMAA)_n-R_F$  and  $R_F-(ACMO)_n-R_F$  oligomers to give the nonflammable characteristic in their nanocomposite cores even after calcination at 800 °C.

In order to clarify the presence of fluorinated oligomer in the composites before and after calcination at 800 °C, the FT-IR spectra of  $R_F-(DMAA)_n-R_F/CaCO_3$  nanocomposites

possessing no weight loss behavior (Run 7 in Table 1-1) have been measured, and the results are shown in Figs. 1-10 and 1-11.

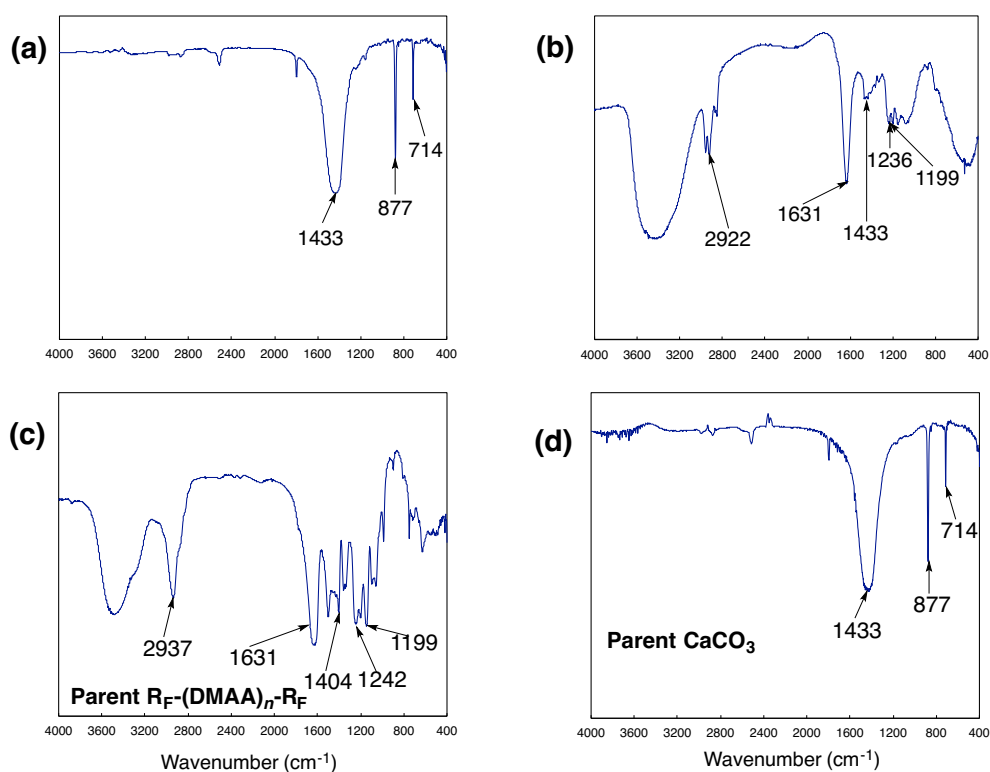


Fig. 1-10 FT-IR spectra of  $\text{R}_F\text{-(DMAA)}_n\text{-R}_F/\text{CaCO}_3$  nanocomposites (Run 7 in Table 1-1) before calcination at 800 °C [before (a) and after (b) treatment with 1N HCl and 1, 2-dichloroethane (DE)], parent  $\text{R}_F\text{-(DMAA)}_n\text{-R}_F$  oligomer (c), and parent  $\text{CaCO}_3$  (d)

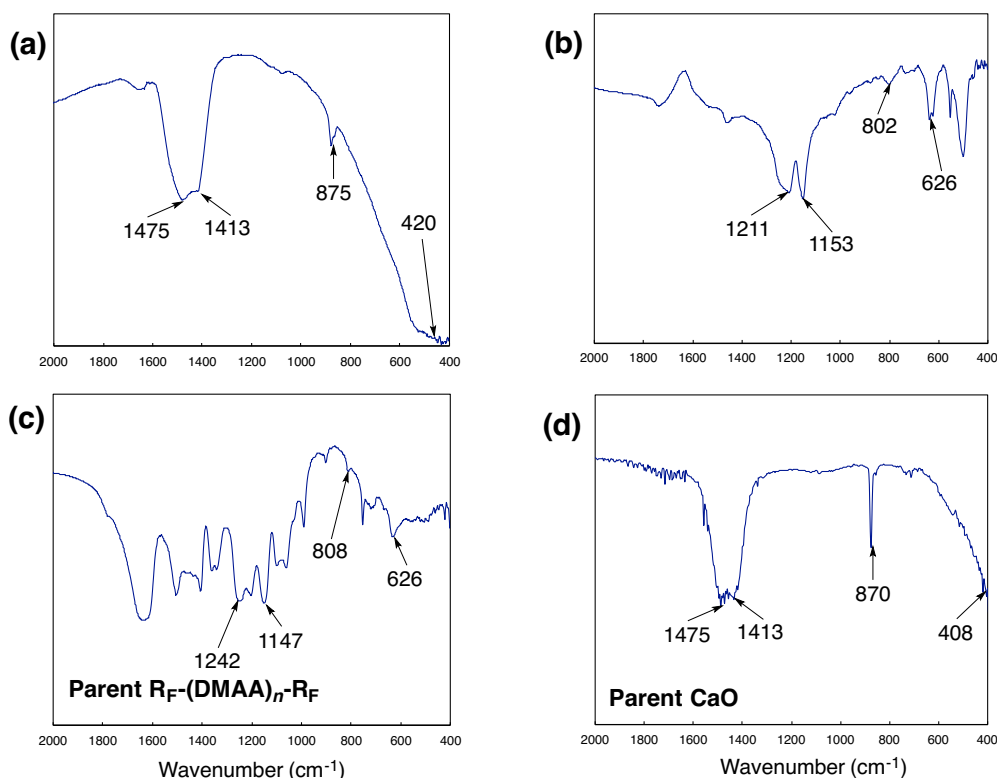


Fig. 1-11 FT-IR spectra of  $R_F-(DMAA)_n-R_F/CaCO_3$  nanocomposites (Run 7 in Table 1-1) after calcination at 800 °C [before (a) and after (b) treatment with 1N HCl and 1, 2-dichloroethane (DE)], parent  $R_F-(DMAA)_n-R_F$  oligomer (c) and parent CaO (d)

As shown in Figs. 1-10-(a) and (d), unexpectedly, any absorption peaks related to the presence of  $R_F-(DMAA)_n-R_F$  oligomer in the nanocomposites before calcination were unable to detect (Fig. 1-10-[a]) to give the same absorption peaks with those of calcium carbonate (see Fig. 1-10-[d]). However, interestingly,  $R_F-(DMAA)_n-R_F/CaCO_3$  nanocomposites after the treatment with 1N HCl and DE showed clear absorption peaks around 2922 (C-H), 1631 (C=O), 1433 (C-N), 1236 (C-N) and 1199 (C-F)  $cm^{-1}$  related to the presence of  $R_F-(DMAA)_n-R_F$  oligomer (see Fig. 1-10-[b]). More interestingly,  $R_F-(DMAA)_n-R_F/CaCO_3$  nanocomposites after calcination at 800 °C were found to give some absorption peaks around

1211 (C-F), 1153 (C-N), 802 (C-C) and 626 (C-C)  $\text{cm}^{-1}$  related to the  $\text{R}_\text{F}-(\text{DMAA})_n-\text{R}_\text{F}$  oligomer by the treatment of the nanocomposites with 1N HCl and DE (see Fig. 1-11-[b]). In contrast, the corresponding nanocomposites before the treatment with 1N HCl and DE were unable to give such absorption peaks (see Fig. 1-11-[a]), and the same FT-IR absorption peaks as those of original CaO (see Fig. 1-11-[d]) were observed. This suggests that calcium carbonate in  $\text{R}_\text{F}-(\text{DMAA})_n-\text{R}_\text{F}/\text{CaCO}_3$  nanocomposites can give a transformation to calcium oxide during the calcination process.

It has been already reported that fluoroalkyl end-capped *N*-(1, 1-dimethyl-3-oxobutyl) acrylamide oligomer  $\{\text{R}_\text{F}-(\text{CH}_2\text{CHC}(=\text{O})\text{NHCMe}_2\text{CH}_2\text{C}(=\text{O})\text{Me})_n-\text{R}_\text{F}:$   
 $\text{R}_\text{F}-(\text{DOBAA})_n-\text{R}_\text{F}\}/\text{silica}$  nanocomposites, which were prepared by the sol-gel reactions of tetraethoxysilane (TEOS) with silica nanoparticle in the presence of the corresponding oligomer under alkaline conditions, can exhibit no weight loss behavior in proportion to the contents of the oligomer in the composites.<sup>20)</sup> In the  $\text{R}_\text{F}-(\text{DOBAA})_n-\text{R}_\text{F}/\text{silica}$  nanocomposite, amido bands related to the oligomer in the composites were not detected by FT-IR spectra measurements at room temperature, indicating that the extremely strong molecular-level combination imparted by both the amido groups in oligomer and the residual silanol groups in the silica gel matrices should afford the perfect restriction of the vibration of such amido groups even at room temperature conditions.<sup>20, 21)</sup>

In this way, these findings suggest that the present fluorinated nanocomposites can exhibit no weight loss characteristic toward fluorinated oligomers in the calcium carbonate nanocomposite matrices even after calcination at 800 °C. Especially, this finding would be due to the effective interaction between fluorinated oligomers and calcium carbonate in the nanocomposite matrices, leading to the perfect restriction of the vibration related to  $R_F-(DMAA)_n-R_F$  oligomer in the calcium carbonate nanocomposites before calcination even at room temperature conditions.

### **1.3.3. Application to the surface modification of poly(methyl methacrylate) films by using fluoroalkyl end-capped oligomers/calcium carbonate nanocomposites before and after calcination at 800 °C**

It was previously reported that fluoroalkyl end-capped oligomers are applicable to the surface modification of traditional organic polymers such as PMMA, and these fluorinated oligomers can be arranged regularly above the PMMA surface to exhibit a strong oleophobicity imparted by end-capped fluoroalkyl groups.<sup>22)</sup> Additionally, it was already reported that fluoroalkyl end-capped oligomers/calcium carbonate nanocomposites were applied to the surface modification of PMMA to exhibit a good oleophobicity imparted by

fluorine on the surface.<sup>23)</sup> Therefore, it is of particular interest to apply the present fluorinated nanocomposite particles possessing no weight loss characteristic to the surface modification of PMMA in order to confirm the presence of fluorinated oligomers/calcium carbonate nanocomposites (Runs 1, 4, 7 and 10 in Table 1-1) after calcination. The contact angles of dodecane on the modified PMMA film surfaces treated with these nanocomposites after calcination were measured. The contact angles of dodecane on the modified PMMA film surface treated with the corresponding fluorinated nanocomposites before calcination have been also measured under similar conditions, for comparison. These results are shown in Table 1-2.

Table 1-2 Contact angles of dodecane on the modified PMMA films treated with  $R_F-(M)_n-R_F/CaCO_3$  nanocomposites<sup>a), b)</sup> before and after calcination at 800 °C (In all cases, the reverse side has dodecane contact angle of 0°)

R <sub>F</sub> -(M) <sub>n</sub> -R <sub>F</sub> /CaCO <sub>3</sub> nanocomposites	Contact angle (degree)	Film thickness (μm)
	Dodecane Surface side	
R <sub>F</sub> -(M) <sub>n</sub> -R <sub>F</sub> in nanocomposites		
After calcination		
R <sub>F</sub> -(ACA) <sub>n</sub> -R <sub>F</sub>	24	202
R <sub>F</sub> -(MES) <sub>n</sub> -R <sub>F</sub>	22	209
R <sub>F</sub> -(DMAA) <sub>n</sub> -R <sub>F</sub>	16	244
R <sub>F</sub> -(ACMO) <sub>n</sub> -R <sub>F</sub>	18	264
Before calcination		
R <sub>F</sub> -(ACA) <sub>n</sub> -R <sub>F</sub>	51	232
R <sub>F</sub> -(MES) <sub>n</sub> -R <sub>F</sub>	33	226
R <sub>F</sub> -(DMAA) <sub>n</sub> -R <sub>F</sub>	42	241
R <sub>F</sub> -(ACMO) <sub>n</sub> -R <sub>F</sub>	12	232
Non-treated	0	202

a) Used nanocomposites: Run 1, 4, 7 and 10 in Table 1-1

b) Concentration of  $R_F-(M)_n-R_F/CaCO_3$  nanocomposites based on PMMA: 1%

As shown in Table 1-2, contact angles of dodecane on the modified PMMA film surfaces treated with fluorinated nanocomposites before calcination shows significantly large values ( $12^{\circ} \sim 51^{\circ}$ ) to exhibit a good oleophobicity imparted by fluorine on the PMMA surface. The contact angles of dodecane on each reverse side was  $0^{\circ}$ , indicating that the fluorinated nanocomposites can be dispersed effectively above the polymer surface during the cast film formation. Interestingly, dodecane contact angle values on the modified PMMA film surfaces treated with fluorinated nanocomposites after calcination at  $800^{\circ}\text{C}$  also showed larger values ( $16^{\circ} \sim 24^{\circ}$ ), quite similar to those before calcination, although the dodecane contact angle value of non-treated PMMA film surface is  $0^{\circ}$ . In addition, the contact angle of dodecane on the poly(tetrafluoroethylene) (Teflon<sup>TR</sup>) plate surface have been measured under the similar conditions, and the obtained value was  $22^{\circ}$ . Thus, the present fluorinated nanocomposites even after calcination can exhibit the similar surface active characteristic to that of Teflon<sup>TR</sup>. From these findings, the present fluorinated oligomers should exhibit a nonflammable characteristic in calcium carbonate nanocomposite cores even after calcination at  $800^{\circ}\text{C}$  to exhibit a good oleophobicity imparted by fluorine in oligomers on the modified PMMA film surface.

Previously, it was reported that fluoroalkyl end-capped oligomers containing amido protons or higher acidic protons than carboxyl groups, such as sulfo groups and carboxyl groups possessing electron-withdrawing  $\text{CF}_3$  units as neighboring groups can be used as novel

fluorinated functional materials possessing a perfectly nonflammable characteristic even after calcination at 800 °C for the composite reactions with silica nanoparticles and TEOS under alkaline conditions.<sup>12, 21, 24 ~ 26)</sup> It is also suggested that ammonium hexafluorosilicate can be easily formed during the nanocomposite reactions to give a nonflammable characteristic toward the fluorinated oligomers in the silica gel matrices.<sup>12, 21, 24 ~ 26)</sup> In particular, the formation of ammonium hexafluorosilicate during the nanocomposite reactions is due to the dehydrofluorination between fluorine and acidic protons in fluorinated oligomer catalyzed by ammonia in the presence of silica nanoparticles as cocatalyst, and the obtained hydrogen fluoride should react with silica nanoparticles to afford tetrafluorosilane and finally ammonium hexafluorosilicate in the presence of ammonia.<sup>12, 21, 24 ~ 26)</sup> It has been very recently reported that the aromatic compounds possessing acidic hydroxyl protons such as bisphenol AF can exhibit a nonflammable characteristic even after calcination at 800 °C in calcium fluoride nanocomposite matrices through not only the hydrogen bonding interaction between fluorine in calcium fluoride and acidic hydroxyl protons in Ar-OH but also the electrostatic interaction between the electronegative oxygens in Ar-OH and electropositive calcium atoms in calcium fluoride.<sup>27)</sup> Therefore, it is suggested that the present fluorinated oligomer/calcium carbonate nanocomposites should exhibit a nonflammable characteristic even after calcination at 800 °C, owing to the effect interaction (F --- Ca) between fluorines in the oligomers and



calcium moieties in the calcium carbonate nanocomposite matrices. Because, the bond-strengthening effect in Ca-F bond (132 kcal or 552 kJ/mol)<sup>28)</sup> can be easily observed, as well as the Si-F bond (129 kcal or 540 kJ/mol)<sup>29, 30)</sup> in ammonium hexafluorosilicate.

## 1.4. Conclusion

A variety of fluoroalkyl end-capped oligomers/calcium carbonate composites have been succeeded in preparing by the reactions of calcium chloride with sodium carbonate in the presence  $R_F-(ACA)_n-R_F$ ,  $R_F-(MES)_n-R_F$ ,  $R_F-(DMAA)_n-R_F$  and  $R_F-(ACMO)_n-R_F$  oligomers. These fluorinated composites thus obtained were found to exhibit a good dispersibility and stability in a variety of solvents. DLS measurements of these composites before and after calcination at 800 °C show that these composites are nanometer size-controlled fine nanoparticles from 25 to 114 nm and 20 to 85 nm, respectively. Thermal stability of these nanocomposites was studied by the use of TGA measurement.  $R_F-(ACA)_n-R_F/$ ,  $R_F-(MES)_n-R_F/$ ,  $R_F-(DMAA)_n-R_F/$  and  $R_F-(ACMO)_n-R_F/CaCO_3$  nanocomposites, in which each theoretical oligomer content in the composites is 19 %, can exhibit no weight loss corresponding to the contents of oligomers even after calcination at 800 °C.  $R_F-(ACA)_n-R_F/CaCO_3$  nanocomposites, in which the theoretical oligomer contents in the composites are 36 ~ 53 %, were found to exhibit a clear weight loss corresponding to the contents of oligomer in the composites after calcination at 800 °C. In contrast,  $R_F-(MES)_n-R_F/$ ,  $R_F-(DMAA)_n-R_F/$  and  $R_F-(ACMO)_n-R_F/CaCO_3$  nanocomposites afforded a slight weight loss behavior after calcination under similar conditions. It was clarified that each fluorinated oligomer/ $CaCO_3$

nanocomposite possessing no weight loss behavior after calcination was applied to the surface modification of PMMA to exhibit a good oleophobic characteristic imparted by fluorine in the composites, as well as that before calcination. Thus, the present fluorinated oligomers/calcium carbonate nanocomposites have high potential for the development of novel nonflammable materials into a wide variety of fields.

## References

- 1) W. R. Dolbier Jr, *J. Fluorine Chem.*, **126**, 157 (2005).
- 2) J. Scheirs (Ed.), *Modern Fluoropolymers*, Wiley, Chichester (1997).
- 3) B. Ameduri and B. Boutevin, *Well-Architected Fluoropolymers: Synthesis: Properties and Applications*, Elsevier, Amsterdam (2004).
- 4) B. Ameduri, *Chem. Rev.*, **109**, 6632 (2009).
- 5) B. Ameduri and B. Boutevin, *J. Fluorine Chem.*, **104**, 53 (2000).
- 6) H. Sawada, *Chem. Rev.*, **96**, 1779 (1996).
- 7) H. Sawada, *J. Fluorine Chem.*, **105**, 219 (2000).
- 8) H. Sawada, *Prog. Polym. Sci.*, **32**, 509 (2007).
- 9) H. Sawada, *Polym. J.*, **39**, 637 (2007).
- 10) H. Sawada, *Polym. Chem.*, **3**, 46 (2012).
- 11) H. Sawada, T. Narumi, S. Kodama, M. Kamijo, R. Ebara, M. Sugiya, and Y. Iwasaki, *Colloid Polym. Sci.*, **285**, 977 (2007).
- 12) H. Sawada, H. Kakehi, T. Tashima, Y. Nishiyama, M. Miura, and N. Isu, *J. Appl. Polym. Sci.*, **112**, 3482 (2009).
- 13) H. Sawada, Y.-F. Gong, Y. Minoshima, T. Matsumoto, M. Nakayama, M. Kosugi, and T. Migita, *J. Chem. Soc., Chem. Commun.*, 537 (1992).

- 14) H. Sawada, Y. Yoshino, Y. Ikematsu, and T. Kawase, *Eur. Polym. J.*, **36**, 231 (2000).
- 15) H. Sawada, A. Ohashi, M. Baba, T. Kawase, and Y. Hayakawa, *J. Fluorine Chem.*, **79**, 149 (1996).
- 16) H. Sawada, T. Kawase, K. Yamashita, and Y. Hayakawa, *J. Chem. Soc., Chem. Commun.*, 827 (1996).
- 17) F. Morel, V. Bounor-Legare, E. Espuche, O. Persyn, and M. Lacroix, *Eur. Polym. J.*, **48**, 919 (2012).
- 18) O. Grassmann and P. Lobmann, *Chem. Eur. J.*, **9**, 1310 (2003).
- 19) O. Grassmann and P. Lobmann, *Biomaterials*, **25**, 277 (2004).
- 20) H. Sawada, T. Tashima, and S. Kodama, *Polym. Adv. Technol.*, **19**, 739 (2008).
- 21) H. Sawada, T. Tashima, H. Kakehi, Y. Nishiyama, M. Kikuchi, M. Miura, Y. Sato, and N. Isu, *Polym. J.*, **42**, 167 (2010).
- 22) H. Sawada, K. Yanagida, Y. Inaba, M. Sugiya, T. Kawase, and T. Tomita, *Eur. Polym. J.*, **37**, 1433 (2001).
- 23) H. Sawada, Y. Shikauchi, H. Kakehi, Y. Katoh, and M. Miura, *Colloid Polym. Sci.*, **285**, 499 (2007).
- 24) H. Sawada, T. Tashima, Y. Nishiyama, M. Kikuchi, G. Kostov, Y. Goto, and B. Ameduri, *Macromolecules*, **44**, 1114 (2011).

- 25) H. Sawada, M. Kikuchi, and M. Nishida, *J. Polym. Sci. Part A; Polym. Chem.*, **49**, 1070 (2011).
- 26) H. Sawada, X. Liu, Y. Goto, M. Kikuchi, T. Tashima, and M. Nishida, *J. Colloid Interface Sci.*, **356**, 8 (2011).
- 27) T. Saito, M. Nishida, H. Fukaya, H. Kakehi, Y. Kato, M. Miura, N. Isu, and H. Sawada, *Colloid Polym. Sci.*, **291**, 945 (2013).
- 28) G.-D. Blue, J. W. Green, R. G. Bautista, and J. L. Margrave, *J. Phys. Chem.*, **67**, 877 (1963).
- 29) L. Pauling, *The Chemical Bond*, Cornell University Press, New York, (1967).
- 30) R. Walsh, *Acc. Chem. Res.*, **14**, 246 (1981).

## CHAPTER 2

### **Low Molecular Weight Aromatic Compounds Possessing Nonflammable and Flammable Characteristics in Calcium Fluoride Nanocomposite Matrices after Calcination at 800 °C**

## 2.1. Introduction

Much attractive attention has been paid to advanced hybrid organic-inorganic composites because of exhibiting a large variety of extraordinary characteristics deriving from the synergism between the properties of each individual material.<sup>1~3)</sup> A great interest has also been focused on the studies involving hybrids based on blends of oxides such as silica and organic polymers dispersed well at molecular levels.<sup>4~8)</sup> In general, the thermal stability of these organic-inorganic composites decreases extremely compared to that of the corresponding parent inorganic materials because of the presence of organic polymers in the composites.<sup>9, 10)</sup> However, It has been recently reported that fluoroalkyl end-capped oligomers containing amido protons and higher acidic protons than carboxyl groups, such as sulfo groups and carboxyl groups possessing electron-withdrawing CF<sub>3</sub> units as neighboring groups, in silica nanocomposite matrices can exhibit a nonflammable characteristic even after calcination at 800 °C through the formation of ammonium hexafluorosilicate during the nanocomposite reactions under alkaline conditions.<sup>11 ~ 14)</sup> Effective interactions between ammonium hexafluorosilicate and these fluorinated oligomers in silica gel matrices should enable the corresponding oligomers to afford a nonflammable characteristic.<sup>15 ~ 17)</sup> The formation of ammonium hexafluorosilicate during this nanocomposite reaction under alkaline conditions



can be attributed to the very strong (129 kcal or 540 kJ/mol) Si-F bond.<sup>18, 19)</sup> The bond-strengthening effect of fluorine also appears in Ca-F bond (132 kcal or 552 kJ/mol).<sup>20)</sup> Thus, it is suggested that the strength of Ca-F bond in  $\text{CaF}_2$  should give rise to a nonflammable behavior toward usual organic compounds in calcium fluoride matrices through a combination of the very strong Ca-F bond and the intermolecular hydrogen bonding between fluorine in  $\text{CaF}_2$  and hydrogen in an organic compound. This chapter shows that low molecular weight aromatic compounds such as bisphenol AF, bisphenol A and bisphenol F can exhibit a nonflammable characteristic in calcium fluoride matrices even after calcination at 800 °C.

## **2.2. Experimental**

### **2.2.1 Measurements**

Dynamic light scattering (DLS) measurements were measured by using Otsuka Electronics DLS-7000 HL (Tokyo, Japan). Fourier-transform infrared (FT-IR) spectra were measured using Shimadzu FTIR-8400 FT-IR spectrophotometer (Kyoto, Japan). Field emission scanning electron micrographs (FE-SEM) were obtained using JEOL JSM-7000F (Tokyo, Japan). X-ray diffraction (XRD) measurements were performed by the use of Mac Science M18XHF-SRA (Tokyo, Japan). Thermal analyses were recorded on Bruker axS TG-DTA2000SA differential thermobalance (Kanagawa, Japan). Ultraviolet-visible (UV-vis) spectra were measured by using Shimadzu UV-1800 UV-vis spectrophotometer (Kyoto, Japan).  $^1\text{H}$  magic-angle spinning (MAS) nuclear magnetic resonance (NMR) spectra were measured at room temperature using Varian Unity INOVA 300 (Tokyo, Japan). High-performance liquid chromatography (HPLC) analyses were conducted on a Shimadzu LC-20AD (Kyoto, Japan) using 95 % aqueous methanol solution as the eluent.

### 2.2.2. Materials

Bisphenol AF, bisphenol A, bisphenol F and 1-(2-naphthyl)ethanol [Naph-EtOH] were purchased from Tokyo Kasei Kogyo Co., Ltd. (Tokyo, Japan). Biphenyl, potassium fluoride and calcium chloride were purchased from Wako Pure Chemical Industries (Osaka, Japan).

### 2.2.3. Preparation of calcium fluoride/bisphenol AF nanocomposites

To a methanol solution (7 ml) of bisphenol AF (100 mg) was added the mixture of 0.2 mol/dm<sup>3</sup> aqueous potassium fluoride solution (10 ml), 0.5 mol/dm<sup>3</sup> aqueous calcium chloride solution (2 ml), and 25 % aqueous ammonia solution (1 ml). This mixture was stirred with a magnetic stirring bar at room temperature for 1 day, and then was centrifuged for 30 min. The obtained product was washed with water several times. The expected calcium fluoride/bisphenol AF nanocomposite powders thus obtained were dried in vacuo at 50 °C for 1 day to afford purified particle powders (71 mg). UV-vis spectra of the collected aqueous solutions were measured to determine the unreacted bisphenol AF (the amount of residual bisphenol AF, 63 mg). The expected CaF<sub>2</sub>/bisphenol AF nanocomposites showed the following FT-IR spectra: FT-IR (per centimeter) 3346 (OH), 968, 879 (C-H in aromatic ring),

and 416 (Ca-F). Other calcium fluoride/aromatic compound nanocomposites were also prepared under similar conditions. These obtained  $\text{CaF}_2$ /aromatic compound nanocomposites showed the following FT-IR spectra;

$\text{CaF}_2$ /bisphenol A nanocomposites: 3341 (OH), 2970 (C-H), 1599, 1512 (C=C in aromatic ring), 877, 833 (C-H in aromatic ring), 420 (Ca-F)

$\text{CaF}_2$ /bisphenol F nanocomposites: 3416 (OH), 2971 (C-H), 1612, 1512 (C=C in aromatic ring), 1241 (C-H in aromatic ring), 401 (Ca-F)

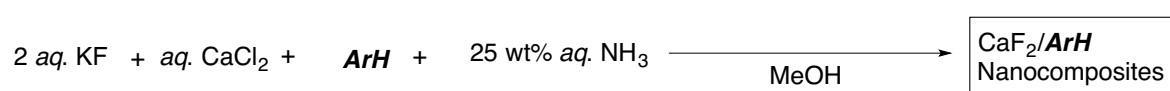
$\text{CaF}_2$ /biphenyl nanocomposites: 3088, 3059, 729 (C-H in aromatic ring), 1597 (C=C in aromatic ring), 418 (Ca-F)

$\text{CaF}_2$ /Naph-EtOH nanocomposites: 3321 (OH), 2970, 2926 (C-H), 1599, 1452 (C=C in aromatic ring), 902, 862 (C-H in aromatic ring), 414 (Ca-F)

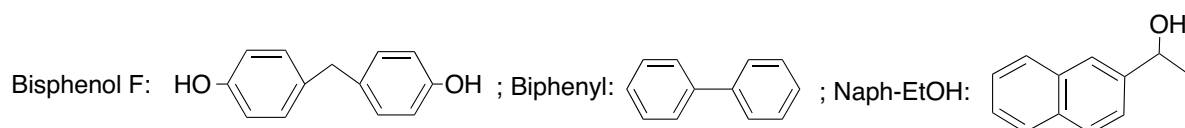
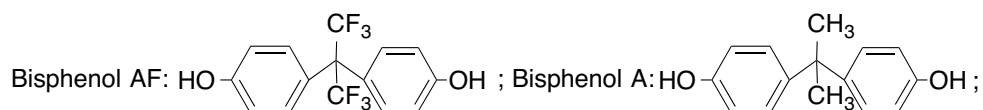
## 2.3. Results and discussion

### 2.3.1. Preparation of calcium fluoride/low molecular weight aromatic compound nanocomposites

Potassium fluoride reacted with calcium chloride in the presence of a variety of low molecular weight aromatic compounds [*ArH*], such as bisphenol AF, bisphenol A, bisphenol F, biphenyl and Naph-EtOH under alkaline conditions at room temperature to yield the corresponding  $\text{CaF}_2/\text{ArH}$  composites. Original calcium fluoride particles were also prepared under similar conditions, for comparison. These results were shown in Scheme 2-1 and Table 2-1.



**ArH:** Bisphenol AF, Bisphenol A, Bisphenol F, Biphenyl, Naph-EtOH



Scheme 2-1

Table 2-1 Preparation of CaF<sub>2</sub>/**ArH** nanocomposites

Run	<b>ArH</b> (mg)	aq. KF (mmol)	aq. CaCl <sub>2</sub> (mmol)	aq. 25 % NH <sub>3</sub> (ml)	Yield <sup>a</sup> (%)	Size of composites <sup>b</sup> (nm ± STD)
1	Bisphenol AF (100)	2.0	1.0	1	40	61.7 ± 11.2 (41.1 ± 9.2) <sup>c)</sup>
2	Bisphenol A (100)	2.0	1.0	1	35	60.4 ± 11.7 (99.7 ± 18.4) <sup>c)</sup>
3	Bisphenol F (100)	2.0	1.0	1	40	73.1 ± 13.8 (63.5 ± 8.9) <sup>c)</sup>
4	Biphenyl (100)	2.0	1.0	1	53	63.5 ± 4.5 (43.8 ± 8.5) <sup>c)</sup>
5	Naph-EtOH (100)	2.0	1.0	1	44	43.8 ± 4.8 (41.9 ± 5.5) <sup>c)</sup>
Parent CaF <sub>2</sub>	-	2.0	1.0	1	33	53.3 ± 11.6 (48.7 ± 9.6) <sup>c)</sup>

<sup>a</sup>Yield were based on CaF<sub>2</sub> and **ArH**<sup>b</sup>Determined by dynamic light scattering (DLS) measurements in methanol<sup>c</sup>Size of composites after calcination at 800 °C

As shown in Scheme 2-1 and Table 2-1, the expected CaF<sub>2</sub>/**ArH** composites were obtained in 35 ~ 53 % isolated yields. These obtained composite white powders were found to exhibit a good dispersibility and stability in not only water but also in traditional organic solvents such as MeOH, 2-propanol, tetrahydrofuran (THF), 1, 2-dichloroethane (DE), dimethyl sulfoxide (DMSO) and *N,N*-dimethylformamide (DMF). Thus, the size of the composites in Table 2-1 has been measured by the use of DLS measurements at 25 °C, and these results are also shown in Table 2-1.

Table 2-1 shows that the obtained composites are nanometer size-controlled fine particles (44 ~ 73 nm) in methanol solutions. The sizes of CaF<sub>2</sub>/bisphenol AF nanocomposites and original CaF<sub>2</sub> particles in a variety of solvents have been measured by DLS measurements at

25 °C, and these results are shown in Fig. 2-1.

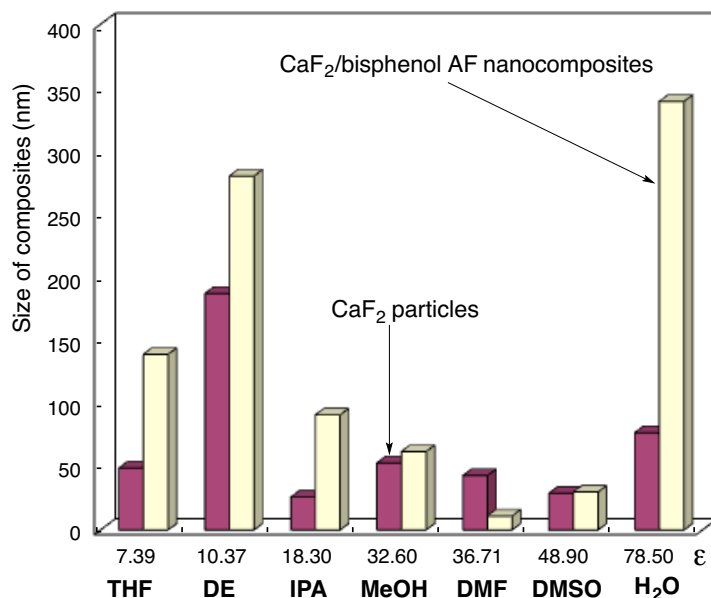


Fig. 2-1 Relationship between the size of CaF<sub>2</sub>/bisphenol AF nanocomposites (or CaF<sub>2</sub> particles) and the dielectric constant ( $\epsilon$ ) of solvents

As shown in Fig. 2-1, the sizes of the nanocomposites and parent CaF<sub>2</sub> particles were 11 ~ 339 nm and 26 ~ 186 nm, respectively, and the sizes of the composites and CaF<sub>2</sub> particles were also very sensitive to the dielectric constants. A higher or lower dielectric constant solvent, such as water and DE could afford an increase of the particle size of the composites and CaF<sub>2</sub> particles. Especially, more effective increase of the particle size of the composites than CaF<sub>2</sub> nanoparticles could be observed in each solvent except for DMF and DMSO.

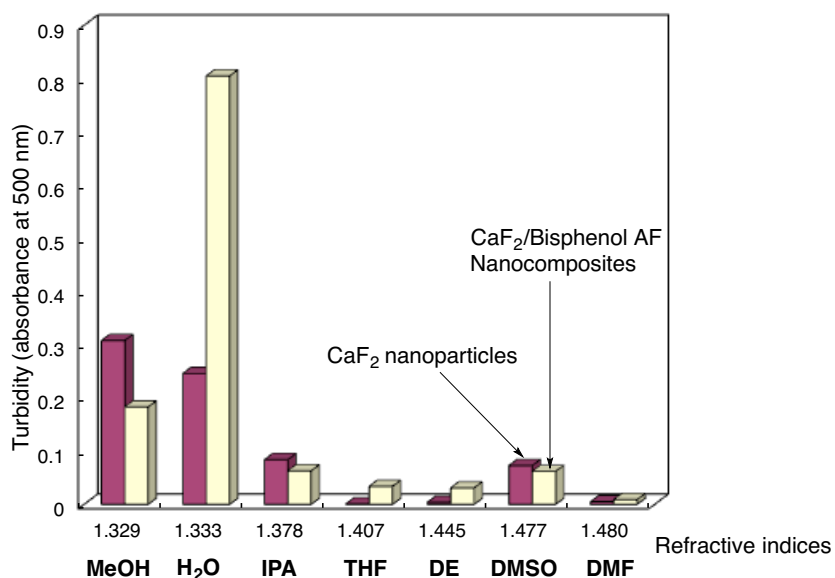


Fig. 2-2 Relationship between the turbidity (absorbance at 500 nm) of  $\text{CaF}_2$ /bisphenol AF nanocomposites (or  $\text{CaF}_2$  nanoparticles) and the refractive indices of a variety of solvents

The turbidity of the well-dispersed nanocomposites and parent  $\text{CaF}_2$  particles is extremely sensitive to the refractive indices of a variety solvents, as shown in Fig. 2-2, and the effective decrease of turbidity for  $\text{CaF}_2$ /bisphenol AF nanocomposites was observed in THF, DE and DMF to afford the transparent colorless solutions. Especially, the lowest turbidity was observed in DMF, indicating that the refractive index of the present  $\text{CaF}_2$ /bisphenol AF nanocomposites is around 1.48. In contrast, the lowest turbidity of parent  $\text{CaF}_2$  particles was observed in THF, indicating the refractive index of  $\text{CaF}_2$  is around 1.40. This value well corresponds to that (1.399) of previously reported one.<sup>21, 22)</sup> The results for the different particle sizes and turbidity between the present nanocomposites and original  $\text{CaF}_2$  particles in Figs. 2-1 and 2-2 suggest that bisphenol AF should be effectively incorporated into calcium



fluoride nanocomposite matrices.

### **2.3.2. Thermal stability of calcium fluoride/low molecular weight aromatic compound nanocomposites**

In order to clarify the presence of aromatic compounds in  $\text{CaF}_2$  nanocomposites, thermal stability of the nanocomposites in Table 2-1 has been studied by the use of thermogravimetric analyses (TGA) measurements, in which the weight loss of these nanocomposites was measured by raising the temperature around 800 °C at a 10 °C/min heating rate under air atmospheric conditions, and the results for the weight loss at 800 °C were shown in Fig. 2-3.

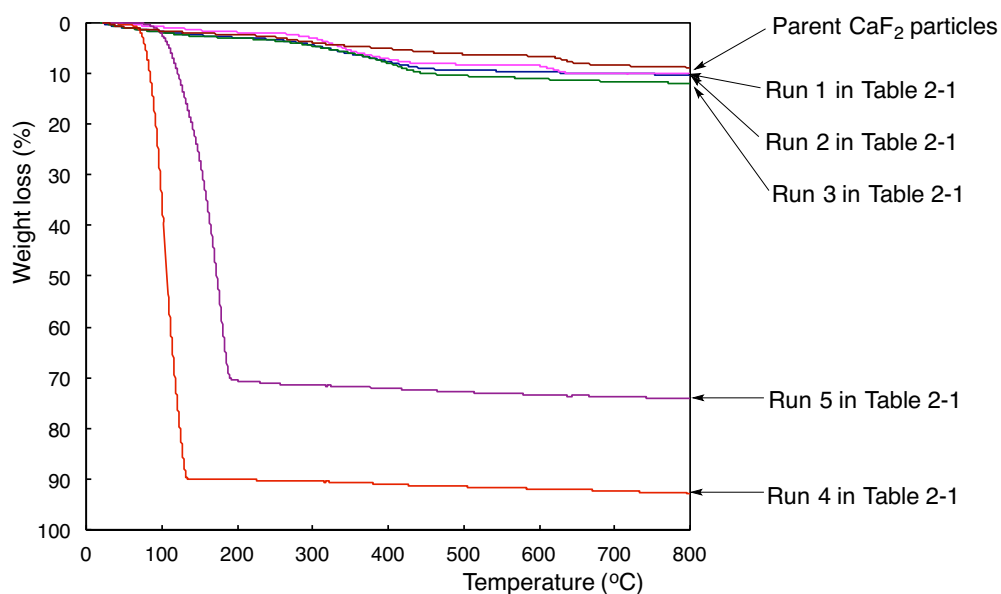


Fig. 2-3 Thermogravimetric analyses of  $\text{CaF}_2/\text{ArH}$  nanocomposites: **ArH**: bisphenol AF (Run 1 in Table 2-1), bisphenol A (Run 2 in Table 2-1), bisphenol F (Run 3 in Table 2-1), biphenyl (Run 4 in Table 2-1), Naph-EtOH (Run 5 in Table 2-1), and  $\text{CaF}_2$  nanoparticles (see Table 2-1)

As shown in Runs 4 and 5 in Fig. 2-3,  $\text{CaF}_2/\text{biphenyl}$  and  $\text{CaF}_2/\text{Naph-EtOH}$  nanocomposites, of whose composites possess neither hydroxyl groups nor acidic hydroxyl groups, respectively, were found to exhibit a clear weight loss at 800 °C corresponding to the contents of aromatic compounds in the composites. Parent biphenyl and Naph-EtOH can also exhibit a perfect weight loss around 120 and 190 °C, respectively, under similar conditions. Unexpectedly,  $\text{CaF}_2/\text{bisphenol AF}$ ,  $\text{CaF}_2/\text{bisphenol A}$  and  $\text{CaF}_2/\text{bisphenol F}$  nanocomposites possessing acidic hydroxyl groups were found to afford no weight loss behavior at 800 °C, of whose weight loss is well consistent with that of the parent  $\text{CaF}_2$  nanoparticles (see Runs 1 ~ 3 in Fig. 2-3). In contrast, the corresponding parent aromatic compounds such as bisphenol AF, bisphenol A and

bisphenol F can give a perfect weight loss around 240, 280 and 280 °C (93 % weight loss), respectively. This finding suggests that acidic hydroxyl groups in aromatic compounds should play an important role for no weight loss behavior of the present calcium fluoride nanocomposites.

The FE-SEM images of methanol solutions of CaF<sub>2</sub>/bisphenol AF nanocomposites (Run 1 in Table 2-1) before and after calcination at 800 °C have been studied, and the results are shown in Fig. 2-4.

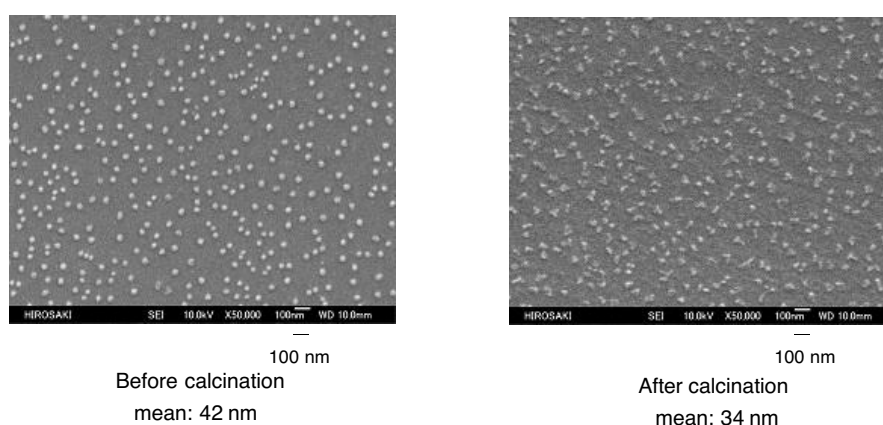


Fig. 2-4 FE-SEM images of well-dispersed methanol solutions of CaF<sub>2</sub>/bisphenol AF nanocomposites (Run 1 in Table 2-1) before and after calcination at 800 °C

Electron micrographs of the nanocomposites before and after calcination at 800 °C showed the formation of composite fine particles with a mean diameter of 42 and 34 nm, respectively, and it was demonstrated that the appearance of white nanocomposite powders did not change at all before and after calcination at 800 °C. Sizes of calcium fluoride/*ArH* nanocomposites in

Table 2-1 after calcination at 800 °C were also measured in methanol by using DLS measurements. The sizes of the composites were nanometer size-controlled (42 ~ 100 nm: see Table 2-1), and almost the same values as those before calcination have been obtained.

Fig. 2-5 shows separately the XRD spectra of CaF<sub>2</sub>/bisphenol AF nanocomposites (Run 1 in Table 2-1) before and after calcination at 800 °C. The XRD spectra of parent CaF<sub>2</sub> nanoparticles in Table 2-1 were also demonstrated in Fig. 2-5, for comparison.

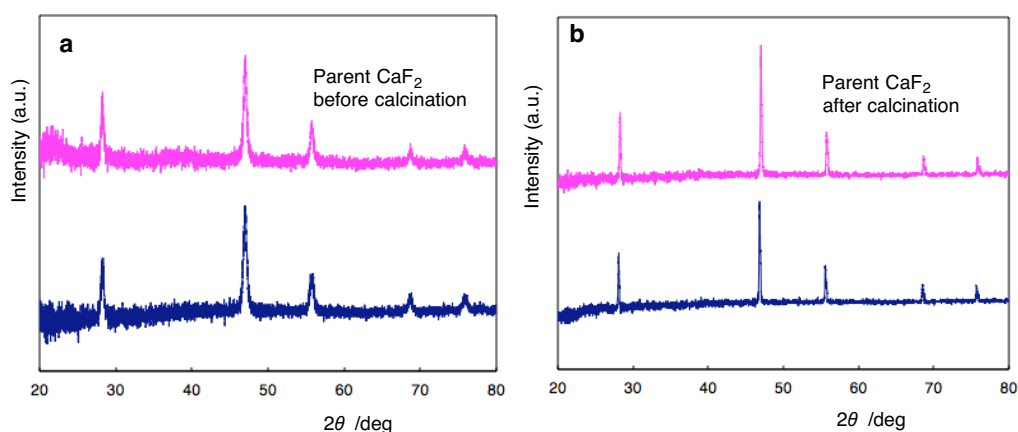


Fig. 2-5 XRD patterns of CaF<sub>2</sub>/bisphenol AF nanocomposites (Run 1 in Table 2-1) before (a) and after (b) calcination at 800 °C

The characteristic peaks of the nanocomposites before and after calcination were completely agreement with those of the parent CaF<sub>2</sub> particles. This finding suggests that calcium fluoride can be essentially incorporated into the architecture of nanocomposite frameworks before and after calcination.

The UV-vis spectra of well-dispersed methanol solutions of CaF<sub>2</sub>/bisphenol AF

nanocomposites before and after calcination at 800 °C have been measured to clarify the presence of bisphenol AF in the composites, and the results were shown in Fig. 2-6.

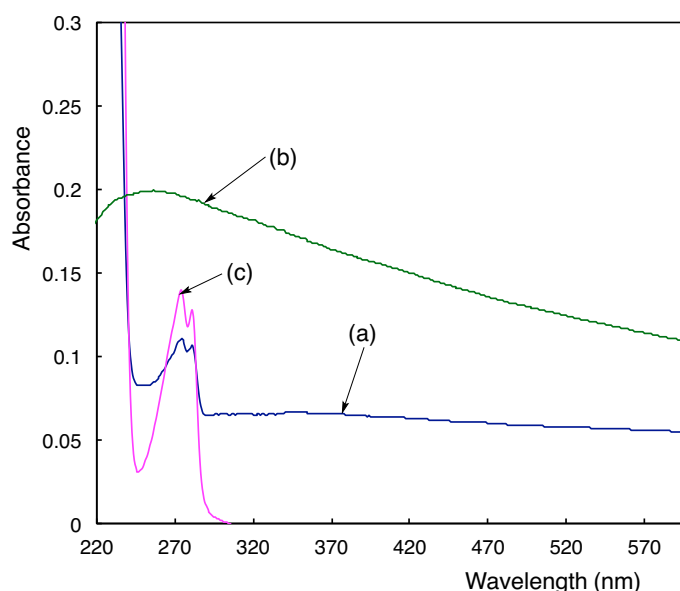


Fig. 2-6 UV-vis spectra of  $\text{CaF}_2$ /bisphenol AF ( $0.2 \text{ g/dm}^3$ ; Run 1 in Table 2-1) before (a) and after (b) calcination at 800 °C, and parent bisphenol AF ( $0.06 \text{ mmol/dm}^3$ ; c) in methanol solutions

As shown in Fig. 2-6-a, the calcium fluoride nanocomposites were able to exhibit a clear absorption band at 274 nm related to bisphenol AF. UV-vis spectra of bisphenol AF in the composites before calcination are quite similar to that of parent bisphenol AF (see Fig. 2-6-c) in methanol. The amount of bisphenol AF in the nanocomposites was estimated by the use of the molar absorption coefficient of bisphenol AF in methanol and the content of bisphenol AF in the composites was 10 %. In contrast, UV-vis spectra of the nanocomposites after calcination were found to exhibit a relatively broad absorption peak around 272 nm (see Fig.

2-6-b), indicating that bisphenol AF should interact with calcium fluoride to give such broad peak during the calcination process.

The amounts of bisphenol A, bisphenol F, biphenyl and Naph-EtOH in the composites before calcination were also estimated to be 9, 7, 95 and 75 %, respectively, under similar conditions. Bisphenol A and bisphenol F in the composites after calcination can exhibit similar broad absorption peaks around 260 nm (original bisphenol A and bisphenol F:  $\lambda_{\text{max}} = 279$  nm; see Figs. 2-7 and 2-8). However, absorption peaks related to biphenyl and Naph-EtOH in the composites after calcination have been completely disappeared (see Figs. 2-9 and 2-10).

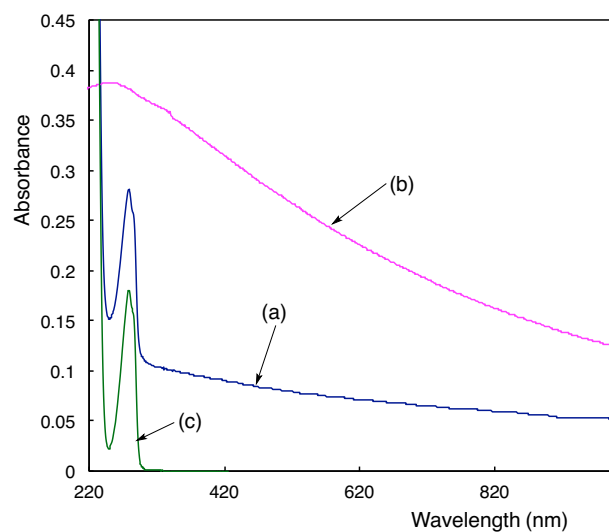


Fig. 2-7 UV-vis spectra of  $\text{CaF}_2$ /bisphenol A ( $0.2 \text{ g/dm}^3$ ; Run 2 in Table 2-1) before (a) and after (b) calcination at  $800^\circ\text{C}$ , and parent bisphenol A ( $0.05 \text{ mmol/dm}^3$ ; c) in methanol solutions

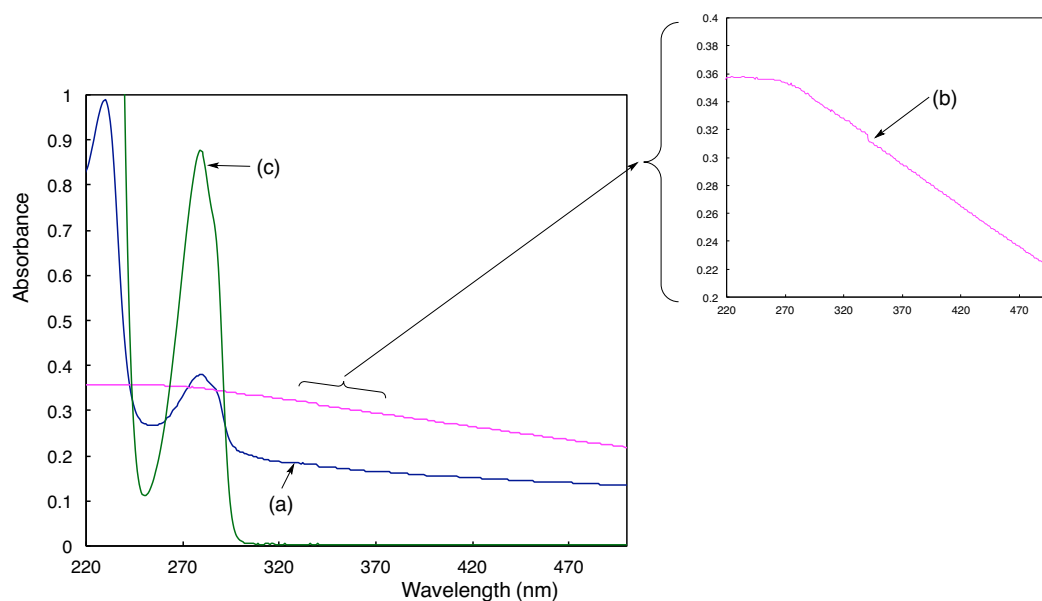


Fig. 2-8 UV-vis spectra of  $\text{CaF}_2$ /bisphenol F ( $0.2 \text{ g/dm}^3$ ; Run 3 in Table 2-1) before (a) and after (b) calcination at  $800^\circ\text{C}$ , and parent bisphenol F ( $0.15 \text{ mmol/dm}^3$ ; c) in methanol solutions

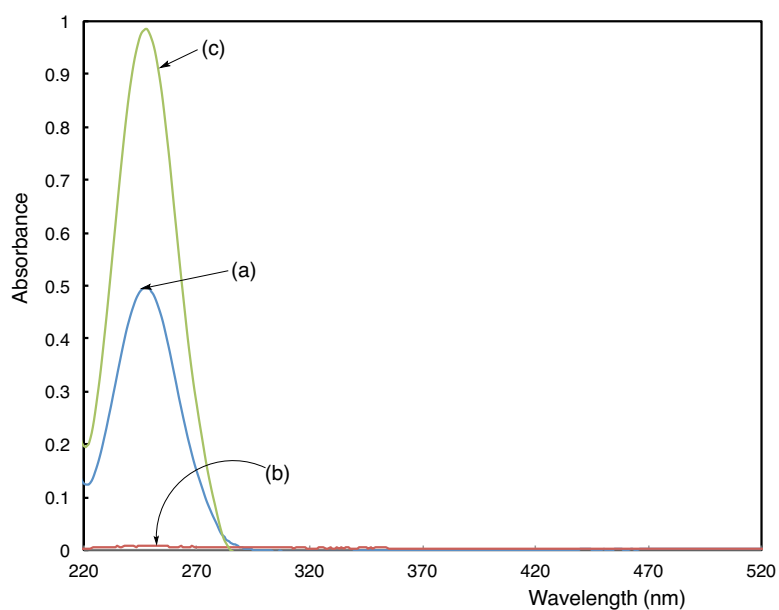


Fig. 2-9 UV-vis spectra of  $\text{CaF}_2$ /biphenyl ( $5 \text{ mg/dm}^3$ ; Run 4 in Table 2-1) before (a) and after (b) calcination at  $800^\circ\text{C}$ , and parent biphenyl ( $0.06 \text{ mmol/dm}^3$ ; c) in methanol solutions

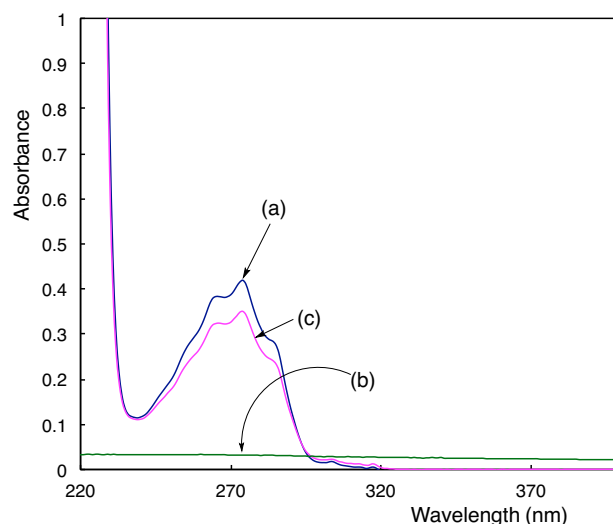


Fig. 2-10 UV-vis spectra of  $\text{CaF}_2/\text{Naph-EtOH}$  ( $0.02 \text{ g/dm}^3$ ; Run 5 in Table 2-1) before (a) and after (b) calcination at  $800^\circ\text{C}$ , and parent Naph-EtOH ( $0.23 \text{ mmol/dm}^3$ ; c) in methanol solutions

In order to clarify the presence of aromatic compounds in the present calcium fluoride nanocomposites, the amount of unreacted bisphenol AF in the nanocomposite reaction shown in Scheme 2-1 and Table 2-1 was estimated to be 63 mg by using UV-vis spectra measurements. Therefore, bisphenol AF: 37 mg (used bisphenol AF for composite reaction: 100 mg, see Run 1 in Table 2-1) was effectively incorporated into calcium fluoride composite matrices to afford the expected calcium fluoride/bisphenol AF nanocomposites. From this finding, since the content of bisphenol AF in calcium fluoride nanocomposites is 52 % ( $37/71 \times 100$ ) [isolated yield of this composite: 71 mg (see Run 1 in Table 2-1)], its TGA curve should exhibit a clear weight loss corresponding to the content (52 %) of bisphenol AF after calcination at  $800^\circ\text{C}$ ; however, the present calcium fluoride/bisphenol AF nanocomposites can exhibit no weight loss even after calcination at  $800^\circ\text{C}$  as shown in Run 1 in Fig. 2-3. The



amounts of unreacted bisphenol A, bisphenol F, biphenyl and Naph-EtOH for the nanocomposite reactions in Scheme 2-1 and Table 2-1 were also determined under similar conditions, and the contents of aromatic compounds in the composites in Table 2-1 are as follows:

The amounts of unreacted <b>ArH</b>	Contents of <b>ArH</b> in the composites
Bisphenol AF: 63 mg	52 % (37/71 x 100)
Bisphenol A: 72 mg	43 % (26/65 x 100)
Bisphenol F: 81 mg	27 % (19/71 x 100)
Biphenyl: 0.1 mg	95 % (99.9/105 x 100)
Naph-EtOH: 38 mg	79 % (62/78 x 100)

The contents of bisphenol A and bisphenol F in the composites are estimated to be 43 and 27 %, respectively; however, the corresponding TGA curves cannot exhibit a clear weight loss corresponding to the content of each aromatic compound as shown in Runs 2 and 3 in Fig. 2-3. On the other hand, biphenyl and Naph-EtOH possessing neither hydroxyl groups nor acidic hydroxyl groups, respectively, were found to exhibit a usual weight loss in the composites corresponding to the contents of these aromatic compounds as shown in Runs 4 and 5 in Fig. 2-3.

The thermal stability of hybrids based on the simple blends of bisphenol AF (45 mg) and original CaF<sub>2</sub> particles (26 mg) has been also studied, for comparison, and the TGA curve was shown in Fig. 2-11-c.

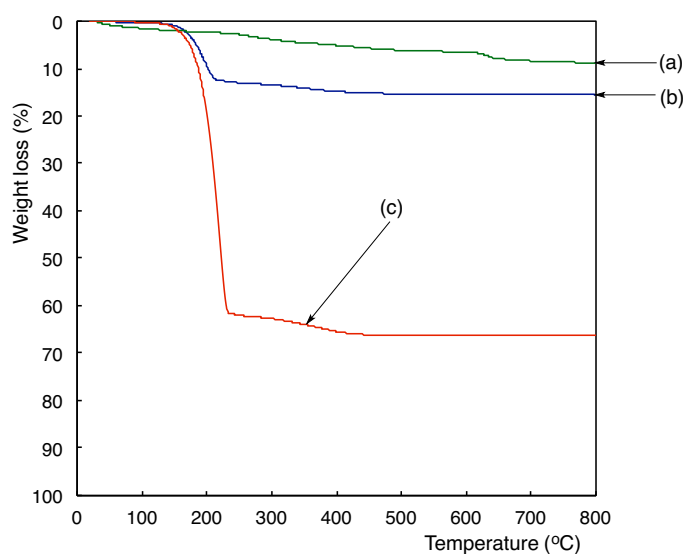
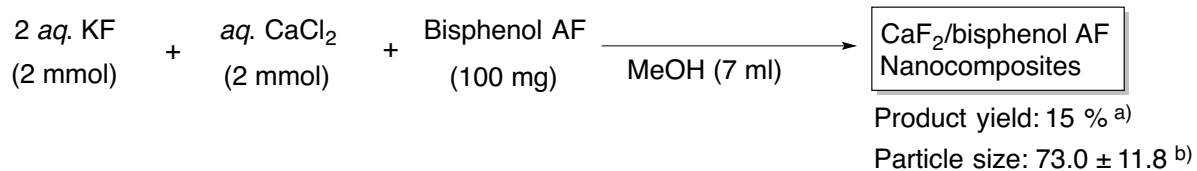


Fig. 2-11 Thermogravimetric analyses of parent  $\text{CaF}_2$  particles (a),  $\text{CaF}_2$ /bisphenol AF nanocomposites, which were prepared under no catalytic conditions (b), and hybrids based on the blends of  $\text{CaF}_2$  particles and bisphenol AF (c)

The simple blend hybrids based on bisphenol AF and  $\text{CaF}_2$  particles afforded a clear weight loss corresponding to the content of bisphenol AF in the blend hybrids. In addition, calcium fluoride/bisphenol AF nanocomposites were tried to prepare under no catalytic conditions as shown in Scheme 2-2.



a) Yield based on  $\text{CaF}_2$  and bisphenol AF

b) Determined by dynamic light scattering measurements in methanol solutions

Scheme 2-2

As shown in Scheme 2-2, the calcium fluoride/bisphenol AF nanocomposites have been prepared in 15 % isolated yield. However, this nanocomposite was found to exhibit a clear weight loss corresponding to the content of bisphenol AF during the calcination process as in Fig. 2-11-b. From these findings, it was demonstrated that acidic hydroxyl groups are essential for no weight loss of low molecular weight aromatic compounds in calcium fluoride composites. Nanocomposite reactions under alkaline conditions as shown in Scheme 2-1 are also essential for no weight loss behavior toward the calcium fluoride nanocomposites.

To verify the presence of bisphenol AF in the nanocomposites before and after calcination at 800 °C,  $^1\text{H}$  MAS NMR of bisphenol AF nanocomposites were measured, and the results were shown in Fig. 2-12.

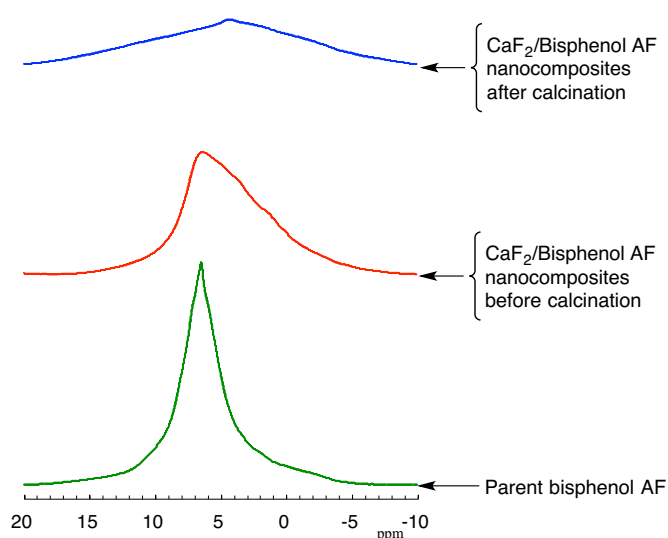


Fig. 2-12  $^1\text{H}$  MAS NMR spectra of  $\text{CaF}_2$ /bisphenol AF nanocomposites before and after calcination at 800 °C

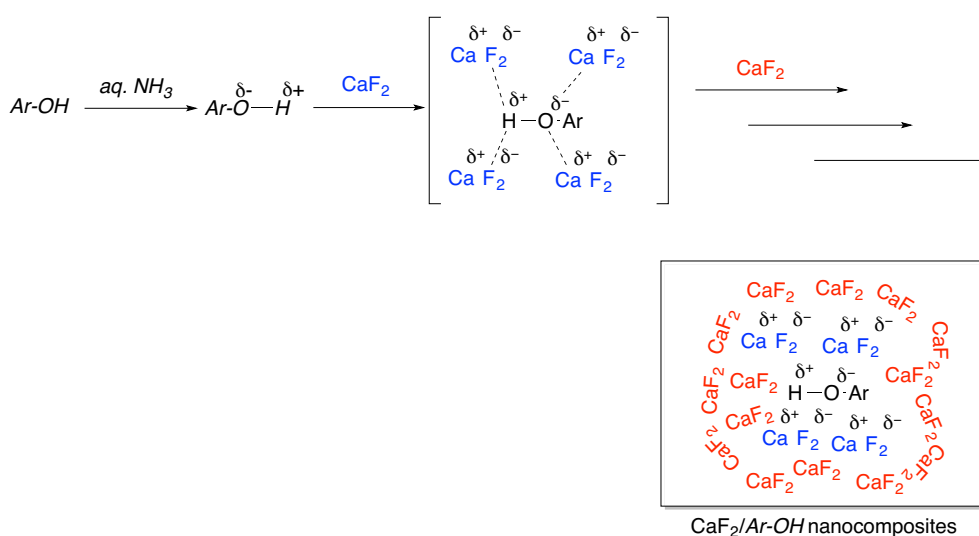
As shown in Fig. 2-12, the broad peaks around 2 ~ 10 ppm related to the presence of aromatic protons in bisphenol AF in the composites were observed before and after calcination. This finding suggests that bisphenol AF should exhibit a nonflammable characteristic in calcium fluoride composite cores even after calcination at 800 °C.

In addition, HPLC (eluent, 5 % aqueous methanol solution) analyses were studied by using the supernatant aqueous methanol solution of calcium fluoride/bisphenol AF nanocomposites (Run 1 in Table 2-1), which were obtained by the centrifugal separation of the corresponding well-dispersed nanocomposites 65 % aqueous methanol solution, and then were filtered through a 0.45 µm PTFE membrane. HPLC analyses showed the peak related to bisphenol AF in the nanocomposites before and after calcination, of whose retention times are the same: 5.9 min (retention time of parent bisphenol AF is 6.0 min under similar conditions). This finding also suggests that bisphenol AF should exhibit a nonflammable characteristic in the composite cores even after calcination.

In conclusion, it was demonstrated that aromatic compounds possessing acidic hydroxyl groups, such as bisphenol AF, bisphenol A and bisphenol F can exhibit a nonflammable characteristic in calcium fluoride nanocomposite matrices even after calcination at 800 °C. In contrast, aromatic compounds possessing neither hydroxyl groups nor acidic hydroxyl groups, respectively, such as biphenyl and Naph-EtOH afforded usual weight loss corresponding to the

contents of these compounds in calcium fluoride nanocomposite matrices during the calcination process. Previously, it was reported that hexafluorosilicate anions obtained in the nanocomposite reactions of fluoroalkyl end-capped acrylic acid oligomer with tetraethoxysilane and silica nanoparticles in the presence of bisphenol AF under alkaline conditions can afford the synergistic interactions derived from not only hydrogen bonding interaction between the fluorines in hexafluorosilicate and hydrogen atoms in bisphenol AF but also noncovalent Si-F interactions between the silica gel in the composites and hexafluorosilicate, and such effective interactions should enable encapsulated bisphenol AF to exhibit a perfectly nonflammable characteristic at 800 °C.<sup>23)</sup> In addition, it is well known that traditional organic salts such as pyridinium, aminopyridinium and acridinium salts can interact with hexafluorosilicate anion to have two- and three-dimensional framework topologies through the strong H-F hydrogen bonds.<sup>24 ~ 31)</sup> Therefore, the present aromatic compounds such as bisphenol AF can exhibit a nonflammable characteristic in calcium fluoride nanocomposite matrices through an effective hydrogen bonding interaction between acidic hydroxyl protons in aromatic compounds (Ar-OH) and fluorine in calcium fluoride. Especially, nanocomposite reactions with these aromatic compounds (Ar-OH) under alkaline conditions in Scheme 2-1 should afford  $\text{Ar-O}^{\delta-}\text{-H}^{\delta+}$  species to interact with calcium fluoride, due to the presence of acidic hydroxyl groups in Ar-OH. Such  $\text{Ar-O}^{\delta-}\text{-H}^{\delta+}$  species would interact with

calcium fluoride through not only the hydrogen bonding interaction between fluorine in calcium fluoride and acidic hydroxyl protons in Ar-OH but also the electrostatic interaction between the electronegative oxygens in Ar-OH and electropositive calcium atoms in calcium fluoride to afford the expected calcium fluoride/Ar-OH nanocomposites possessing a nonflammable characteristic as in Scheme 2-3. Thus, aromatic compounds possessing neither acidic hydroxyl groups nor hydroxyl groups, respectively, can exhibit a usual flammable characteristic in calcium fluoride nanocomposites.



Scheme 2-3 Schematic illustration for the formation of CaF<sub>2</sub>/Ar-OH nanocomposites

In fact, theoretical study with the Gaussian09, Revision A. 02<sup>32)</sup> for the optimization of stable calcium fluoride/bisphenol AF composite structure obtained through the interaction of bisphenol AF with tetramolecular calcium fluorides shows that intermolecular hydrogen

bonidng interactions between fluorine in calcium fluoride and acidic hydroxyl protons in bisphenol AF are essential for the architecture of stable nanocomposites as shown in Fig. 2-13. In addition, Fig. 2-14 shows that electrostatic interaction between oxygen atoms in bisphenol AF and calcium atoms in calcium fluorides is also essential for the architecture of stable tetramolecular calcium fluorides/bisphenol AF composites under similar conditions.

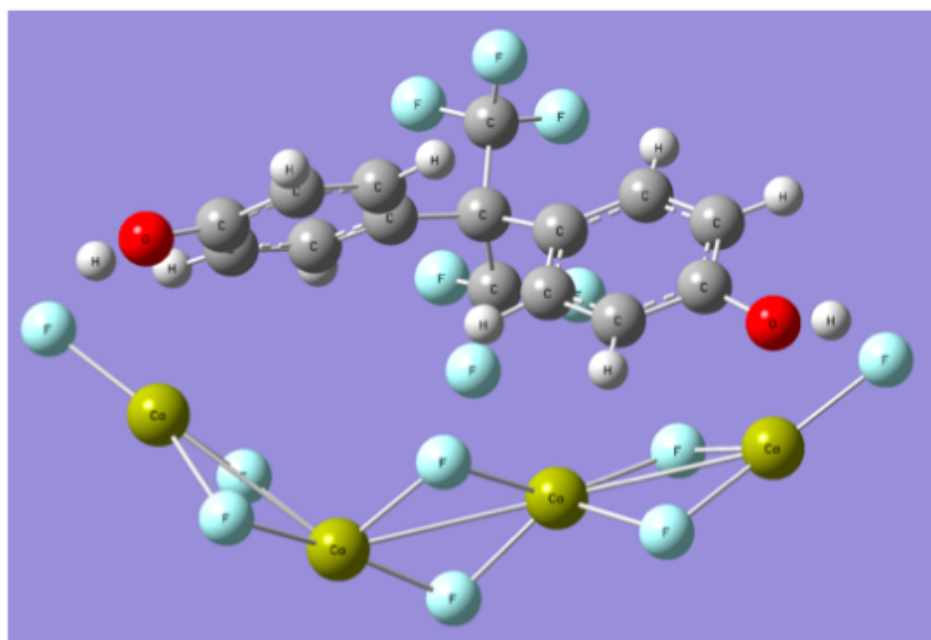


Fig. 2-13 Optimization of stable calcium fluoride/bisphenol AF composite structure obtained through the interaction of bisphenol AF with tetramolecular calcium fluorides (fluorine-hydrogen interaction) by using Gaussian09, Revision A.02

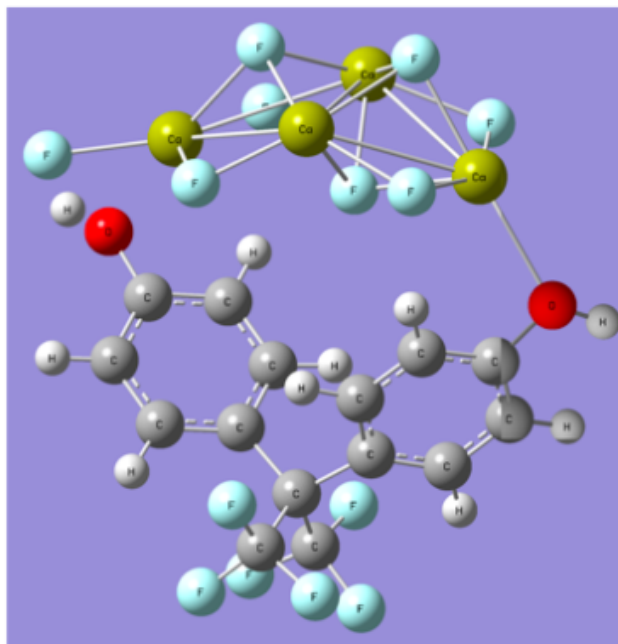


Fig. 2-14 Optimization of stable calcium fluoride/bisphenol AF composite structure obtained through the interaction of bisphenol AF with tetramolecular calcium fluorides (oxygen-calcium interaction) by using Gaussian09, Revision A.02

In this way, it was verified that low molecular weight aromatic compounds possessing acidic hydroxyl groups can exhibit a nonflammable characteristic in the calcium fluoride nanocomposite matrices even after calcination. Especially, the present preparative method of these fluorinated nanocomposites is very simple and easy. Thus, this technology has high potential for the development of nonflammable materials into a wide variety of fields.



## 2.4. Conclusion

Calcium chloride reacted with potassium fluoride in the presence of low molecular weight aromatic compounds (*ArH*) such as bisphenol AF, bisphenol A, bisphenol F, biphenyl, and 1-(2-naphthyl)ethanol under alkaline conditions to afford new calcium fluoride/*ArH* composites. DLS and FE-SEM measurements show that these calcium fluoride/*ArH* composites are nanometer size-controlled fine particles and have a good dispersibility and stability in water, tetrahydrofuran, 1, 2-dichloroethane, methanol, dimethyl sulfoxide, *N,N*-dimethylformamide, and 2-propanol. Interestingly, aromatic compounds possessing acidic hydroxyl groups in the calcium fluoride nanocomposites were found to exhibit a nonflammable characteristic even after calcination at 800 °C, although the corresponding aromatic compounds possessing neither acidic hydroxyl groups nor hydroxyl groups in the nanocomposites exhibited a usual flammable characteristic under similar conditions. In contrast, calcium fluoride/*ArH* nanocomposites, which were prepared under no catalytic conditions, afforded a clear weight loss corresponding to the contents of *ArH* in the composites to exhibit a usual flammable characteristic.

## References

- 1) P. Gomez-Romero and C. Sanchez (Eds), *Functional Hybrid Materials*, Wiley, Weinheim (2004).
- 2) C. J. Brinker and G. W. Schere, *Sol-Gel Science*, Academic Press, Boston (1990).
- 3) M. Pedroso, M. Dias, C. Azuma, G. R. San, and C. Mothe, *Colloid Polym. Sci.*, **281**, 19 (2003).
- 4) Y.-L. Liu and S.-H. Li, *Macromol. Rapid Commun.*, **25**, 1392 (2004).
- 5) M. K. Harmer, W. E. Farneth, and Q. Sun, *J. Am. Chem. Soc.*, **118**, 7708 (1996).
- 6) J.-W. Cho and K.-I. Sul, *Fibers Polym.*, **2**, 135 (2001).
- 7) S. Yano, N. Okubo, and K. Takahashi, *Macromol. Symp.*, **108**, 270 (1996).
- 8) P. Fabbri, M. Messori, M. Montecchi, S. Nannarone, L. Pasquali, F. Pilati, C. Tonelli, and M. Toselli, *Polymer*, **47**, 1055 (2006).
- 9) Y.-C. Chen, C.-C. Tsai, and Y.-D. Lee, *J. Polym. Sci., Part A: Polym. Chem.*, **42**, 1789 (2004).
- 10) J. Shin, D. W. Cho, W. Bae, and H. Kim, *Colloid Polym. Sci.*, **288**, 63 (2010).
- 11) H. Sawada, *Polym. Chem.*, **3**, 46 (2012).
- 12) H. Sawada, T. Narumi, S. Kodama, M. Kamijo, R. Ebara, M. Sugiya, and Y. Iwasaki,

- Colloid Polym. Sci.*, **285**, 977 (2007).
- 13) H. Sawada, H. Kakehi, T. Tashima, Y. Nishiyama, M. Miura, and N. Isu, *J. Appl. Polym. Sci.*, **112**, 3482 (2009).
- 14) H. Sawada, X. Liu, Y. Goto, M. Kikuchi, T. Tashima, and M. Nishida, *J. Colloid Interface Sci.*, **356**, 8 (2011).
- 15) H. Sawada, T. Tashima, H. Kakehi, Y. Nishiyama, M. Kikuchi, M. Miura, Y. Sato, and N. Isu, *Polym. J.*, **42**, 167 (2010).
- 16) H. Sawada, T. Tashima, Y. Nishiyama, M. Kikuchi, Y. Goto, G. Kostov, and B. Ameduri, *Macromolecules*, **44**, 1114 (2011).
- 17) H. Sawada, Y. Matsuki, Y. Goto, S. Kodama, M. Sugiya, and Y. Nishiyama, *Bull. Chem. Soc. Jpn.*, **83**, 75 (2010).
- 18) L. Pauling, *The Chemical Bond*, Cornell University Press, New York (1967).
- 19) R. Walsh, *Acc. Chem. Res.*, **14**, 246 (1981).
- 20) G.-D. Blue, J. W. Green, R. G. Bautista, and J. L. Margrave, *J. Phys. Chem.*, **67**, 877 (1963).
- 21) <http://www.crystran.co.uk/calcium-fluoride-caf2.htm>
- 22) W. J. Tropf, *Opt. Eng.*, **34**, 1369 (1995).
- 23) H. Sawada, M. Kikuchi, and M. Nishida, *J. Polym. Sci., Part A: Polym. Chem.*, **49**, 1070

(2011).

- 24) V. O. Gelmboldt, E. V. Ganin, M. S. Fonari, L. V. Koroeva, Y. E. Ivanov, and M. M. Botoshansky, *J. Fluorine Chem.*, **130**, 428 (2009).
- 25) G. J. Reiß, *Acta Cryst.*, **C54**, 1489 (1998).
- 26) A. F. Jalboutm Z. Y. Jiang, A. Ouasri, H. Jeghnou, A. Rhandour, M. C. Dhamelincourt, P. Dhamelincourt, and A. Mazzah, *Vib. Spectroc.*, **33**, 21 (2003).
- 27) B. D. Conley, B. C. Yearwood, S. Parkin, and D. A. Atwood, *J. Fluorine Chem.*, **115**, 155 (2002).
- 28) V. O. Gelmboldt, E. V. Ganin, and K. V. Domasevitch, *Acta Cryst.*, **C63**, o530 (2007).
- 29) A. F. Jalboutm, A. Ouasri, H. Jeghnou, and A. Rhandour, *Vib. Spectrosc.*, **44**, 94 (2007).
- 30) C. A. Mattia, O. Ortona, R. Puliti, G. Cascarano, and C. Giacovazzo, *J. Mol. Struct.*, **350**, 63 (1995).
- 31) R. Thaimattarn, M Szafran, Z. Dega-Szafran, and M. Jaskolski, *Acta Cryst.*, **B64**, 483 (2008).
- 32) All calculations were performed using the Gaussian09, Revision A.02. The structures were fully optimized using the B3LYP functional with the 6-31G(d) basis set. All structures were characterized by frequency calculation, and energies were corrected by the zero point energy. See: M. J. Frisch, G. W. Trucks, H. B. Schlegel, G. E. Scuseria, K. N.

Kudin, J. R. Cheeseman, J. A. Montgomery Jr, T. Vreven, K. N. Kudin, J. C. Burant et al.,

Gaussian03, Revision C.02; Gaussian, Inc., C. T. Wallingford (2004).

## CHAPTER 3

### **Reaction of Fluorinated Aliphatic Alcohols with Calcium Chloride: Formation of the Fluorinated Alcohol/Calcium Fluoride Nanocomposites – Thermal Stability and Application to the Surface Modification of These Nanocomposites**

### 3.1. Introduction

Fluorinated polymers are well-known to possess a wide variety of unique properties such as surface active property, high thermal stability and chemical resistance in comparison with the traditional hydrocarbon polymers.<sup>1 ~ 7)</sup> In these fluorinated polymers, partially fluoroalkylated polymers such as fluoroalkyl end-capped oligomers [ $R_F-(M)_n-R_F$ ;  $R_F$  = fluoroalkyl groups;  $M$  = radical polymerizable monomers] are attractive functional materials, because they exhibit various unique properties such as surface active properties and nanometer size-controlled molecular aggregates which cannot be achieved by the corresponding non-fluorinated and randomly or block-type fluoroalkylated ones.<sup>8 ~ 14)</sup> Especially, fluoroalkyl end-capped oligomeric aggregates can interact with numerous guest molecules such as fullerene, carbon nanotube, organic dyes, and metal nanoparticles to afford the corresponding fluorinated oligomers/guest molecules nanocomposites.<sup>14 ~ 20)</sup> In fact, fluoroalkyl end-capped oligomers/calcium carbonate nanocomposites can be easily prepared by the reaction of calcium chloride with sodium carbonate in the presence of the corresponding oligomers under alkaline conditions.<sup>21, 22)</sup> Fluorinated oligomers in the calcium carbonate nanocomposite matrices can provide a non-flammable characteristic even after calcination at 800 °C.<sup>22)</sup> This interesting characteristic is due to the effect interaction between fluorine atoms in the

oligomers and calcium atoms in the calcium carbonate ( $\text{F}^{\cdots}\text{Ca}$ ), which would be derived from the bond-strengthening effect in Ca-F bond (132 kcal or 552 kJ/mol).<sup>23)</sup> In addition, low molecular weight aromatic compounds possessing the acidic hydroxyl protons such as bisphenol AF can exhibit a non-flammable characteristic even after calcination at 800 °C in the calcium fluoride nanocomposite matrices through not only the hydrogen-bonding interaction between fluorines in calcium fluoride and acidic hydroxyl protons in aromatic compounds but also the electrostatic interaction between the electronegative oxygen in the aromatic compound and the electropositive calcium atoms in calcium fluoride.<sup>24)</sup> Therefore, it is deeply desirable to develop the novel non-flammable fluorinated functional materials imparted by  $\text{F}^{\cdots}\text{Ca}$  interactions. This chapter shows that the specified fluorinated aliphatic alcohol possessing the internal higher acidic methylene units neighboring fluorines in the main chain can react with calcium chloride under alkaline conditions to afford the corresponding fluorinated alcohol/calcium fluoride nanocomposites. The nanocomposites thus obtained can provide no weight loss characteristic in the calcium fluoride nanocomposite matrices even after calcination at 800 °C. Furthermore, the nanocomposites after calcination at 800 °C are applicable to the surface modification of poly(methyl methacrylate) (PMMA) to exhibit good oleophobicity and lower refractive indices imparted by the longer fluoroalkyl unit in the composites on the modified PMMA film surfaces, as well as that before calcination. These



results will be described in this chapter.

## **3.2. Experimental**

### **3.2.1 Measurements**

Dynamic light scattering (DLS) measurements were measured by using Otsuka Electronics DLS-7000 HL (Tokyo, Japan). Fourier-transform infrared (FT-IR) spectra were measured by using Shimadzu FTIR-8400 FT-IR spectrophotometer (Kyoto, Japan). Field emission scanning electron micrographs (FE-SEM) were recorded on JEOL JSM-7000F (Tokyo, Japan). X-ray diffraction (XRD) measurements were performed by the use of Rigaku Miniflex 600 (Tokyo, Japan). Thermal analyses were recorded on Bruker axs TG-DTA2000SA differential thermobalance (Kanagawa, Japan). Ultraviolet-visible (UV-vis) spectra were measured by the use of Shimadzu UV-1800 UV-vis spectrophotometer (Kyoto, Japan). The contact angles were measured by the use of Kyowa Interface Science Drop Master 300 (Saitama, Japan).  $^1\text{H}$  NMR spectra were measured by using JEOL JNM-400 (400 MHz) FT NMR SYSTEM (Tokyo, Japan). Refractive indices were measured by using Abbe refractometer NAR-1T, Atago Co., Ltd. (Tokyo, Japan).

### 3.2.2. Materials

1*H*, 1*H*, 2*H*, 2*H*-nonafluoro-1-hexanol (FA-4), 1*H*, 1*H*, 2*H*, 2*H*-tridecafluoro-1-*n*-octanol (FA-6), 1*H*, 1*H*, 2*H*, 2*H*-heptadecafluoro-1-decanol (FA-8), 1*H*, 1*H*, 2*H*, 2*H*, 6*H*, 6*H*-nonadecafluoro-1-undecanol (DTFA), 2, 3, 3, 3-tetrafluoro-2-[1, 1, 2, 3, 3, 3-hexafluoro-2-(heptafluoropropoxy) propoxy]-1-propanol (PO-3-OH) and 2, 4, 4, 5, 7, 7, 8, 10, 10, 11, 13, 13, 14, 16, 16, 17, 17, 18, 18, 18-icosafuoro-2, 5, 8, 11, 14-pentakis(trifluoromethyl)-3, 6, 9, 12, 15-pentaoxaoctadecane-1-ol (PO-6-OH) were received from Unimatec Co., Ltd., (Ibaraki, Japan). Calcium chloride was purchased from Wako Pure Chemical Industries (Osaka, Japan).

### 3.2.3. Preparation of 1*H*, 1*H*, 2*H*, 2*H*, 6*H*, 6*H*-nonadecafluoro-1-undecanol (DTFA)/calcium fluoride nanocomposites

To a methanol solution (5.0 ml) of 1*H*, 1*H*, 2*H*, 2*H*, 6*H*, 6*H*-nonadecafluoro-1-undecanol (DTFA) [C<sub>4</sub>F<sub>9</sub>CH<sub>2</sub>C<sub>5</sub>F<sub>10</sub>C<sub>2</sub>H<sub>4</sub>OH; (500 mg)] was added the mixture of 0.5 mol/dm<sup>3</sup> calcium chloride methanol solution (4 ml) and 25 wt% aqueous ammonia solution (3 ml). This mixture was stirred with a magnetic stirring bar at room temperature for 1 day, and then was

centrifuged for 30 min. The obtained crude product was washed with methanol several times. The expected DTFA/calcium fluoride nanocomposite powders thus obtained were dried in vacuo at 50 °C for 1 day to afford the purified composites powders (100 mg). The obtained DTFA/CaF<sub>2</sub> nanocomposites showed the following FT-IR spectra: FT-IR (cm<sup>-1</sup>) 3489 (O-H), 1234, 1084 (C-F), 1138 (C-O), 876 (C-H), 415 (Ca-F).

#### **3.2.4. Preparation of modified poly(methyl methacrylate) films treated with 1*H*, 1*H*, 2*H*, 2*H*, 6*H*, 6*H*-nonadecafluoro-1-undecanol (DTFA)/calcium fluoride nanocomposites before and after calcination at 800 °C**

Modified poly(methyl methacrylate) [PMMA] films were prepared by casting the tetrahydrofuran solutions (25 ml) containing PMMA (990 mg) and the DTFA/calcium fluoride nanocomposites before and after calcination at 800 °C (10 mg) on the glass plates. The solvent was evaporated at room temperature, and the films formed were peeled off and dried at 50 °C for 24 h under vacuum to afford the modified PMMA films.

### 3.3. Results and discussion

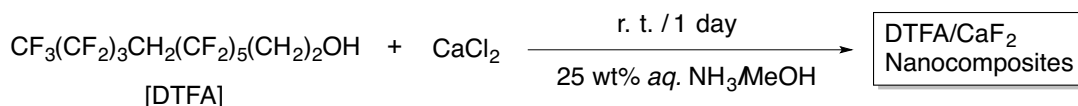
#### 3.3.1. Preparation of 1*H*, 1*H*, 2*H*, 2*H*, 6*H*, 6*H*-nonadecafluoro-1-undecanol (DTFA)/calcium fluoride nanocomposites by using calcium chloride

A variety of fluorinated aliphatic alcohols illustrated in Fig. 3-1 were tried to react with calcium chloride in methanol under alkaline conditions.

Abbreviation	Structure	Abbreviation	Structure
FA-4:	$\text{CF}_3(\text{CF}_2)_3(\text{CH}_2)_2\text{OH}$	PO-3-OH:	$\text{CF}_3\text{CF}_2\text{CF}_2\text{O}-\overset{\text{CF}_3}{\underset{ }{\text{C}}}\text{FCF}_2\text{O}-\overset{\text{CF}_3}{\underset{ }{\text{C}}}\text{FCH}_2\text{OH}$
FA-6:	$\text{CF}_3(\text{CF}_2)_5(\text{CH}_2)_2\text{OH}$		
FA-8:	$\text{CF}_3(\text{CF}_2)_7(\text{CH}_2)_2\text{OH}$	PO-6-OH:	$\text{CF}_3\text{CF}_2\text{CF}_2\text{O}-\overset{\text{CF}_3}{\underset{ }{\text{C}}}\text{FCF}_2\text{O})_4-\overset{\text{CF}_3}{\underset{ }{\text{C}}}\text{FCH}_2\text{OH}$
DTFA:	$\text{CF}_3(\text{CF}_2)_3\text{CH}_2(\text{CF}_2)_5(\text{CH}_2)_2\text{OH}$		

Fig. 3-1 Molecular structures and abbreviations of fluorinated aliphatic alcohols used

However, these fluorinated aliphatic alcohols except for the DTFA were unable to react with calcium chloride. Only the DTFA was found to react with calcium chloride to afford the DTFA/calcium fluoride composites under similar conditions. These results are shown in Scheme 3-1 and Table 3-1.



Scheme 3-1

Table 3-1 Preparation of the DTFA/CaF<sub>2</sub> nanocomposites

Run	DTFA	NH <sub>3</sub>	CaCl <sub>2</sub>	Yield <sup>a)</sup> (%)	Size of nanocomposites <sup>b)</sup>	
	(mg)	(ml)	(mmol)		before calcination (nm)	after calcination (nm)
1	500	0	2.0	0	-	-
2	500	1.0	2.0	10	28.9 ± 3.4	38.3 ± 7.2
3	500	3.0	2.0	20	22.5 ± 2.7	26.6 ± 3.8
4	116	1.0	2.0	12	28.2 ± 3.6	25.3 ± 5.4
5	500	5.0	2.0	18	37.7 ± 8.5	34.1 ± 6.0

a) Yield was based on the used DTFA

b) Determined by dynamic light scattering (DLS) measurements in methanol

As shown in Scheme 3-1 and Table 3-1, the expected DTFA/calcium fluoride composites were obtained in 10 ~ 20 % isolated yields under alkaline conditions; although the corresponding composites were not isolated at all in the absence of ammonia. The obtained composites were found to exhibit a good dispersibility and stability not only in water but also in traditional organic solvents such as methanol, 2-propanol, tetrahydrofuran (THF), 1, 2-dichloroethane (DE), dimethyl sulfoxide (DMSO) and *N, N*-dimethylformamide (DMF). Thus, the average particle sizes of these composites in methanol have been measured by using the dynamic light scattering measurements (DLS), and the results are also shown in Table 3-1.

The size of each composite before and after calcination at 800 °C is nanometer size-controlled fine particles from 23 to 38 nm levels.

The XRD spectra of these nanocomposite powders have been measured to verify the crystalline structure of the composites. The XRD spectra of the original calcium fluoride and calcium chloride were also measured, for comparison. The results are shown in Fig. 3-2.

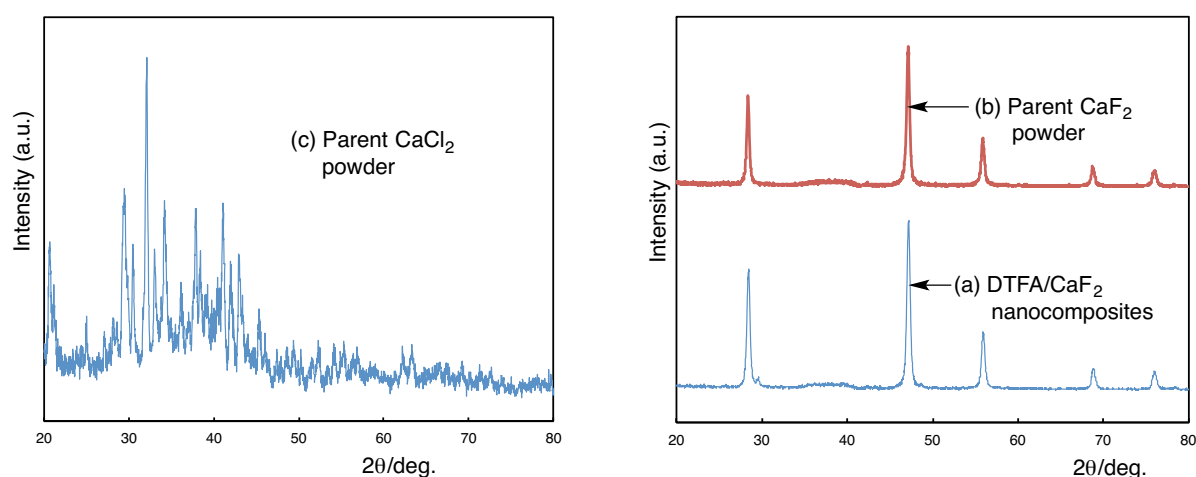


Fig. 3-2 X-ray diffraction (XRD) of the DTFA/ $\text{CaF}_2$  nanocomposites [(a): Run 4 in Table 3-1], parent  $\text{CaF}_2$  powder (b), and parent  $\text{CaCl}_2$  powder (c)

As shown in Fig. 3-2, XRD spectra of the nanocomposites show the characteristic peaks related to calcium fluoride, of whose peaks are quite similar to those of the parent calcium fluoride, indicating that calcium chloride should react with the DTFA to afford the DTFA/ $\text{CaF}_2$  nanocomposites.

The turbidity of the well-dispersed DTFA/ $\text{CaF}_2$  nanocomposites and the parent  $\text{CaF}_2$

particles is extremely sensitive to the refractive indices of a variety of solvents (see Fig. 3-3).

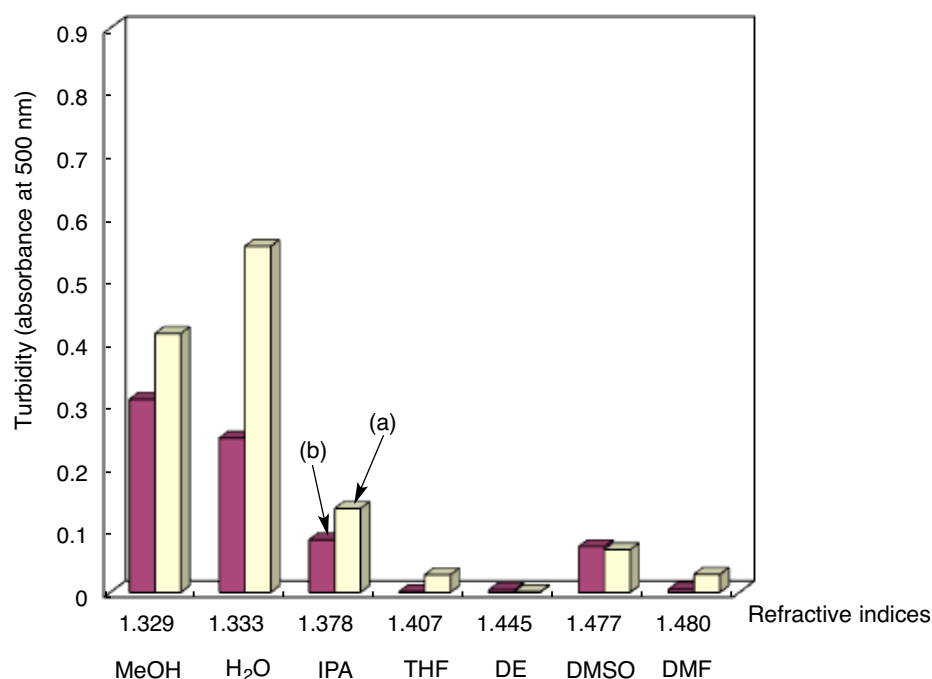


Fig. 3-3 Relationship between the turbidity (absorbance at 500 nm) of DTFA/CaF<sub>2</sub> nanocomposites [(a): Run 4 in Table 3-1] (or the parent CaF<sub>2</sub> particles (b)) and the refractive indices of a variety of solvents

Especially, the effective decrease of the turbidity for the DTFA/CaF<sub>2</sub> nanocomposites was observed in THF and 1, 2-dichloroethane (DE) to afford the transparent colorless solutions. The lowest turbidity was observed in THF, suggesting that the refractive index of the DTFA/CaF<sub>2</sub> nanocomposites is around 1.407. In contrast, it was demonstrated that the turbidity of the parent CaF<sub>2</sub> particles in THF becomes higher than that of the DTFA/CaF<sub>2</sub> nanocomposites. This finding is due to the presence of the DTFA units in the nanocomposites, and the DTFA should be effectively incorporated into the calcium fluoride nanocomposite



matrices.

In this way, it is suggested that the formation of calcium fluoride is due to the dehydrofluorination between the higher acidic protons and fluorines in the DTFA under alkaline conditions to interact with calcium chloride. In order to clarify the formation of calcium fluoride through the nanocomposite reactions illustrated in Scheme 3-1, the potential energy change for the formation of the deprotonated DTFA anions have been studied by using molecular orbital calculation with the Gaussian 03.<sup>25)</sup> For neutral DTFA and its deprotonated anions, the equilibrium geometry was optimized with the RHF/6-31G(d) method, while potential energy at the optimized geometry was recalculated with the density functional theory at the B3LYP/6-311+G(d, p) level. The potential energy change for the formation of the deprotonated FA-6 anions was also studied by using the same computational procedure, for comparison. These results are demonstrated in Figs. 3-4 and 3-5.

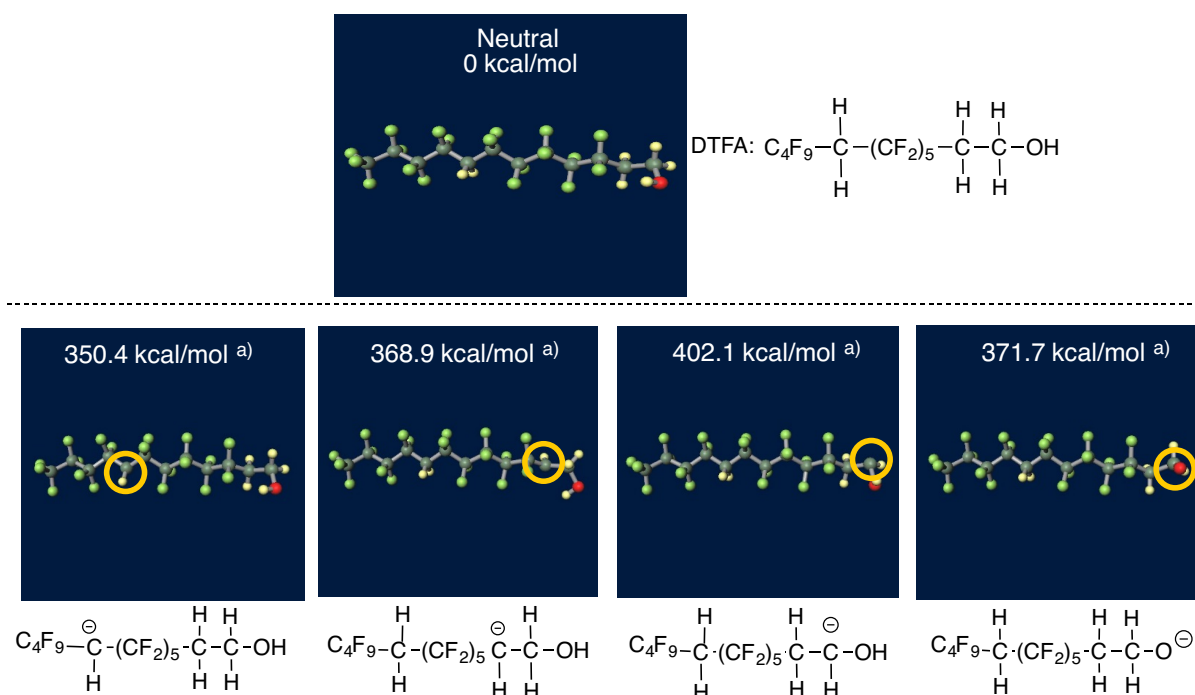


Fig. 3-4 Potential energy change for the formation of the deprotonated DTFA anions,<sup>a)</sup> calculated at the B3LYP/6-311+G(d,p)//RHF/6-31G(d) level: a) Compared with the energy of neutral DTFA

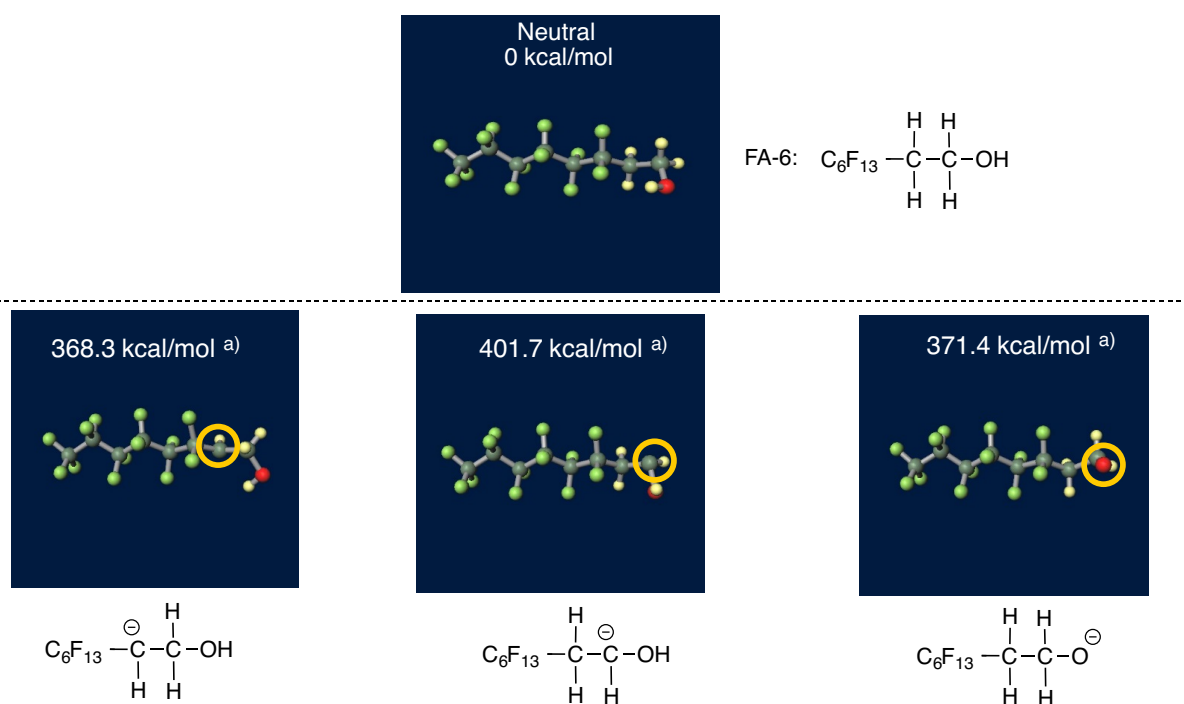


Fig. 3-5 Potential energy change for the formation of the deprotonated FA-6 anions,<sup>a)</sup> calculated at the B3LYP/6-311+G(d,p)//RHF/6-31G(d) level: a) Compared with the energy of neutral FA-6

The potential energy change for the formation of each deprotonated DTFA anion in Fig. 3-4 shows that the methylene protons introduced between the  $C_4F_9$ - and the  $-(CF_2)_5$ - units in the DTFA [ $C_4F_9$ - $CH_2$ -( $CF_2$ ) $_5$ - $CH_2CH_2OH$ ] should possess a higher acidity compared with that of the other protons in the DTFA. The potential energy change for the formation of the deprotonated FA-6 anions also shows the higher acidity of the internal methylene protons neighboring fluorines in the DTFA. Therefore, it is suggested that the dehydrofluorination should proceed between the internal methylene protons and the neighboring fluorines in the DTFA.

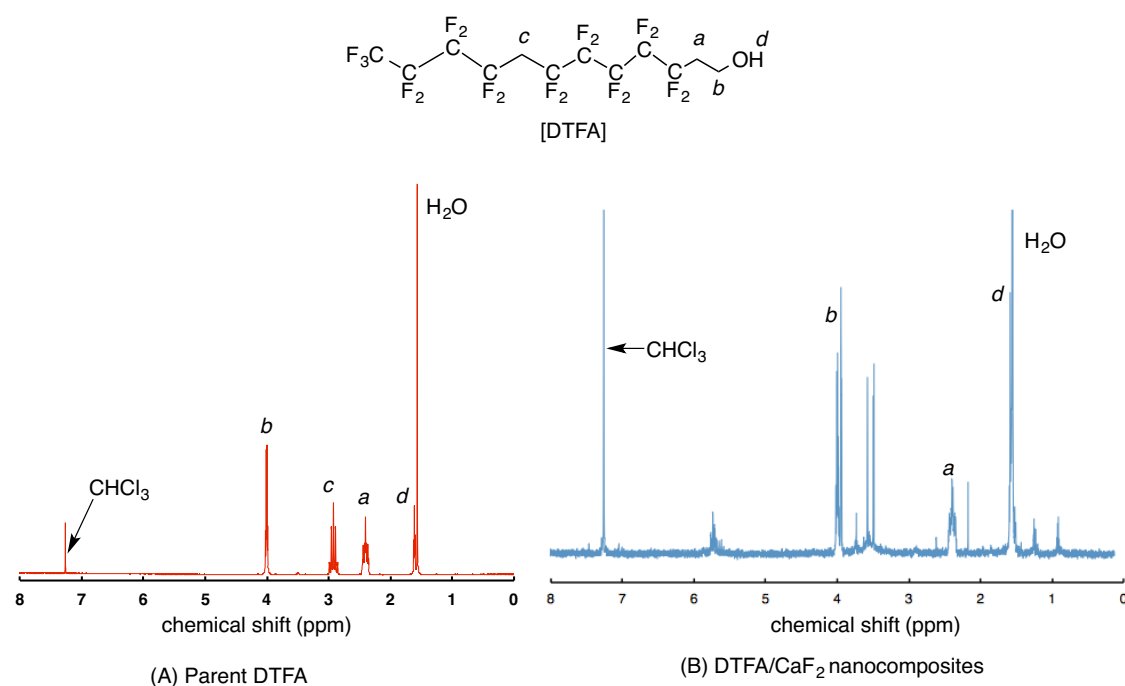


Fig. 3-6  $^1H$  NMR spectra of the parent DTFA (A) and the DTFA/ $CaF_2$  nanocomposites [(B): Run 4 in Table 3-1] in  $CDCl_3$

In fact,  $^1\text{H}$  NMR spectra of well-dispersed chloroform- $d_1$  solution containing the DTFA/ $\text{CaF}_2$  nanocomposites [Fig. 3-6-(B)] show that the peak around at 2.9 ppm related to the methylene protons in the parent DTFA [Fig. 3-6-(A)] has been completely disappeared through the nanocomposite reaction with calcium chloride. The DTFA/ $\text{CaF}_2$  nanocomposites also afforded the characteristic peaks around 5.8 ppm related to the formation of the olefinic protons as shown in Fig. 3-6-(B). These results suggest that the dehydrofluorination between the internal methylene protons and the neighboring fluorines in the DTFA should proceed under alkaline conditions in the presence of calcium chloride to produce the olefinic moieties in the nanocomposites. It was previously reported that the similar dehydrofluorinations between the methylene units and the neighboring fluorines in poly(vinylidene fluoride) can proceed under alkaline conditions to provide the olefinic units.<sup>26 ~ 29)</sup>

### **3.3.2. Thermal stability of 1*H*, 1*H*, 2*H*, 2*H*, 6*H*, 6*H*-nonadecafluoro-1-undecanol (DTFA)/calcium fluoride nanocomposites**

Thermal stability of the DTFA/ $\text{CaF}_2$  nanocomposites in Table 3-1 have been studied by the use of thermogravimetric analyses (TGA) measurements, in which the weight loss of the nanocomposites was measured by raising the temperature around 800 °C at a 10 °C/min

heating rate under air atmospheric conditions. The results are shown in Fig. 3-7.

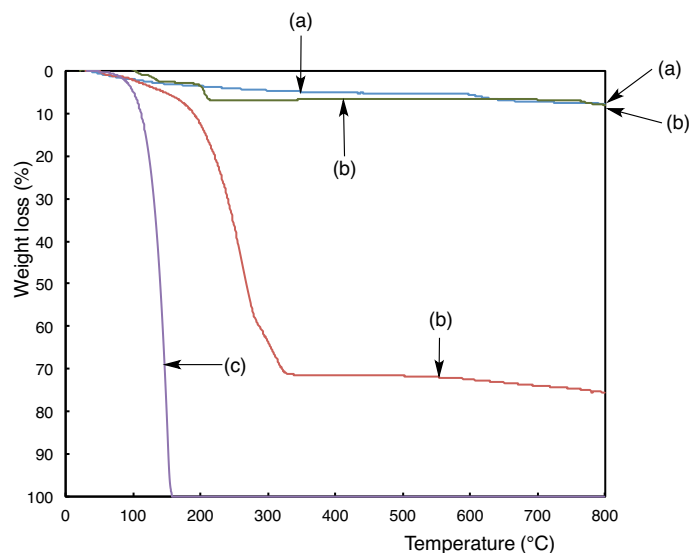


Fig. 3-7 Thermogravimetric analyses of DTFA/CaF<sub>2</sub> nanocomposites [(a): Run 3 in Table 3-1], the composites isolated from the supernatant solution in the preparation of the nanocomposites [(b): Run 3 in Table 3-1], the parent DTFA (c) and the parent CaCl<sub>2</sub> powder (d)

As shown in Fig. 3-7, the composites isolated from the supernatant solution in the preparation of the DTFA/CaF<sub>2</sub> nanocomposites [Fig. 3-7-(b)] exhibited a clear weight loss corresponding to the content of the unreacted DTFA in the composites after calcination at 800 °C, and the content of the unreacted DTFA was estimated to be 463 mg by using this weight loss curve at 800 °C. Thus, 37 mg [500 mg (DTFA used for the composite reaction) – 463 mg (unreacted DTFA)] of DTFA should be incorporated into the calcium fluoride nanocomposite matrices to provide the expected DTFA/CaF<sub>2</sub> nanocomposites in 20 % (100 mg) isolated yield (see Run 3 in Table 3-1). From this finding, it is suggested that the DTFA/CaF<sub>2</sub> nanocomposites would provide the 37 % (37/100 x 100) weight loss after

calcination. However, interestingly, the DTFA/CaF<sub>2</sub> nanocomposites were found to exhibit no weight loss behavior even after calcination at 800 °C [see Fig. 7-(a)], of whose TGA curve is quite similar to that of the original calcium chloride [see Fig. 7-(d)]. No weight loss behavior after calcination at 800 °C was similarly observed in each nanocomposite illustrated in Runs 2, 4 and 5 in Table 3-1. This finding suggests that the incorporated DTFA into the nanocomposite matrices can provide the no weight loss characteristic even after calcination at 800 °C.

It has been already reported that the aromatic compounds possessing the acidic hydroxyl protons such as bisphenol AF can exhibit a non-flammable characteristic even after calcination at 800 °C in the calcium fluoride nanocomposite matrices through not only the hydrogen-bonding interaction between fluorines in calcium fluoride and acidic hydroxyl protons in the aromatic compounds but also the electrostatic interaction between the electronegative oxygens in the hydroxyl groups and electropositive calcium atoms in calcium fluoride.<sup>24)</sup> Therefore, the present DTFA/CaF<sub>2</sub> nanocomposites should exhibit a non-flammable characteristic even after calcination at 800 °C in calcium fluoride nanocomposite matrices through not only the hydrogen-bonding interaction between fluorine in calcium fluoride and hydroxyl protons in the DTFA but also the electrostatic interaction between the electronegative oxygen or fluorine atoms in the DTFA and electropositive calcium atoms in calcium fluoride.

FE-SEM measurements for the DTFA/CaF<sub>2</sub> nanocomposites (Run 3 in Table 3-1) were studied before and after calcination at 800 °C, and the results are shown in Fig. 3-8.

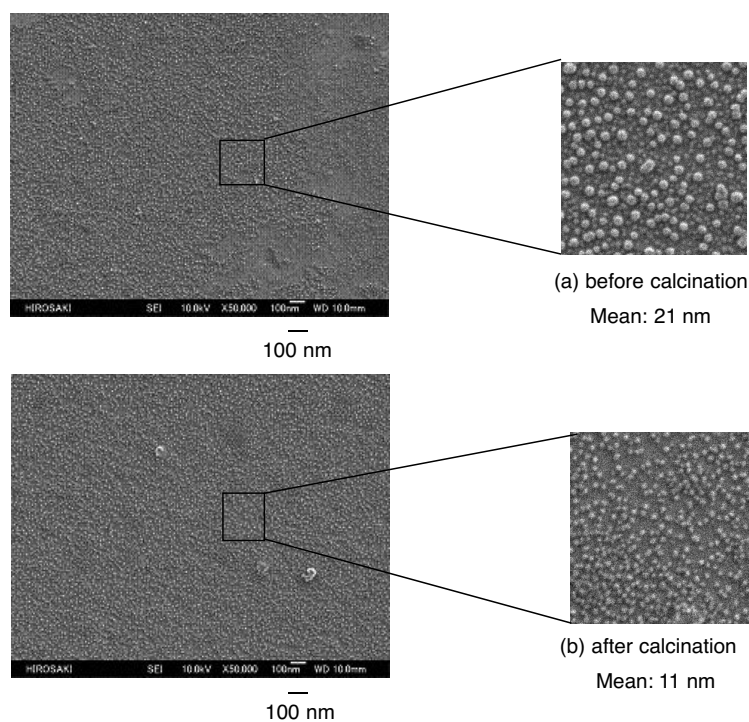


Fig. 3-8 FE-SEM images of well-dispersed methanol solutions of DTFA/CaF<sub>2</sub> nanocomposites (Run 3 in Table 3-1) before (a) and after (b) calcination at 800 °C

Electron micrographs of the nanocomposites before and after calcination at 800 °C show the formation of the composite fine nanoparticles with mean diameters of 21 nm and 11 nm, respectively. The similar particle sizes for the composites before and after calcination were obtained in DLS (see Run 3 in Table 3-1) and FE-SEM measurements, respectively.

### 3.3.3. Surface modification of poly(methyl methacrylate) by using 1*H*, 1*H*, 2*H*, 2*H*, 6*H*, 6*H*-nonadecafluoro-1-undecanol (DTFA)/calcium fluoride nanocomposites before and after calcination at 800 °C

It is of particular interest to apply the present DTFA/CaF<sub>2</sub> nanocomposite fine particles possessing no weight loss characteristic into the surface modification of the traditional organic polymers such as PMMA [poly(methyl methacrylate)] in order to confirm the presence of the DTFA possessing longer fluoroalkyl unit in the nanocomposites before and even after calcination at 800 °C. The modified PMMA films (content of the composites based on PMMA: 1 wt%) treated with the DTFA/CaF<sub>2</sub> nanocomposite (Run 3 in Table 3-1) have been prepared before and after calcination (see Fig. 3-9).

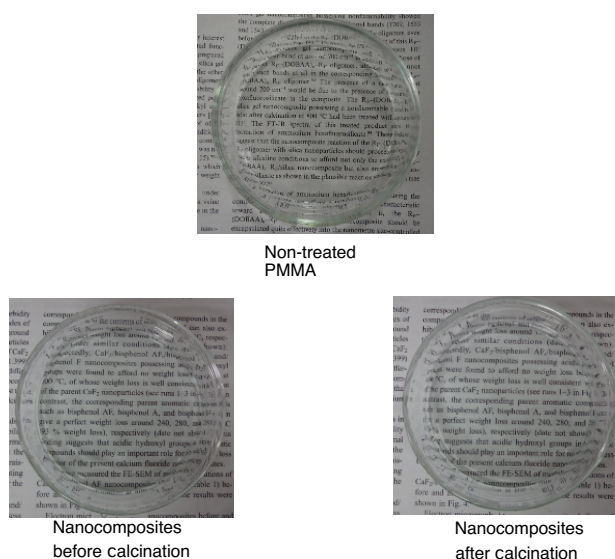


Fig. 3-9 Photograph of the modified PMMA films treated with the DTFA/CaF<sub>2</sub> nanocomposites\* before and after calcination at 800 °C (Run 3 in Table 3-1) and the non-treated original PMMA film  
\*) The contents of the composites before and after calcination are 1 wt % based on PMMA, respectively



The transparency and the wetting behavior for oil toward the modified PMMA films were studied by the use of transmittance at 500 nm of UV-vis spectra and the dodecane contact angle measurements, respectively. The results are shown in Fig. 3-10 and Table 3-2.

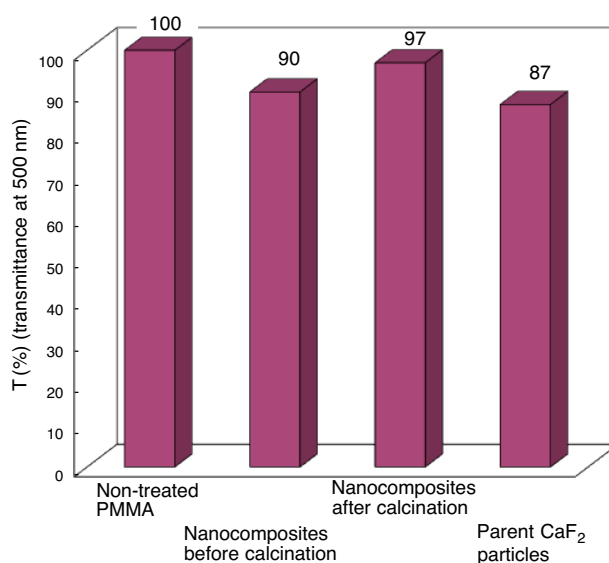


Fig. 3-10 Transmittance of the modified PMMA films treated with the DTFA/CaF<sub>2</sub> nanocomposites\* before and after calcination at 800 °C (Run 3 in Table 3-1) and parent CaF<sub>2</sub> particles\*

\*) The contents of the composites and CaF<sub>2</sub> particles are 1 wt% based on PMMA, respectively

Table 3-2 Contact angles of dodecane on the modified PMMA films treated with the DTFA/CaF<sub>2</sub> nanocomposites (Run 3 in Table 3-1) before and after calcination at 800 °C<sup>a</sup>) and the parent CaF<sub>2</sub> particles<sup>a</sup>)

	Contact angle (degree)		
	Dodecane		Film thickness (μm)
	Surface side	Reverse side	
DTFA/CaF <sub>2</sub> nanocomposites before calcination	46	0	207
DTFA/CaF <sub>2</sub> nanocomposites after calcination	39	0	205
Treated with Parent CaF <sub>2</sub>	0	0	200
Non-treated PMMA	0	0	201
PTFE [poly(tetrafluoroethylene)] plat	22	-	-

a) Concentration of the DTFA/CaF<sub>2</sub> nanocomposites before and after calcination at 800 °C and the parent CaF<sub>2</sub> particles based on the used PMMA are 1 wt %, respectively

Fig. 3-10 shows that the transparency (90 % and 97 %) of the modified PMMA films treated with the DTFA/CaF<sub>2</sub> nanocomposites before and after calcination is similar to that of the non-treated PMMA film, although the parent CaF<sub>2</sub> particles exhibit the relatively lower transparency toward the modified film. This finding would be due to the formation of very fine nanoparticles of the DTFA/CaF<sub>2</sub> nanocomposites before and even after calcination (see Fig. 3-8).

Dodecane contact angle values on the modified PMMA film surfaces treated with the DTFA/CaF<sub>2</sub> nanocomposites before and after calcination at 800 °C are 46° and 39°, respectively; although the parent PMMA film and the modified PMMA film treated with the CaF<sub>2</sub> particles are 0° (surface and reverse side) (see Table 3-2). A higher dodecane contact

angle value:  $39^\circ$  is due to the presence of the DTFA units in the composite matrices even after calcination. Especially, such higher dodecane contact angle values ( $39 \sim 46^\circ$ ) reveal the effective surface arrangement of the fluoroalkyl units in the nanocomposites before and even after calcination above the modified PMMA film surface to provide a higher oleophobic characteristic, compared with that (dodecane contact angle value:  $22^\circ$ ) of the traditional PTFE [poly(tetrafluoroethylene)] plate.

In order to clarify the surface arrangement behavior of the fluoroalkyl units in the DTFA/CaF<sub>2</sub> nanocomposites before and after calcination, the refractive indices of modified PMMA film treated with the DTFA/CaF<sub>2</sub> nanocomposites have been measured before and after calcination at  $800^\circ\text{C}$ . The refractive indices of the modified PMMA film treated with the parent CaF<sub>2</sub> particles have been also measured under similar conditions, for comparison. These results are shown in Fig. 3-11.

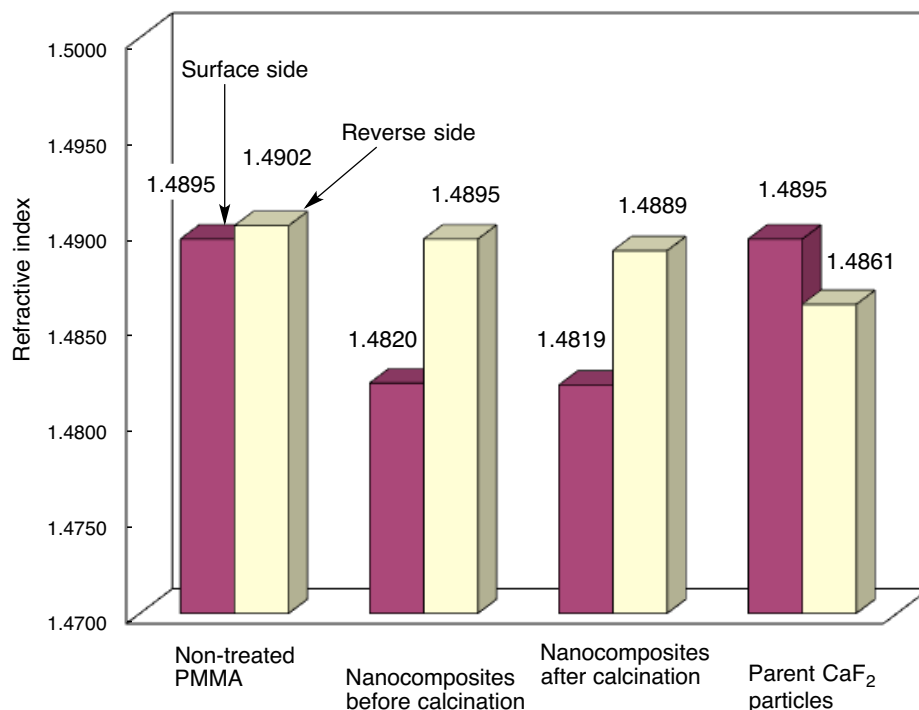


Fig. 3-11 Refractive indices of modified PMMA film surface and reverse sides treated with the DTFA/CaF<sub>2</sub> nanocomposites (Run 3 in Table 3-1) before and after calcination at 800 °C and with the parent CaF<sub>2</sub> particles

Refractive indices of the modified PMMA film treated with the DTFA/CaF<sub>2</sub> nanocomposites were found to reduce effectively on the surface side. A similar result was obtained in the DTFA/CaF<sub>2</sub> nanocomposites after calcination. On the other hand, the significant difference of the refractive indices cannot be observed between the surface and reverse sides of the original PMMA film and the modified PMMA film treated with the parent CaF<sub>2</sub> particles. Therefore, it was verified that the present DTFA/CaF<sub>2</sub> nanocomposites before and even after calcination can provide the higher surface arrangement ability of the fluoroalkyl units in the composites toward the traditional organic polymers such as PMMA.

### 3.4. Conclusion

A variety of fluorinated aliphatic alcohols were applied to the nanocomposite reactions with calcium chloride under alkaline conditions. In these fluorinated alcohols, only 1*H*, 1*H*, 2*H*, 2*H*, 6*H*, 6*H*-nonadecafluoro-1-undecanol (DTFA) was found to react with calcium chloride under alkaline conditions to afford the DTFA/CaF<sub>2</sub> nanocomposites. This reactivity is due to the presence of the higher acidic protons (internal methylene units neighboring fluorines in the DTFA) than the other fluorinated aliphatic alcohols, and the dehydrofluorination between the higher acidic protons and fluorines in the DTFA should proceed under alkaline conditions to provide the DTFA/CaF<sub>2</sub> nanocomposites. Interestingly, the DTFA/CaF<sub>2</sub> nanocomposites were found to exhibit no weight loss behavior corresponding to the contents of the DTFA in the nanocomposites even after calcination at 800 °C. The DTFA/CaF<sub>2</sub> nanocomposites before and after calcination at 800 °C were applied to the surface modification of PMMA to exhibit good oleophobicity and lower refractive indices imparted by the longer fluoroalkyl units in the composites on the modified surfaces. Thus, the present DTFA/CaF<sub>2</sub> nanocomposites have high potential for the development of novel thermally stable fluorinated functional materials possessing the surface active characteristic into a wide variety of fields.

## References

- 1) B. Ameduri and B. Boutevin, *J. Fluorine Chem.*, **104**, 53 (2000).
- 2) W. R. Dolbier Jr., *J. Fluorine Chem.*, **126**, 157 (2005).
- 3) T. Imae, *Curr. Opin. Colloid Interface Sci.*, **8**, 307 (2003).
- 4) K. Johns and G. Stead *J. Fluor. Chem.*, **104**, 5 (2000).
- 5) M. M. Renfrew and E. E. Lewis, *Ind. Eng. Chem.*, **38**, 870 (1946).
- 6) K. Matsumoto, M. Kubota, H. Matsuoka, and H. Yamaoka, *Macromolecules*, **32**, 7122 (1999).
- 7) F. Boschet, G. Kostov, B. Ameduri, A. Jackson, and B. Boutevin, *Polym. Chem.*, **3**, 217 (2012).
- 8) H. Sawada, Y.-F. Gong, Y. Minoshima, T. Matsumoto, M. Nakayama, M. Kosugi, and T. Migita, *J. Chem. Soc., Chem. Commun.*, 537, (1992).
- 9) H. Sawada, Y. Minoshima, and H. Nakajima, *J. Fluorine Chem.*, **65**, 169 (1992).
- 10) H. Sawada, *Chem. Rev.*, **96**, 1779 (1996).
- 11) H. Sawada, *J. Fluorine Chem.*, **105**, 219 (2000).
- 12) H. Sawada, *Prog. Polym. Sci.*, **32**, 509 (2007).
- 13) H. Sawada, *Polym. J.*, **39**, 637 (2007).

- 14) H. Sawada, *Polym. Chem.*, **3**, 46 (2012).
- 15) H. Sawada, K. Ikeno, and T. Kawase, *Macromolecules*, **35**, 4306 (2002).
- 16) H. Sawada, T. Narumi, M. Kiyohara, and M. Baba, *J. Fluorine Chem.*, **128**, 1416 (2007).
- 17) H. Sawada, T. Tashima, H. Kakehi, Y. Nishiyama, M. Kikuchi, M. Miura, Y. Sato, and N. Isu, *Polym. J.*, **42**, 167 (2010).
- 18) H. Sawada, S. Izumi, K. Sasazawa, and M. Yoshida, *J. Colloid Interface Sci.*, **377**, 76 (2012).
- 19) M. Mugisawa and H. Sawada, *Langmuir*, **24**, 9215 (2008).
- 20) S. Guo, T. Ogasawara, T. Saito, H. Kakehi, Y. Kato, M. Miura, N. Isu, and H. Sawada, *Colloid Polym. Sci.*, **291**, 2947 (2013).
- 21) H. Sawada, Y. Shikauchi, H. Kakehi, Y. Katoh, and M. Miura, *Colloid Polym. Sci.*, **285**, 499 (2007).
- 22) T. Saito, H. Kakehi, Y. Kato, M. Miura, N. Isu, and H. Sawada, *Polym. Adv. Technol.*, **24**, 532 (2013).
- 23) G.-D. Blue, J. W. Green, R. G. Bautista, and J. L. Margrave, *J. Phys. Chem.*, **67**, 877 (1963).
- 24) T. Saito, M. Nishida, H. Fukaya, H. Kakehi, Y. Kato, M. Miura, N. Isu, and H. Sawada, *Colloid Polym. Sci.*, **291**, 945 (2013).

- 25) Gaussian 03, Revision D. 02, M. J. Frisch, G. W. Trucks, H. B. Schlegel, G. E. Scuseria, M. A. Robb, J. R. Cheeseman, J. A. Montgomery, Jr., T. Vreven, K. N. Kudin, J. C. Burant, J. M. Millam, S. S. Iyengar, J. Tomasi, V. Barone, B. Mennucci, M. Cossi, G. Scalmani, N. Rega, G. A. Petersson, H. Nakatsuji, M. Hada, M. Ehara, K. Toyota, R. Fukuda, J. Hasegawa, M. Ishida, T. Nakajima, Y. Honda, O. Kitao, H. Nakai, M. Klene, X. Li, J. E. Knox, H. P. Hratchian, J. B. Cross, V. Bakken, C. Adamo, J. Jaramillo, R. Gomperts, R. E. Stratmann, O. Yazyev, A. J. Austin, R. Cammi, C. Pomelli, J. W. Ochterski, P. Y. Ayala, K. Morokuma, G. A. Voth, P. Salvador, J. J. Dannenberg, V. G. Zakrzewski, S. Dapprich, A. D. Daniels, M. C. Strain, O. Farkas, D. K. Malick, A. D. Rabuck, K. Raghavachari, J. B. Foresman, J. V. Ortiz, Q. Cui, A. G. Baboul, S. Clifford, J. Cioslowski, B. B. Stefanov, G. Liu, A. Liashenko, P. Piskorz, I. Komaromi, R. L. Martin, D. J. Fox, T. Keith, M. A. Al-Laham, C. Y. Peng, A. Nanayakkara, M. Challacombe, P. M. W. Gil, B. Johnson, W. Chen, M. W. Wong, C. Gonzalez, and J. A. Pople, Gaussian, Inc., Wallingford CT, 2004.
- 26) R. Crowe and J. P. S. Badyal, *J. Chem. Soc., Chem. Commun.*, 958 (1991).
- 27) H. Kise and H. Ogata, *Polym. Chem.*, **21**, 3443 (1983).
- 28) G. J. Ross, J. F. Watts, M. P. Hill, and P. Morrissey, *Polymer*, **41**, 1685 (2000).
- 29) G. J. Ross, J. F. Watts, M. P. Hill, and P. Morrissey, *Polymer*, **42**, 403 (2001).



## CHAPTER 4

**Facile Creation of Superoleophobic and Superhydrophilic Surface by Using Fluoroalkyl End-capped Vinyltrimethoxysilane Oligomer/Calcium Silicide Nanocomposites – Development of These Nanocomposites to Environmental Cyclical Type-Fluorine Recycle Through Formation of Calcium Fluoride**

## 4.1. Introduction

Fluoropolymers have broad technological applications in a numerous fields, due to their exhibiting high thermal and oxidative stability, low dielectric constant, low moisture absorption, low flammability, low surface energy, excellent biocompatibility, and excellent resistance to most chemicals.<sup>1~3)</sup> Recent developments in the field of fluoropolymers serve to illustrate the distinctive role of fluorine in material science.<sup>4, 5)</sup> In fact, perfluorinated polymers such as poly(tetrafluoroethylene) (PTFE) possess an excellent thermal resistance [ $T_{\text{dec}}$  578 °C ( $T_{\text{dec}}$  defined as the temperature at which 10 % of the mass is lost after heating)] due to the bond-strengthening effect of fluorine for the C-C and C-F bonds in fluorinated polymers, although the traditional organic polymers, such as poly(vinyl chloride), poly(ethylene), poly(propylene), and poly(styrene) are well known for decomposing completely at around 400 ~ 500 °C.<sup>6 ~ 11)</sup> Thus, the fluoropolymers/inorganic composite materials have high potential to develop the novel fluorinated functional materials imparted by both fluorines in polymers and the inorganic materials. Fluorinated polymers/inorganic composites such as PTFE/silica composites and [poly(vinylidene fluoride)s] (PVDF)/silica composites have been already prepared through the sol-gel process, and their thermal stability has been studied in detail by using thermogravimetric analyses (TGA) measurements.<sup>12, 13)</sup>

However, these composite materials exhibit a clear weight loss corresponding to the content of each polymer in the composites at around 500 ~ 600 °C as well as that of the parent PTFE or PVDF.<sup>12, 13)</sup> On the other hand, during the comprehensive studies on the nanocomposite reactions of partially fluoroalkylated polymers, such as fluoroalkyl end-capped oligomers with the inorganic materials,<sup>14 ~ 21)</sup> Fluoroalkyl end-capped vinyltrimethoxysilane oligomer [ $R_F-(CH_2CHSi(OMe)_3)_n-R_F$ ;  $R_F-(VM)_n-R_F$ ;  $R_F$  = fluoroalkyl group] was found to undergo the sol-gel reaction under alkaline conditions in the presence of low molecular weight aromatic compounds such as 1, 1'-bi(2-naphthol) (BINOL) to give the corresponding oligomer/silica nanocomposites [ $R_F-(VM-SiO_2)_n-R_F$ ]-encapsulated BINOL.<sup>22)</sup> Interestingly, encapsulated BINOL can exhibit a nonflammable characteristic even after calcination at 800 °C, although the corresponding oligomer in the nanocomposites affords a usual flammable behavior under similar conditions.<sup>22)</sup> This nonflammable characteristic is due to the formation of ammonium hexafluorosilicate in the composites based on the bond-strengthening effect in Si-F bond (129 kcal or 540 kJ/mol)<sup>23, 24)</sup> during the nanocomposite reactions. Additionally, fluoroalkyl end-capped oligomers/ $CaCO_3$  nanocomposites have been very recently succeeded in preparing by the reactions of calcium chloride with sodium carbonate in the presence of the corresponding oligomers.<sup>25)</sup> These obtained fluorinated oligomers/ $CaCO_3$  nanocomposites were also found to exhibit a nonflammable characteristic toward the fluorinated oligomers in

the nanocomposites even after calcination at 800 °C.<sup>25)</sup> This interesting characteristic is due to the effect interaction between fluorine atom in the oligomer and calcium atom in the calcium carbonate (F-Ca), which would be derived from the bond-strengthening effect in Ca-F bond (132 kcal or 552 kJ/mol).<sup>26)</sup>  $R_F-(VM)_n-R_F$  oligomer also undergoes the sol-gel reaction under alkaline conditions to afford the corresponding fluorinated oligomer/silica nanoparticles  $[R_F-(VM-SiO_2)_n-R_F]$ .<sup>27)</sup> The modified glass surface treated with the  $R_F-(VM-SiO_2)_n-R_F$  oligomeric nanoparticles can exhibit a completely hydrophobic (superhydrophobic) characteristic (a water contact angle of 180°) with a non-wetting property against water droplet.

<sup>27)</sup> From these findings, the study on the nanocomposite reactions of  $R_F-(VM)_n-R_F$  oligomer with the inorganic particles possessing not only the silicon but also the calcium units is of particular interest from the developmental viewpoints of new fluorinated functional materials. This chapter shows that calcium silicide ( $CaSi_2$ ) particles, which are composed of calcium and silicon, can be applied to the nanocomposite reactions with  $R_F-(VM)_n-R_F$  oligomer under alkaline conditions to give the expected  $R_F-(VM-SiO_2)_n-R_F/CaSi_2$  nanocomposites. In addition, it has been found that the obtained  $R_F-(VM-SiO_2)_n-R_F/CaSi_2$  nanocomposites are applicable to the facile creation of the superoleophobic and superhydrophilic surface. These results will be described in this chapter.

## **4.2. Experimental**

### **4.2.1 Measurements**

Dynamic light scattering (DLS) measurements were measured by using Otsuka Electronics DLS-7000HL (Tokyo, Japan). Fourier-transform infrared (FT-IR) spectra were measured using Shimadzu FTIR-8400 FT-IR spectrophotometer (Kyoto, Japan). Field emission scanning electron micrographs (FE-SEM) and energy dispersive X-ray (EDX) spectra were recorded using JEOL JSM-7000F (Tokyo, Japan). X-ray diffraction (XRD) measurements were performed by the use of Rigaku Miniflex 600 (Tokyo, Japan). Thermal analyses were recorded on Bruker axs TG-DTA2000SA differential thermobalance (Kanagawa, Japan). The contact angles were measured by the use of Kyowa Interface Science Drop Master 300 (Saitama, Japan). Dynamic force microscope (DFM) was measured by using SII NanoTechnology Inc. E-sweep (Chiba, Japan). X-ray photoelectron spectroscopy (XPS) measurements were performed by the use of Shimadzu ESCA 3400 (Kyoto, Japan).

#### 4.2.2. Materials

Vinyltrimethoxysilane (VM) was used as received from Dow Corning Toray Co., Ltd., (Tokyo, Japan). Calcium silicide particles were purchased from AZmax Corporation (Chiba, Japan). Fluoroalkyl end-capped vinyltrimethoxysilane oligomer [ $R_F-(CH_2CHSi(OMe)_3)_n-R_F$ ;  $R_F-(VM)_n-R_F$ ;  $R_F = CF(CF_3)OC_3F_7$ ;  $M_n = 730$ ] was synthesized by reaction of fluoroalkanoyle peroxide with the corresponding monomer according to the previously reported methods.<sup>28)</sup>

#### 4.2.3. Preparation of fluoroalkyl end-capped vinyltrimethoxysilane oligomer/calcium silicide nanocomposites [ $R_F-(VM-SiO_2)_n-R_F/CaSi_2$ ]

To methanol solution (5 ml) of fluoroalkyl end-capped vinyltrimethoxysilane oligomer [ $R_F-(VM)_n-R_F$ ;  $R_F = CF(CF_3)OC_3F_7$  (100 mg)] were added  $CaSi_2$  particles (100 mg) and 28 wt% aqueous ammonia solution (2.0 ml). The mixture was stirred with a magnetic stirring bar at 25 °C for 5 h. After the solvent was evaporated off, methanol was added to the obtained crude products. The methanol suspension was stirred with magnetic stirring bar at room temperature for 1 day and then centrifuged for 30 min. The expected fluorinated nanocomposites were easily separated from the methanol suspension. Fluorinated composite

powders thus obtained were dried in vacuo at 50 °C for 1 day to yield purified composite powders (158 mg). The obtained  $R_F-(VM-SiO_2)_n-R_F/CaSi_2$  nanocomposites showed the following FT-IR spectra;

FT-IR ( $cm^{-1}$ ): 1334 (C-F), 1147, 1068 (Si-O-Si), and 808 (C-C).

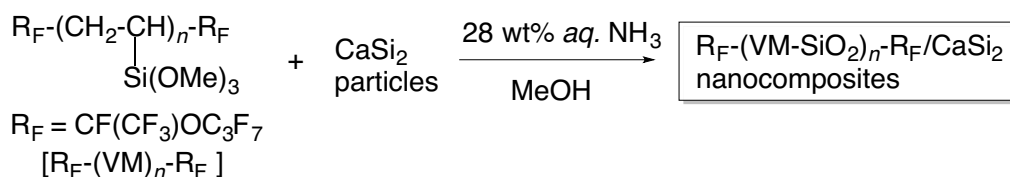
#### **4.2.4. Preparation of modified glass treated with $R_F-(VM-SiO_2)_n-R_F/CaSi_2$ nanocomposites by dipping method**

To a methanol solution (5.0 ml) containing  $R_F-(VM)_n-R_F$  oligomer (100 mg) were added  $CaSi_2$  particles (100 mg) and 28 wt% aqueous ammonia solution (2.0 ml). The mixture was stirred with a magnetic stirring bar at 25 °C for 5 h. The glass plate (18 x 18 mm<sup>2</sup> pieces) was dipped into the methanol solution of  $R_F-(VM-SiO_2)_n-R_F/CaSi_2$  nanocomposites at room temperature and left for 1 min. This was lifted from the solution at constant rate and dried at room temperature for 1 day under vacuum to afford the modified glass.

### 4.3. Results and discussion

#### 4.3.1. Preparation of fluoroalkyl end-capped vinyltrimethoxysilane oligomer/calcium silicide nanocomposites [R<sub>F</sub>-(VM-SiO<sub>2</sub>)<sub>n</sub>-R<sub>F</sub>/CaSi<sub>2</sub>]

Calcium silicide has been well known as environment friendly semiconductor materials, and much attention has been focused in calcium silicide for silicon planar technology as narrow band gap semiconductor.<sup>29 ~ 34)</sup> However, studies on the applications of calcium silicide particles into the organic polymer/inorganic composite materials have been very limited so far. Thus, fluoroalkyl end-capped vinyltrimethoxysilane oligomer [R<sub>F</sub>-(VM)<sub>n</sub>-R<sub>F</sub>] was applied to the preparation of the corresponding oligomer/calcium silicide nanocomposites. As shown in Scheme 4-1, R<sub>F</sub>-(VM)<sub>n</sub>-R<sub>F</sub> oligomer reacted with calcium silicide [CaSi<sub>2</sub>] particles under alkaline conditions to give the corresponding R<sub>F</sub>-(VM-SiO<sub>2</sub>)<sub>n</sub>-R<sub>F</sub>/CaSi<sub>2</sub> composites in good isolated yields (49 ~ 79 %). These results are shown in Scheme 4-1 and Table 4-1.



Scheme 4-1



Table 4-1 Preparation of  $R_F-(VM-SiO_2)_n-R_F/CaSi_2$  nanocomposites

Run	$R_F-(VM)_n-R_F$ (mg)	$CaSi_2$ (mg)	Yield <sup>a)</sup> (%)	Size of composites <sup>b)</sup>		Contents of $CaSi_2$ in composites <sup>c)</sup> (%)
				Before calcination (nm)	After calcination (nm)	
1	100	5	49	$61.9 \pm 10.4$	$89.9 \pm 19.2$	1
2	100	10	54	$75.7 \pm 13.7$	$52.8 \pm 7.9$	8
3	100	20	67	$42.1 \pm 4.1$	$96.1 \pm 16.8$	33
4	100	50	56	$41.1 \pm 7.7$	$52.8 \pm 7.9$	48
5	100	100	79	$35.6 \pm 5.1$	$38.4 \pm 5.0$	67
6	100	200	79	$25.2 \pm 5.5$	$23.2 \pm 3.7$	88
7	100	250	77	$27.2 \pm 4.7$	$24.4 \pm 5.4$	94
Parent $CaSi_2$ -		300		$390 \pm 66$	$362 \pm 68$	

a) Yield was based on oligomer and  $CaSi_2$ 

b) Determined by dynamic light scattering (DLS) measurements in methanol

c) Determined by thermogravimetric analyses (TGA)

The  $R_F-(VM-SiO_2)_n-R_F/CaSi_2$  composites thus obtained were found to exhibit a good dispersibility and stability in traditional organic solvents such as methanol, isopropyl alcohol (IPA), tetrahydrofuran (THF), *N,N*-dimethylformamide (DMF), and fluorinated aliphatic solvents (1:1 mixed solvents (AK-225) of 1,1-dichloro-2,2,3,3,3-pentafluoropropane and 1,3-dichloro-1,2,2,3,3-pentafluoropropane) except for water, although the parent  $CaSi_2$  particles have no dispersibility and stability for these solvents.

The size of the  $R_F-(VM-SiO_2)_n-R_F/CaSi_2$  composite particles in methanol was measured by using DLS measurements at 25 °C. The size of the parent  $CaSi_2$  particle was also measured under similar conditions, for comparison, and the results are also shown in Table 4-1.

As shown in Table 4-1, the  $R_F-(VM-SiO_2)_n-R_F/CaSi_2$  composites are nanometer size-controlled fine particles before and even after calcination at 800 °C (average particle size:

$23.2 \pm 3.7 \sim 96.1 \pm 16.8$  nm), compared with those ( $362 \pm 68 \sim 390 \pm 66$  nm) of the parent  $\text{CaSi}_2$  particles.

The field emission scanning electron micrograph (FE-SEM) images of the methanol solutions of  $\text{R}_\text{F}-(\text{VM-SiO}_2)_n-\text{R}_\text{F}/\text{CaSi}_2$  composites (Run 3 in Table 4-1) have been measured before and after calcination at  $800^\circ\text{C}$ . The FE-SEM measurements of parent  $\text{CaSi}_2$  particles were also measured under similar conditions, for comparison. These results are shown in Figs. 4-1 and 4-2.

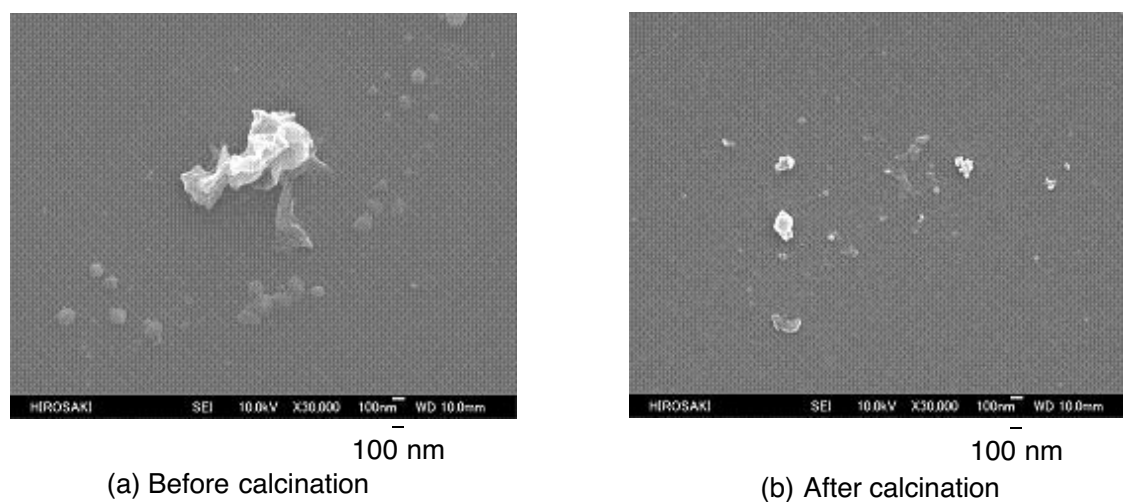


Fig. 4-1 Field Emission Scanning Electron Microscopy (FE-SEM) images of parent  $\text{CaSi}_2$  particles in methanol solutions before (a) and after (b) calcination at  $800^\circ\text{C}$

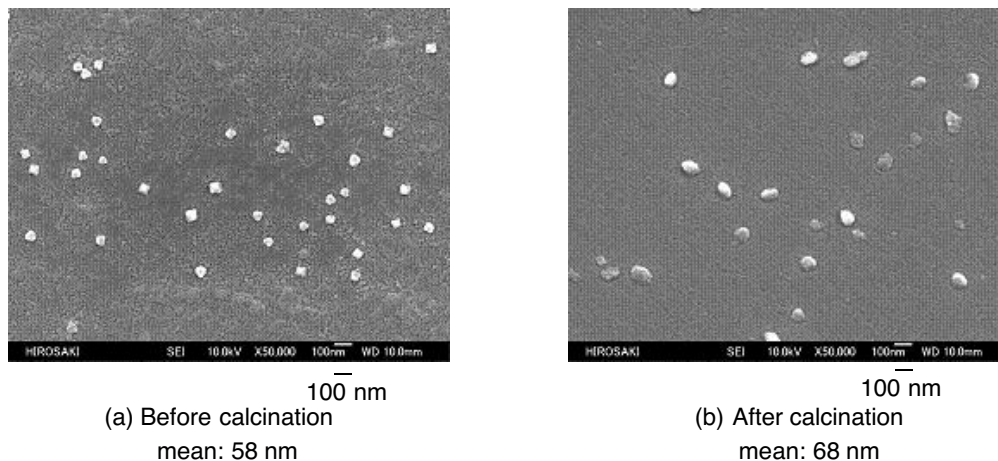


Fig. 4-2 FE-SEM images of  $R_F-(VM-SiO_2)_n-R_F/CaSi_2$  nanocomposites (Run 3 in Table 4-1) in methanol solutions before (a) and after (b) calcination at 800 °C

Electron micrographs show that the shapes of parent  $CaSi_2$  particles before and after calcination at 800 °C are not uniform due to the coagulation or agglomeration of the particles (see Fig. 4-1). However, interestingly, the uniform  $R_F-(VM-SiO_2)_n-R_F/CaSi_2$  composites fine nanoparticles with a mean diameter of 58 ~ 68 nm have been prepared before and even after calcination at 800 °C (see Fig. 4-2). The formation of uniform nanocomposite fine particles indicates that the  $CaSi_2$  particles should be effectively encapsulated into the fluoroalkyl end-capped vinyltrimethoxysilane oligomeric silica nanocomposite cores during the nanocomposite reactions with the corresponding oligomer under alkaline conditions to give the expected  $R_F-(VM-SiO_2)_n-R_F/CaSi_2$  nanocomposite fine particles possessing a good dispersibility and stability toward a variety of organic media.

Thermal stability of  $R_F-(VM-SiO_2)_n-R_F/CaSi_2$  nanocomposites illustrated in Table 4-1 was

studied by the use of thermogravimetric analyses (TGA), in which the weight loss of these nanocomposites was measured by raising the temperature at around 800 °C (the heating rate 10 °Cmin<sup>-1</sup>) in air atmosphere and the results are shown in Fig. 4-3.

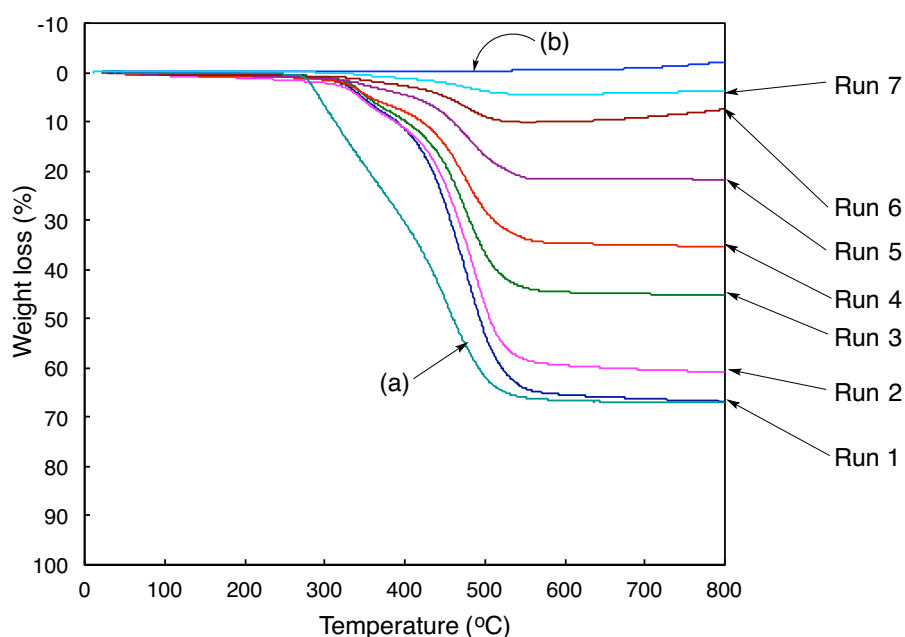


Fig. 4-3 Thermogravimetric analyses of  $R_F-(VM-SiO_2)_n-R_F/CaSi_2$  nanocomposites (Runs 1 ~ 7 in Table 4-1), the parent  $R_F-(VM-SiO_2)_n-R_F$  oligomeric nanoparticles (a), and the parent  $CaSi_2$  particles (b)

The weight loss of the parent  $R_F-(VM-SiO_2)_n-R_F$  oligomeric nanoparticles, which were prepared by the sol-gel reaction of  $R_F-(VM)_n-R_F$  oligomer under alkaline conditions, markedly dropped at around 270 °C and decomposed gradually, reached 67 % at around 530 °C due to the partly formation of silica gel during the calcination process [Fig. 4-3-(a)]. On the other hand, the  $R_F-(VM-SiO_2)_n-R_F/CaSi_2$  nanocomposites were found to decompose significantly

compared with that of the parent  $\text{CaSi}_2$  during the calcination process from room temperature to 800 °C [Fig. 4-3-(b) and Runs 1 ~ 7 in Fig. 4-3]. Thus, the contents of  $\text{CaSi}_2$  particles in the nanocomposites were estimated to be 1 ~ 94 % (see Table 4-1) based on the weight loss of  $\text{CaSi}_2$  particles and the parent  $\text{R}_\text{F}-(\text{VM-SiO}_2)_n-\text{R}_\text{F}$  oligomeric nanoparticles.

#### **4.3.2. Preparation of modified glass treated with $\text{R}_\text{F}-(\text{VM-SiO}_2)_n-\text{R}_\text{F}/\text{CaSi}_2$ nanocomposites by dipping method**

The modified glasses treated with  $\text{R}_\text{F}-(\text{VM-SiO}_2)_n-\text{R}_\text{F}/\text{CaSi}_2$  nanocomposites illustrated in Table 4-1 have been prepared, and the contact angles of dodecane and water for these glass plates were measured by depositing a droplet of dodecane or water (2  $\mu\text{l}$ ) on the modified glass surfaces. These results are shown in Table 4-2.

Table 4-2 Contact angles of water and dodecane on glasses treated with  $R_F-(VM-SiO_2)_n-R_F/CaSi_2$  nanocomposites

Run <sup>a</sup>	Contents of $CaSi_2$ in composites <sup>b</sup> (%)	Contact angle (degree) <sup>a)</sup>							
		Dodecane	Water						
			Time						
			0 m	5 m	10 m	15 m	20 m	25 m	30 m
1	1	70	180 <sup>c</sup>	-	-	-	-	-	-
2	8	72	180 <sup>c</sup>	-	-	-	-	-	-
3	33	76	114	106	95	84	78	52	0
4	48	63	121	116	107	101	85	57	0
5	67	118	129	0	-	-	-	-	-
6	88	94	90	0	-	-	-	-	-
7	94	74	67	0	-	-	-	-	-
Parent $R_F-(VM-SiO_2)_n-R_F$ oligomeric nanoparticles		48	180 <sup>c</sup>	-	-	-	-	-	-
Parent $CaSi_2$		0	0	-	-	-	-	-	-
Non-treated Glass		0	50						

<sup>a</sup> Each Run No. corresponds to that of Table 4-1<sup>b</sup> See Table 4-1<sup>c</sup> A time dependence was not observed for 30 min

As shown in Table 4-2, the contact angles of dodecane and water on the modified glass surfaces treated with the  $R_F-(VM-SiO_2)_n-R_F/CaSi_2$  nanocomposites showed large values 63 ~ 118° and 114 ~ 180°, respectively, of whose values can exhibit highly oleophobic and hydrophobic characteristics imparted by fluoroalkyl segments in the composites. Of particular interest, the  $R_F-(VM-SiO_2)_n-R_F/CaSi_2$  nanocomposites (Run 5 in Table 4-2) afforded the highest dodecane contact angle value: 118° to give the superoleophobic characteristic on the modified surface.

Water and dodecane contact angle values on the modified glass surface treated with the parent  $CaSi_2$  particles were found to become 0° in each case, although the water contact angle

value of the non-treated glass surface is  $52^\circ$  (see Table 4-2). Interestingly, water contact angle values on the modified glass surfaces treated with  $R_F-(VM-SiO_2)_n-R_F/CaSi_2$  nanocomposites are very sensitive for the change of the contents of  $CaSi_2$  in the composites, and the lower contents of  $CaSi_2$  in the composites: 1 ~ 8 % enabled the modified surfaces to give the superhydrophobic characteristic (water contact angle value  $180^\circ$ ) with a non-wetting property against water. A steep time dependence of water contact angle was observed in the cases of the high contents: 33 ~ 48 % of  $CaSi_2$  in the composites. The water contact angles decreased smoothly from  $114 \sim 121^\circ$  to  $0^\circ$  over 30 min to give a superhydrophilicity on the modified surfaces. More interestingly, the more effective decrease of water contact angle values can be observed from  $129 \sim 67^\circ$  to  $0^\circ$  only over 5 min in the cases of the higher contents 67 ~ 94 % of  $CaSi_2$  in the composites, although each dodecane contact angle value can keep its value under similar conditions (see Fig. 4-4).

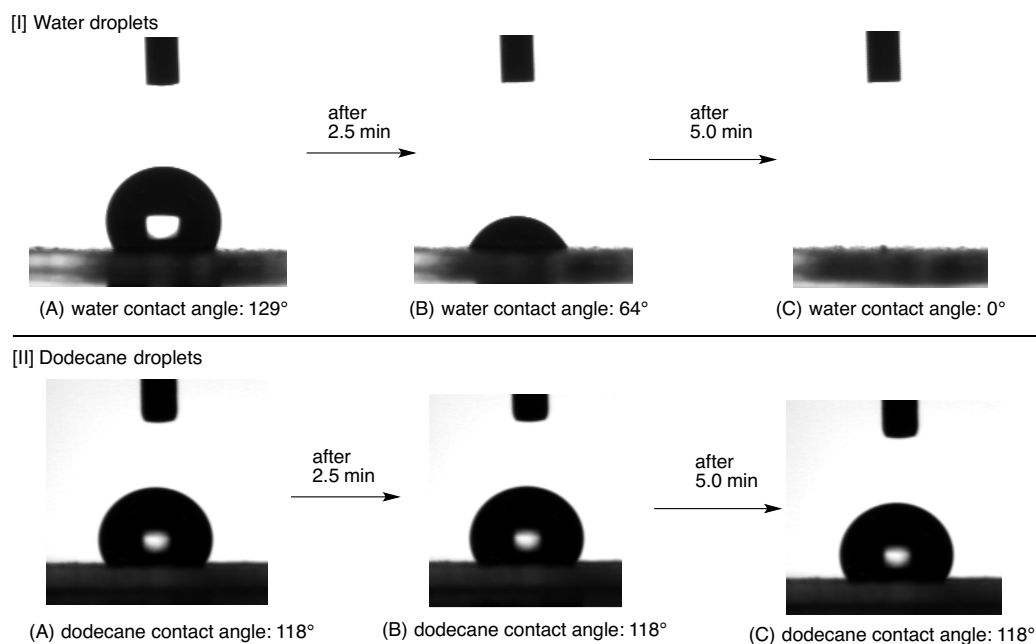


Fig. 4-4 Charge coupled device camera images of the water and dodecane droplets on the modified glass surface treated with  $R_F-(VM-SiO_2)_n-R_F/CaSi_2$  nanocomposites (Run 5 in Table 4-1) [initial contact angle (A), contact angle after 2.5 min (B), and contact angle after 5.0 min (C)]

This finding suggests that at the interface with water, hydrophobic fluoroalkyl segments are replaced by the hydrophilic  $CaSi_2$  particle surface, of whose parent particles can exhibit the water contact angle  $0^\circ$  on the modified surface (see Table 4-2). The  $CaSi_2$  particles in the composites which are composed of the higher contents of  $CaSi_2$  67 ~ 94 % are also likely to be arranged more regularly at the interface. It takes about only 5 min to replace the fluoroalkyl segments by the  $CaSi_2$  units when the environment is changed from air to water. Especially, the good repeatability (3 cycles) for such flip-flop motion between the fluoroalkyl segments and  $CaSi_2$  particles in the nanocomposites (Run 5 in Table 4-2) can be observed for the measurement of the water contact angle as following:



Cycles	0 min	5 min
1 st	129°	0°
2 nd	129°	0°
3 rd	129°	0°

Thus, such flip-flop motion to give the hydrophobic and superhydrophilic characteristics adapted to the environmental change from air to water can be easily observed on the modified surfaces.

In general, highly oleophobic (superoleophobic) surface are realized by lowering the surface energy and enhancing the surface roughness.<sup>35 ~ 43)</sup> The fabrication of superoleophobic surface is difficult due to the lower surface tension of oils than that of water.<sup>44, 45)</sup> The surface roughness is very important for the wetting properties for liquids. Thus, the surface roughness of the modified glasses treated with the parent  $R_F-(VM-SiO_2)_n-R_F$  oligomeric nanoparticles, and with the  $R_F-(VM-SiO_2)_n-R_F/CaSi_2$  nanocomposites, of whose modified surfaces can exhibit the superhydrophobicity (water contact angle 180°: Run 2 in Table 4-2) and both superhydrophilic and superoleophobic characteristics (water and dodecane contact angles 0° and 118°: Run 5 in Table 4-2), respectively, have been studied by using FE-SEM measurements. These results are shown in Figs. 4-5 ~ 4-7.

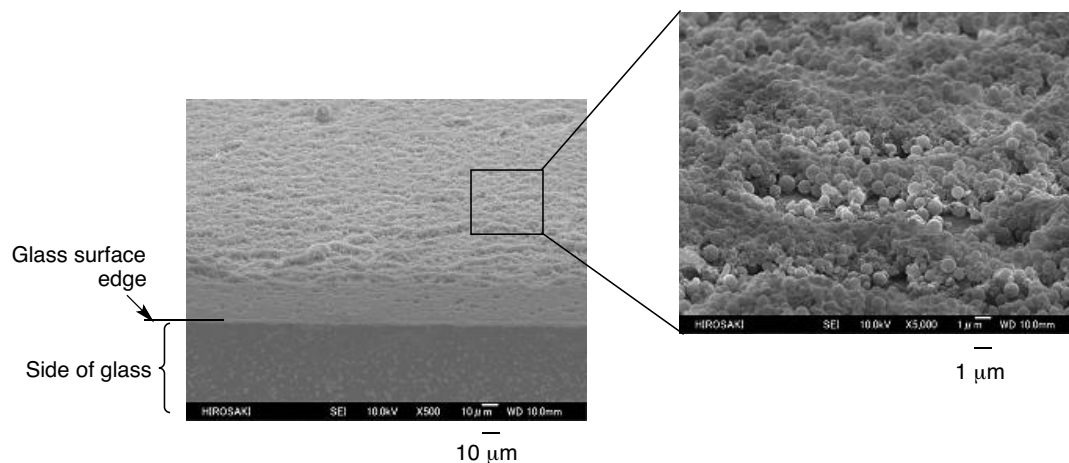


Fig. 4-5 FE-SEM images of glass surface treated with the parent  $R_F-(VM-SiO_2)_n-R_F$  nanoparticles (see Table 4-2)

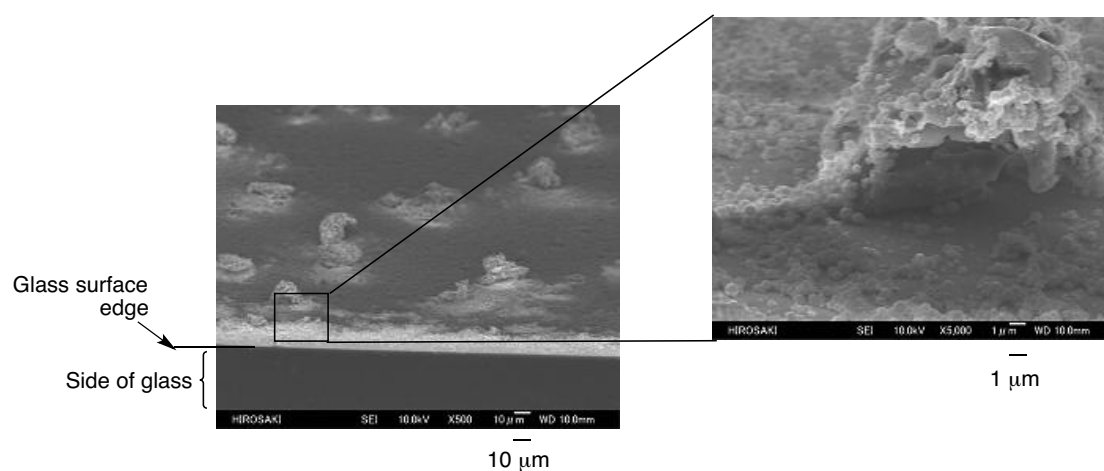


Fig. 4-6 FE-SEM images of glass surface treated with  $R_F-(VM-SiO_2)_n-R_F/CaSi_2$  nanocomposites (Run 2 in Table 4-1)

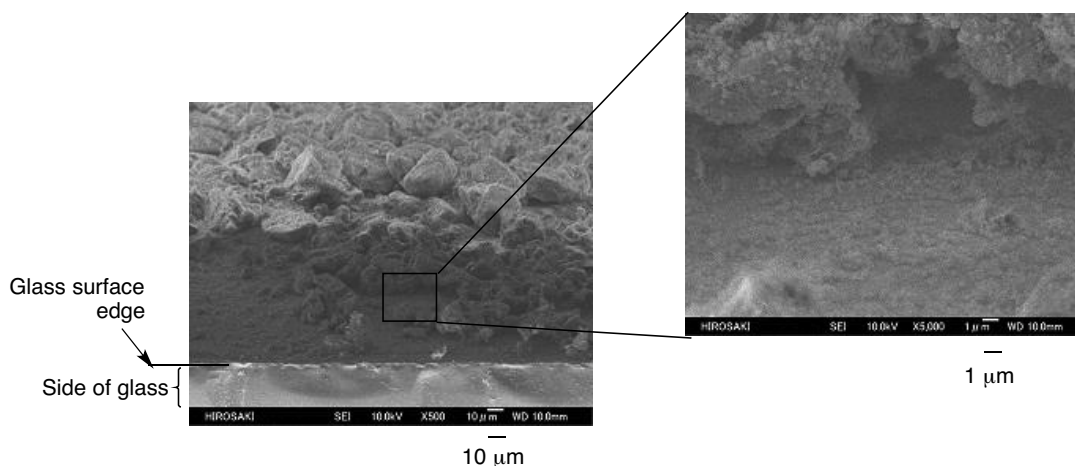


Fig. 4-7 FE-SEM images of glass surface treated with  $R_F-(VM-SiO_2)_n-R_F/CaSi_2$  nanocomposites (Run 5 in Table 4-1)

As shown in Figs. 4-5 and 4-6, the architecture of the effective roughness have been observed on the modified glass surfaces treated with the  $R_F-(VM-SiO_2)_n-R_F/CaSi_2$  nanocomposites (Run 2 in Table 4-2), compared with that of the parent  $R_F-(VM-SiO_2)_n-R_F$  oligomeric nanoparticles. Interestingly, the more enhanced roughness surface was observed in the  $R_F-(VM-SiO_2)_n-R_F/CaSi_2$  nanocomposites possessing the superoleophobic characteristic (dodecane contact angle  $118^\circ$ : Run 5 in Table 4-2) demonstrated in Fig. 4-7.

Dynamic force microscopy (DFM) measurements of these nanocomposites also show that the topographical image of each surface can exhibit a roughness characteristic, and the roughness average:  $R_a$  (127 nm) of the modified glass surface possessing the superoleophobic characteristic [dodecane contact angle  $118^\circ$ ; Fig. 4-8-(c)] is extremely higher than that ( $R_a$  40 nm) of the highly oleophobic surface [dodecane contact angle  $72^\circ$ ; Fig. 4-8-(b)] or that ( $R_a$  7 nm) of the usual oleophobic surface [dodecane contact angle  $48^\circ$ ; Fig. 4-8-(a)].

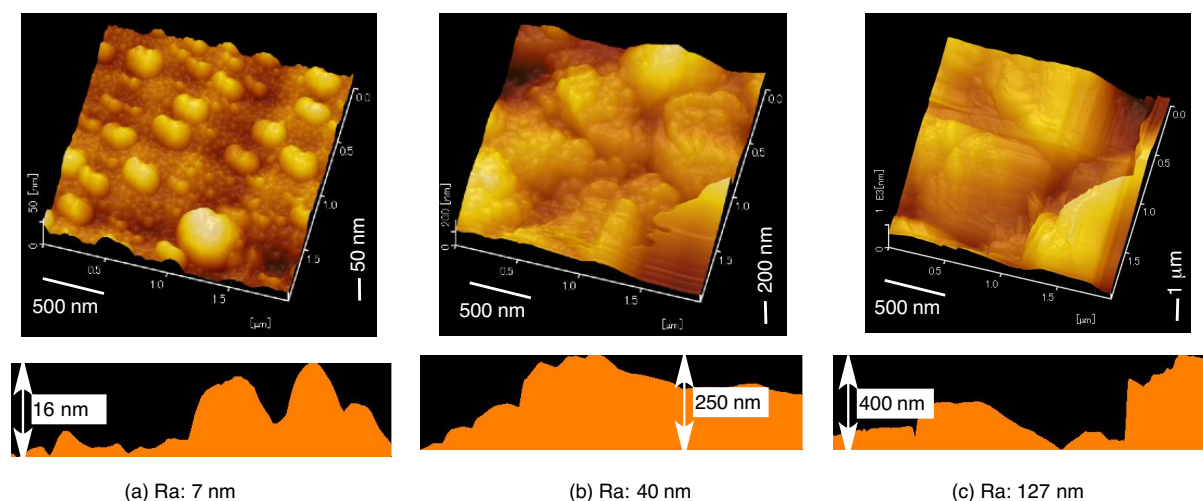


Fig. 4-8 Dynamic force microscopy (DFM) topographic images of the modified glass surface treated with the parent  $R_F-(VM-SiO_2)_n-R_F$  oligomeric nanoparticles (a), the  $R_F-(VM-SiO_2)_n-R_F/CaSi_2$  nanocomposites (Run 2 in Table 4-2) (b), and the  $R_F-(VM-SiO_2)_n-R_F/CaSi_2$  nanocomposites (Run 5 in Table 4-2) (c)

These findings suggest that  $CaSi_2$  particles are essential to the architecture of rough surface, and the higher contents (67 %) of  $CaSi_2$  in the composites are effective for the architecture of the superoleophobic and superhydrophilic fractal surface.

To further confirm the presence of fluoroalkyl segments and  $CaSi_2$  to migrate to the surface, the surface elemental composition has been measured by X-ray photoelectron spectroscopy (XPS) using Ar gas ion etching at the conditions of 1 ~ 2 kV and 10 ~ 20 mA, at which conditions the ion etching rate has been said to be about 5 nm/min. Here, the binding energies of  $F_{1s}$  and  $Ca_{2p}$  for the  $R_F-(VM-SiO_2)_n-R_F/CaSi_2$  nanocomposites (Runs 2 and 5 in Table 4-2) were presented, and the results are shown in Figs. 4-9 and 4-10.

As shown in Fig. 4-9, the peak intensity of the  $F_{1s}$  signal at around 690 eV in the  $R_F-(VM-SiO_2)_n-R_F/CaSi_2$  nanocomposites (Run 2 in Table 4-2) was found to decrease with

increasing the etching times (etching conditions; the first time 1 kV/10 mA for 60 s, the second time 2 kV/20 mA for 300 s). In contrast, the peak intensity of  $\text{Ca}_{2p}$  signal at around 350 eV was found to increase with the increase of the etching times. These findings indicate that fluoroalkyl segments in the composites can be arranged regularly above the modified surface; however, the  $\text{CaSi}_2$  moieties should be encapsulated inside the composite cores in the  $\text{R}_\text{F}-(\text{VM-SiO}_2)_n-\text{R}_\text{F}/\text{CaSi}_2$  nanocomposites, of whose lower content (8 %) of  $\text{CaSi}_2$  in the composites (see Run 2 in Table 4-1).

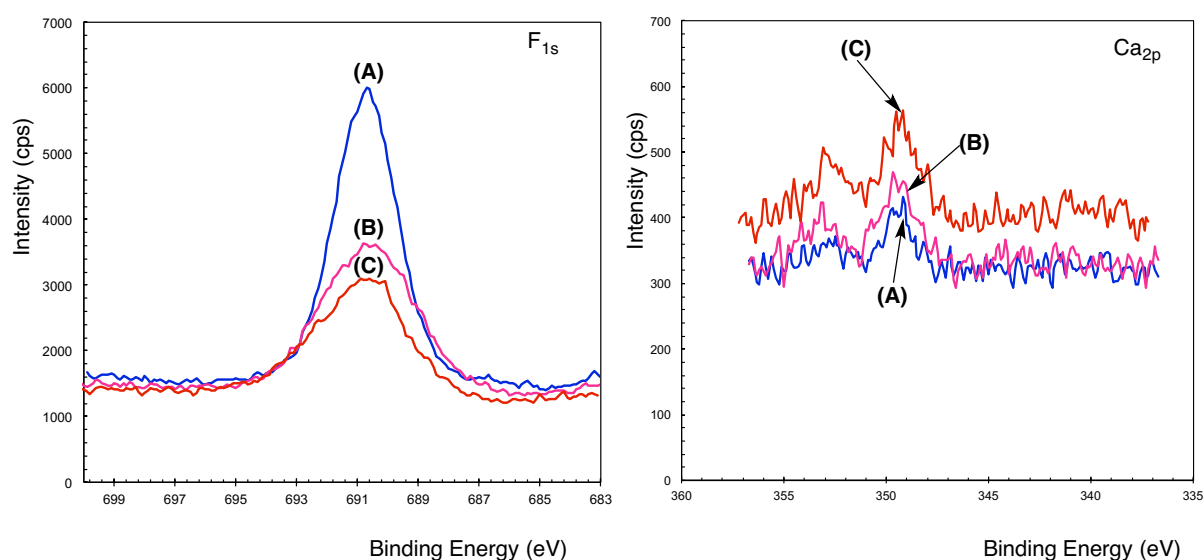


Fig. 4-9 XPS (X-ray Photoelectron Spectroscopy)  $\text{F}_{1s}$  and  $\text{Ca}_{2p}$  spectra of  $\text{R}_\text{F}-(\text{VM-SiO}_2)_n-\text{R}_\text{F}/\text{CaSi}_2$  nanocomposites (Run 2 in Table 4-1) before (A) and after Ar etching [(B): the first time, (C): the second time]

In the case of  $\text{R}_\text{F}-(\text{VM-SiO}_2)_n-\text{R}_\text{F}/\text{CaSi}_2$  nanocomposites, of whose higher content (67 %) of  $\text{CaSi}_2$  in the composites (see Run 5 in Table 4-1), a similar result was obtained in the peak intensity of  $\text{F}_{1s}$  signal as shown in Fig. 4-10; however, the similar peak intensities of  $\text{Ca}_{2p}$

signals were observed before and after the Ar etching, indicating that  $\text{CaSi}_2$  moieties in the composites should be arranged on the surface to exhibit the superhydrophilicity imparted by the  $\text{CaSi}_2$  moieties.

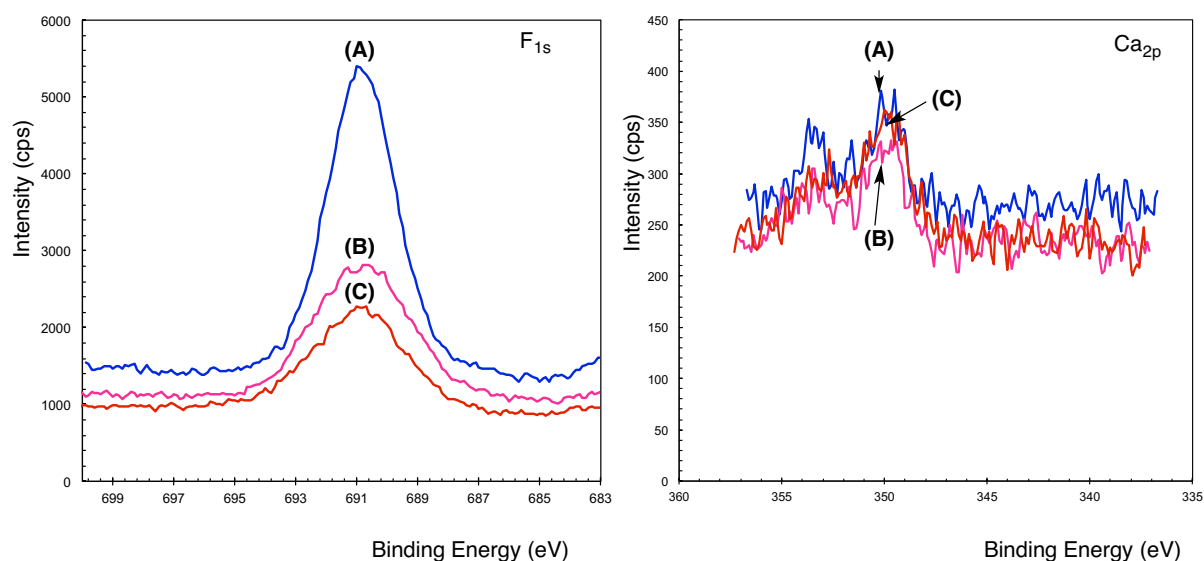


Fig. 4-10 XPS (X-ray Photoelectron Spectroscopy)  $\text{F}_{1s}$  and  $\text{Ca}_{2p}$  spectra of  $\text{R}_F\text{-(VM-SiO}_2)_n\text{-R}_F/\text{CaSi}_2$  nanocomposites (Run 5 in Table 4-1) before (A) and after Ar etching [(B): the first time, (C): the second time]

Fig. 4-3 shows that the thermal stability of  $\text{R}_F\text{-(VM-SiO}_2)_n\text{-R}_F/\text{CaSi}_2$  nanocomposites possessing both the superoleophobicity and superhydrophilicity (Run 5 in Table 4-2) is superior to that of the original  $\text{R}_F\text{-(VM-SiO}_2)_n\text{-R}_F$  oligomeric nanoparticles, because the  $T_{\text{dec}10}$  (defined by a 10 % mass loss 10 °C/min heating rate under air atmosphere conditions) value (461 °C) is higher than that (313 °C) of the original nanoparticles. Such higher thermal stability would be due to the encapsulation of  $\text{CaSi}_2$  particles in the  $\text{R}_F\text{-(VM-SiO}_2)_n\text{-R}_F$  oligomeric nanoparticle cores. In fact, as shown in Fig. 4-11-(B), the dodecane contact angle

values on the modified glass surface treated with the  $R_F-(VM-SiO_2)_n-R_F$  oligomeric nanoparticle after calcination from room temperature to 800 °C were found to decrease effectively from 48 to 0° with increasing the calcination temperatures, and the dodecane contact angle value can keep 0° at above 400 °C, indicating that the  $R_F-(VM-SiO_2)_n-R_F$  oligomeric nanoparticles decompose completely at above 400 °C, quite similar to that of the TGA curve illustrated in Fig. 4-3. On the other hand, the dodecane contact angle values on the modified glass surfaces treated with  $R_F-(VM-SiO_2)_n-R_F/CaSi_2$  nanocomposites after calcination from room temperature to 460 °C can keep an effective oleophobicity imparted by fluoroalkyl segments in the composites (Fig. 4-11-(A)), indicating that thermal stability of the  $R_F-(VM-SiO_2)_n-R_F/CaSi_2$  nanocomposites is superior to that of the parent  $R_F-(VM-SiO_2)_n-R_F$  oligomeric nanoparticles.

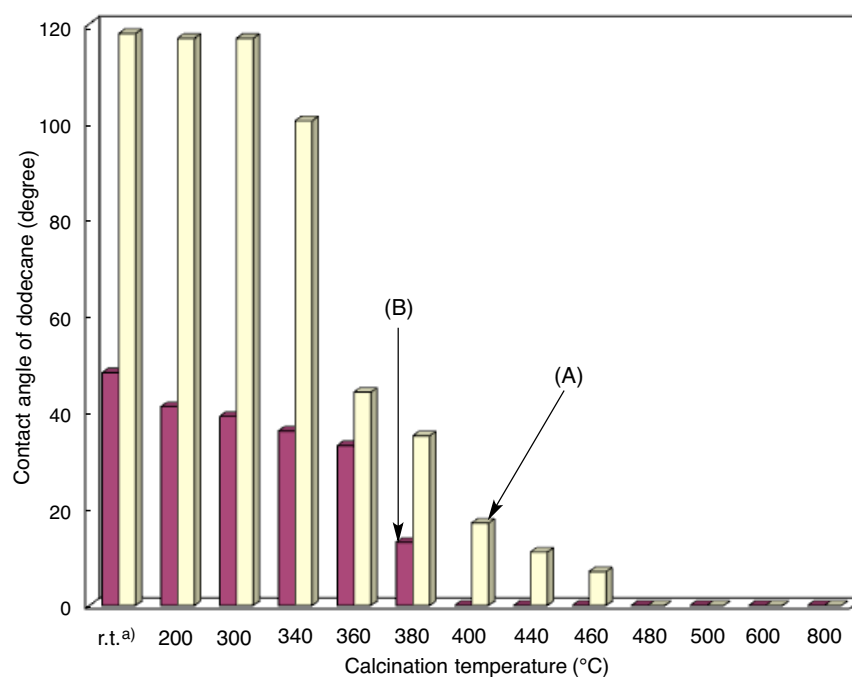


Fig. 4-11 Contact angles of dodecane on the glass surfaces treated with  $R_F-(VM-SiO_2)_n-R_F/CaSi_2$  nanocomposite [Run 5 in Table 4-2: (A)] and the parent  $R_F-(VM-SiO_2)_n-R_F$  oligomeric nanoparticles: (B) before (r.t.) and after calcination from 200 to 800 °C  
a) Room temperature

#### 4.3.3. Crystalline structures of $R_F-(VM-SiO_2)_n-R_F/CaSi_2$ nanocomposites before and after calcination at 800 °C

Fig. 4-11 shows that the fluorinated oligomer in the  $R_F-(VM-SiO_2)_n-R_F/CaSi_2$  nanocomposites can decompose completely at around 480 °C. Thus, the crystalline structures of  $R_F-(VM-SiO_2)_n-R_F/CaSi_2$  nanocomposites (Run 5 in Table 4-2) before and after calcination have been studied by using the XRD spectra measurements, and the results are shown in Fig. 4-12.



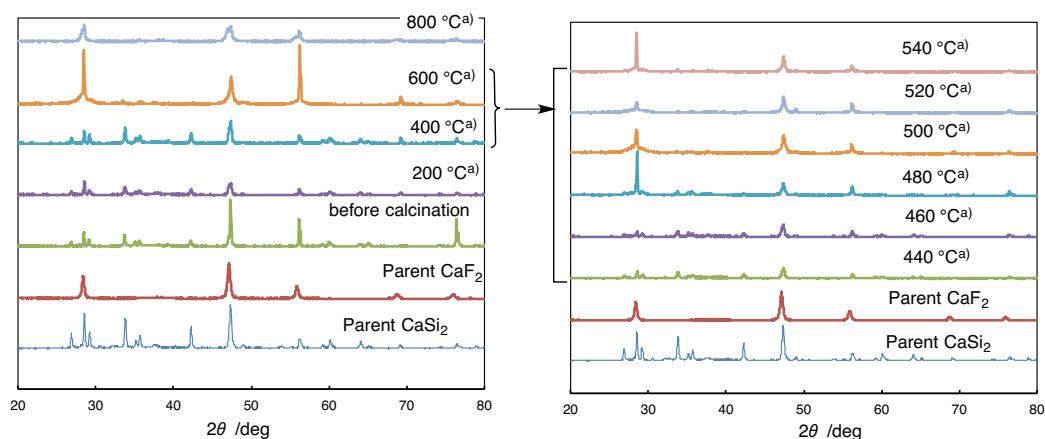


Fig. 4-12 XRD patterns of  $R_F-(VM-SiO_2)_n-R_F/CaSi_2$  nanocomposites (Run 5 in Table 4-2) before and after calcination  
a) Calcination temperature

As shown in Fig. 4-12, the XRD spectra of  $R_F-(VM-SiO_2)_n-R_F/CaSi_2$  nanocomposites before calcination show the characteristic peaks related to calcium silicide in the composites. However, interestingly, XRD spectra of  $R_F-(VM-SiO_2)_n-R_F/CaSi_2$  nanocomposites after calcination at 800 °C show not the presence of calcium silicide but the formation of calcium fluoride, indicating that calcium silicide should react with the fluorinated oligomer in the composites to give calcium fluoride during the calcination process. Especially, calcium fluoride can be quantitatively formed at above the 480 °C as shown in Fig. 4-12, and such calcination temperature is well consistent with that of the effective weight loss of  $R_F-(VM-SiO_2)_n-R_F/CaSi_2$  nanocomposites illustrated in Run 5 in Fig. 4-3.

The EDX spectra of  $R_F-(VM-SiO_2)_n-R_F/CaSi_2$  nanocomposites (Run 5 in Table 4-2) have been measured to clarify the presence of fluorines in the nanocomposites before and after calcination at 800 °C. The EDX measurements of  $R_F-(VM-SiO_2)_n-R_F$  oligomeric nanoparticles

have been also studied under the similar conditions, for comparison. The results are as follows:

Atomic (fluorine) contents (atm. %)			
$R_F-(VM-SiO_2)_n-R_F/CaSi_2$ nanocomposites		$R_F-(VM-SiO_2)_n-R_F$ oligomeric nanoparticles	
Before calcination	After calcination	Before calcination	After calcination
24 %	15 %	17 %	0 %

$R_F-(VM-SiO_2)_n-R_F$  oligomeric nanoparticles cause their pyrolysis by the calcination at 800 °C to decrease the contents of fluorine in the nanoparticles from 17 to 0 %, suggesting that the hydrogen fluoride should be smoothly generated during such calcination process. On the other hand, the residual fluorine content (15 %) in the  $R_F-(VM-SiO_2)_n-R_F/CaSi_2$  nanocomposites can be determined even after calcination at 800 °C, as well as that (24 %) before calcination. This finding indicates that the fluorinated  $CaSi_2$  nanocomposites can give not hydrogen fluoride but the calcium fluoride as the pyrolytic product through such calcination process.

In this way, it was verified that the present  $R_F-(VM-SiO_2)_n-R_F/CaSi_2$  nanocomposites are an effective tool for the formation of thermally stable calcium fluoride during the calcination process. Especially, the present fluorinated nanocomposites can afford the thermally stable calcium fluoride as a fluorine source through the calcination process. Thus, the present composites have high potential for the new environmental cyclical type-fluorine recycling system through the formation of calcium fluoride.

#### 4.4. Conclusion

New fluoroalkyl end-capped vinyltrimethoxysilane oligomer/calcium silicide nanocomposites  $[R_F-(VM-SiO_2)_n-R_F/CaSi_2]$  were prepared by the sol-gel reactions of the corresponding fluorinated oligomer  $[R_F-(VM)_n-R_F]$  with  $CaSi_2$  particles under alkaline condition. These nanocomposites thus obtained were applied to the surface modification of glass to exhibit the both superoleophobic and superhydrophilic characteristics on the modified surface. Especially, the switching behavior between the superhydrophobic and superhydrophilic characteristics can be observed on the modified surfaces by controlling the contents of  $CaSi_2$  in the nanocomposites, and the relatively lower contents: 1 ~ 8 % of  $CaSi_2$  in the composites enable the modified surfaces to give the superhydrophobic characteristic (water contact angle  $180^\circ$ ). On the other hand, the moderate contents: 67 ~ 88 % of  $CaSi_2$  in the composites enabled the modified surfaces to give the both superoleophobic and superhydrophilic surfaces. The DFM measurements showed that the creation of such superoleophobic and superhydrophilic surface is due to the architecture of the fractal surface by combination of appropriate surface roughness with fluoroalkyl segments and the  $CaSi_2$  particles in the nanocomposites. There have been hitherto numerous reports on the creation of the superamphiphobic (superhydrophobic and superoleophobic) surface by achieving low

surface energy and high surface roughness.<sup>42)</sup> We believe that the creation of the present superoleophobic and superhydrophilic surface in the air environment is the first example on the modified glass surface; although the underwater superoleophobic surfaces have attracted a great deal of attention.<sup>46 ~ 48)</sup> More interestingly, it was verified that the present  $R_F-(VM-SiO_2)_n-R_F/CaSi_2$  nanocomposites can give the calcium fluoride as the pyrolytic product, indicating that the present nanocomposites have high potential for the application to the new environmental cyclical type-fluorine recycling system through the formation of calcium fluoride.

## References

- 1) W. R. Dolbier Jr., *J. Fluorine Chem.*, **126**, 157 (2005).
- 2) J. Scheirs, Ed., *Modern Fluoropolymers*, Wiley, Chichester (1997).
- 3) K. Johns and G. Stead, *J. Fluorine Chem.*, **104**, 5 (2000).
- 4) B. Ameduri and B. Boutevin, *Well-Architected Fluoropolymers: Synthesis: Properties and Applications*, Elsevier, Amsterdam (2004).
- 5) B. Ameduri and B. Boutevin, *J. Fluorine Chem.*, **104**, 53 (2000).
- 6) S. Yano, N. Okubo, and K. Takahashi, *Macromol. Symp.*, **108**, 279 (1996).
- 7) P. Fabbri, M. Messori, M. Montecchi, S. Nannarone, L. Pasquali, F. Pilati, C. Tonelli, and M. Toselli, *Polymer*, **47**, 1055 (2006).
- 8) G. David, C. Boyer, J. Tonnar, B. Ameduri, P. Lacroix-Desmazes, and B. Boutevin, *Chem. Rev.*, **106**, 3936 (2006).
- 9) B. Ameduri, *Chem. Rev.*, **109**, 6632 (2009).
- 10) E. Girard, J.-D. Marty, B. Ameduri, and M. Destarac, *ACS Macro. Lett.*, **1**, 270 (2012).
- 11) F. Boschet and B. Ameduri, *Chem. Rev.*, **114**, 927 (2014).
- 12) Y.-C. Chen, C.-C. Lee, and Y.-D. Lee, *J. Polym. Sci., Part A: Polym. Chem.*, **42**, 1789 (2004).

- 13) J. W. Cho and K. I. Sul, *Fibers Polym.*, **2**, 135 (2001).
- 14) H. Sawada, *Chem. Rev.*, **96**, 1779 (1996).
- 15) H. Sawada, *J. Fluorine Chem.*, **105**, 219 (2000).
- 16) H. Sawada, *J. Fluorine Chem.*, **121**, 111 (2003).
- 17) H. Sawada, *Prog. Polym. Sci.*, **32**, 509 (2007).
- 18) H. Sawada, *Polym. Chem.*, **3**, 46 (2012).
- 19) H. Sawada, T. Tashima, H. Kakehi, Y. Nishiyama, M. Kikuchi, M. Miura, Y. Sato, and N. Isu, *Polym. J.*, **42**, 167 (2010).
- 20) H. Sawada, M. Kikuchi, and M. Nishida, *J. Polym. Sci., Part A: Polym. Chem.*, **49**, 1070 (2011).
- 21) H. Sawada, T. Tashima, Y. Nishiyama, M. Kikuchi, G. Kostov, Y. Goto, and B. Ameduri, *Macromolecules*, **44**, 1114 (2011).
- 22) H. Sawada, Y. Matsuki, Y. Goto, S. Kodama, M. Sugiya, and Y. Nishiyama, *Bull. Chem. Soc. Jpn.*, **83**, 75 (2010).
- 23) L. Pauling, *The chemical bond*, Cornell University Press, New York (1967).
- 24) R. Walsh, *Acc. Chem. Res.*, **14**, 246 (1981).
- 25) T. Saito, H. Kakehi, Y. Kato, M. Miura, N. Isu, and H. Sawada, *Polym. Adv. Technol.*, **24**, 532 (2013).

- 26) G.-D. Blue, J. W. Green, R. G. Bautista, and J. L. Margrave, *J. Phys. Chem.*, **67**, 877 (1963).
- 27) H. Sawada, T. Suzuki, H. Takashima, and K. Takishita, *Colloid Polym. Sci.*, **286**, 1569 (2008).
- 28) H. Sawada and M. Nakayama, *J. Chem. Soc., Chem. Commun.*, 677 (1991).
- 29) F. Canepa, M. Napoletano, P. Manfrinetti, and A. Palenzona, *J. Alloys Compds.*, **299**, 20 (2000).
- 30) S. A. Dotsenko, K. N. Galkin, D. A. Bezbabny, D. L. Goroshko, and N. G. Galkin, *Physics Procedia*, **23**, 41 (2012).
- 31) R. Wurz, M. Schmidt, A. Schopke, and W. Fuhs, *Appl. Surface Sci.*, **190**, 437 (2002).
- 32) A. M. Nartowski and I. P. Parkin, *Polyhedron*, **21**, 187 (2002).
- 33) C. Wen, A. Kato, T. Nonomura, and H. Tatsuoka, *J. Alloys Compds.*, **509**, 4583 (2011).
- 34) B. Gillot, G. Wber, H. Souha, and M. Zenkouar, *J. Alloys Compds.*, **270**, 275 (1998).
- 35) X. Yao, Y. Song, and L. Jiang, *Adv. Mater.*, **23**, 719 (2011).
- 36) J. Feng, B. Huang, and M. Zhong, *J. Colloid Interface Sci.*, **336**, 268 (2009).
- 37) R. Taurino, E. Fabbri, M. Messori, F. Pilati, D. Pospiech, and A. Synytska, *J. Colloid Interface Sci.*, **325**, 149 (2008).
- 38) H. Wang, H. Zhou, A. Gestos, J. Fang, and T. Lin, *ACS Appl. Mater. Interfaces.*, **5**,

10221 (2013).

- 39) S.-H. Hsu, Y.-L. Chang, Y.-C. Tu, C. M. Tsai, and W.-F. Su, *ACS Appl. Mater. Interfaces*, **5**, 2991 (2013).
- 40) Y.-T. Cheng and D. E. Rodak, *Appl. Phys. Lett.*, **86**, 144101 (2005).
- 41) S. G. Lee, S. S. Ham, D. Y. Lee, H. Bong, and K. Cho, *Langmuir*, **29**, 15051 (2013).
- 42) K. Liu, Y. Tian, and L. Jiang, *Prog. Mater. Sci.*, **58**, 503 (2013).
- 43) Y. Goto, H. Takashima, K. Takishita, and H. Sawada, *J. Colloid Interface Sci.*, **362**, 375 (2011).
- 44) K. Tsujii, T. Yamamoto, T. Onda, and S. Shibuichi, *Angew. Chem. Int. Ed. Eng.*, **36**, 1011 (1997).
- 45) S. Shibuichi, T. Yamamoto, T. Onda, and K. Tsujii, *J. Colloid Interface Sci.*, **208**, 287 (1998).
- 46) C. Ding, Y. Zhu, M. Liu, L. Feng, M. Wan, and L. Jiang, *Soft Mater.*, **8**, 9064 (2012).
- 47) M. J. Liu, S. T. Wang, Z. X. Wei, Y. L. Song, and L. Jiang, *Adv. Mater.*, **21**, 665 (2009).
- 48) X. Liu, J. Zhou, Z. Xue, J. Gao, J. Meng, S. Wang, and L. Jiang, *Adv. Mater.*, **24**, 3401 (2012).



## CHAPTER 5

### **Facile Creation of Modified Surface Possessing the Controlled Wettability between Superamphiphobic and Superoleophobic-Superhydrophilic Characteristics by Using Perfluorocarboxamides/Calcium Carbonate/ Calcium Fluoride Nanocomposites: Application to the Separation of Oil and Water**

## 5.1. Introduction

There has hitherto been a considerable interest in perfluoroacyl fluorides (PFAFs) because they are key intermediates for the synthesis of a variety of fluorinated polymers. <sup>1)</sup> In fact, the ionic oligomerization of PFAFs with hexafluoropropene oxide (HFPO) can proceed to afford the 1:1 adducts of the acyl fluorides and HFPO. <sup>2)</sup> The photochemical decarbonylation and coupling of fluorinated acyl fluorides [ $R_F-C(=O)F$ ] can afford the coupling products ( $R_F-R_F$ ) with both  $COF_2$  and CO. <sup>3, 4)</sup> Additionally, perfluoroalkanoyl fluorides are useful intermediates for the synthesis of perfluoroalkanoyl peroxides <sup>5)</sup>, and numerous fluoroalkyl end-capped oligomers have been prepared by the oligomerization of traditional radical polymerizable monomers initiated by these peroxides. <sup>6, 7)</sup> For example, fluoroalkanoyl peroxides react with vinyltrimethoxysilane to provide two fluoroalkyl end-capped vinyltrimethoxysilane oligomers in good isolated yields. <sup>8)</sup> These fluoroalkyl end-capped oligomers can undergo the sol-gel reactions under alkaline conditions to afford the corresponding fluorinated oligomeric silica nanoparticles. <sup>9)</sup> Fluoroalkyl end-capped oligomers are also effective for the nanocomposite reactions with not only silica nanoparticles but also calcium carbonate nanoparticles. <sup>10 ~ 13)</sup> Interestingly, fluoroalkyl end-capped oligomers/calcium carbonate nanocomposites can supply the nonflammable characteristic toward the oligomers in the composite matrices even after

calcination at 800 °C.<sup>14)</sup> This is due to the effective interaction between fluorine atoms in the oligomer and calcium atoms in the calcium carbonate (F --- Ca), which would be derived from the bond-strengthening effect in Ca-F bond (132 kcal or 552 kJ/mol).<sup>15)</sup> In this way, the composite reactions of organofluorinated compounds with calcium carbonate fine particles are of particular interest from the developmental viewpoints of new fluorinated functional materials. As mentioned above, perfluoroacyl fluorides are important intermediates toward numerous fluorochemicals. However, perfluoroacyl fluorides react with moisture developing hydrogen fluoride and perfluorocarboxylic acid.<sup>16)</sup> This finding should enable the perfluoroacyl fluorides/calcium carbonate nanocomposites to reveal the novel functionalities through the interaction of calcium carbonate with hydrogen fluoride. This chapter shows that a variety of perfluoroacyl fluorides such as perfluoro-3-(1-piperidiny)propionyl fluoride, perfluoro-2-methyl-3-morpholinopropionyl fluoride, perfluoro-3-di-*n*-propylaminopropionyl fluoride and perfluoro-3-di-*n*-butylaminopropionyl fluoride can react with calcium carbonate nanoparticles under alkaline conditions to provide the corresponding perfluorocarboxamides/calcium carbonate/calcium fluoride nanocomposites. Interestingly, these nanocomposites are applicable to the surface modification of glass, filter paper and polyethylene terephthalate (PET) fabric to exhibit the superamphiphobic and superoleophobic-superhydrophilic characteristics. More interestingly, the controlled

wettability between the superamphiphobic and superoleophobic-superhydrophilic characteristics can be observed by changing the feed ratios of the acyl fluorides and calcium carbonate nanoparticles. In addition, the fluorinated calcium carbonate nanocomposites possessing a superoleophobic-superhydrophilic characteristic are applicable to the separation membrane for not only the mixture of oil and water but also the oil-in-water emulsion. The fluorinated nanocomposites possessing a superamphiphobic characteristic have been applied to the separation membrane for the mixture of fluorocarbon and hydrocarbon. These results will be described in this chapter.

## **5.2. Experimental**

### **5.2.1 Measurements**

Dynamic light scattering (DLS) measurements were measured by using Otsuka Electronics DLS-7000HL (Tokyo, Japan). Field emission scanning electron micrographs (FE-SEM) was recorded using JEOL JSM-7000F (Tokyo, Japan). X-ray diffraction (XRD) measurements were performed by the use of Rigaku Miniflex 600 (Tokyo, Japan). The contact angles were measured by the use of Kyowa Interface Science Drop Master 300 (Saitama, Japan). Dynamic force microscope (DFM) was measured by using SII NanoTechnology Inc. E-sweep (Chiba, Japan). Optical and fluorescence microscopies were measured by using OLYNPUS Corporation BX51 (Tokyo, Japan). Fourier-transform infrared (FT-IR) spectra were recorded using Shimadzu FTIR-8400 FT-IR spectrophotometer (Kyoto, Japan). Attenuated total reflectance fouier transform infrared (ATR-FTIR) spectroscopy was measured by using Agilent Technologies Inc., Varian 670-IR (California, USA).

### 5.2.2. Materials

All perfluoroalkanoyl fluorides were received from Mitsubishi Materials Electronic Chemicals Co., Ltd., (Akita, Japan). Calcium carbonate nanoparticle (average size: 80 nm) was received from Shiraishi Kogyo Kaisha, Ltd., (Hyogo, Japan). Sodium dodecyl sulfate (SDS) was purchased from Wako Pure Chemical Industries (Osaka, Japan).

### 5.2.3. Preparation of perfluorocarboxamides/calcium carbonate/calcium fluoride nanocomposites

To methanol solution (5 ml) containing perfluoro-3-di-*n*-butylaminopropionyl fluoride (PF-DBAPF: 200 mg) were added CaCO<sub>3</sub> nanoparticle (100 mg) and 25 wt % aqueous ammonia solution (2.0 ml). The mixture was stirred with a magnetic stirring bar at 25 °C for 5 h. After the removal of the solvent and ammonia, methanol was added to the obtained crude products. The methanol solution was stirred with magnetic stirring bar at room temperature for 1 day and then centrifuged for 30 min. The expected fluorinated nanocomposites were easily separated from the methanol solution. Fluorinated composite powders thus obtained were dried in vacuo at 50 °C for 1 day to yield the purified composite powders (66 mg). Other

perfluorocarboxamides/ $\text{CaCO}_3$ / $\text{CaF}_2$  nanocomposites were also prepared under similar conditions.

#### **5.2.4. Preparation of modified glass treated with perfluorocarboxamides/calcium carbonate/calcium fluoride nanocomposites**

To methanol solution (5.0 ml) containing PF-DBAPF [280 mg (0.6 mmol)] were added  $\text{CaCO}_3$  nanoparticles [50 mg (0.5 mmol)] and 25 wt % aqueous ammonia solution (2.0 ml). The mixture was stirred with a magnetic stirring bar at 25 °C for 5 h. The glass plates (18 x 18 mm<sup>2</sup> pieces) were dipped into this methanol solution at room temperature and left for 1 min. These were lifted from the solution at constant rate and dried at room temperature for 1 day under vacuum to afford the modified glass. The modified filter papers (25 x 25 mm<sup>2</sup> pieces) and PET fabric swatches (25 x 25 mm<sup>2</sup> pieces) were prepared under similar conditions. The contact angle values for dodecane and water were measured by depositing a drop of dodecane (2 µl) or water (2 µl) on the modified plate surfaces. The contact angle values for dodecane and water were measured by depositing a drop of dodecane (2 µl) or water (2 µl) on the modified plate surfaces. A steep time dependence was observed in the case of the measurements for water contact angle. Thus, the time dependent-water contact angle values

for 30 mins were measured.

#### **5.2.5. Preparation of the surfactant-stabilized oil (dodecane)-in-water emulsion**

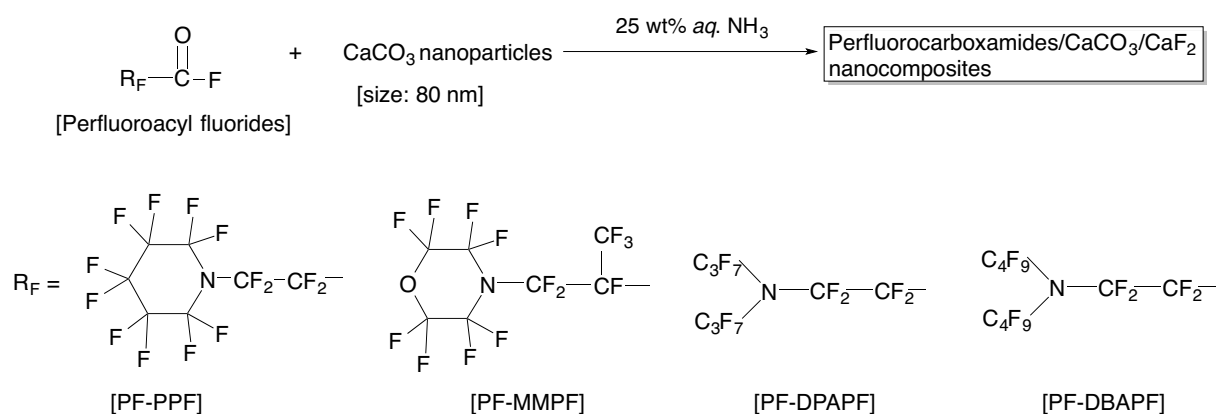
The surfactant (SDS: 300 mg) was added into the mixture of water (5 ml) and dodecane (0.15 ml). The obtained mixture was stirred for 30 min at room temperature to afford the white-colored O/W emulsion.



### 5.3. Results and discussion

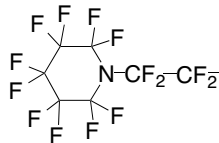
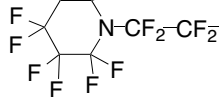
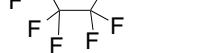
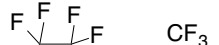
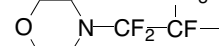


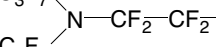


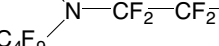

#### 5.3.1. Preparation of perfluorocarboxamides/calcium carbonate/calcium fluoride nanocomposites

Perfluoroacyl fluorides (PFAFs) such as perfluoro-3-(1-piperidiny)propionyl fluoride (PF-PPF), perfluoro-2-methyl-3-morpholinopropionyl fluoride (PF-MMPF), perfluoro-3-di-*n*-propylaminopropionyl fluoride (PF-DPAPF) and perfluoro-3-di-*n*-butylaminopropionyl fluoride (PF-DBAPF) reacted with calcium carbonate nanoparticles under alkaline conditions to afford the corresponding fluorinated  $\text{CaCO}_3/\text{CaF}_2$  composites in 9 ~ 40 % isolated yields. These results are shown in Scheme 5-1 and Table 5-1.



Scheme 5-1

Table 5-1 Preparation of perfluorocarboxamides/CaCO<sub>3</sub>/CaF<sub>2</sub> nanocomposites<sup>a)</sup>

Run	R <sub>F</sub> group in PFAF	PFAF (mg) [mmol]	CaCO <sub>3</sub> (mg) [mmol]	Yield <sup>b)</sup> (%)	Size of Composites <sup>c)</sup> (nm)
1		280 [0.7]	50 [0.5]	12	25.6 ± 5.3
2		200 [0.5]	50 [0.5]	15	27.1 ± 6.2
3		200 [0.5]	100 [1.0]	40	30.7 ± 6.8
4		280 [0.7]	50 [0.5]	12	36.4 ± 9.3
5		200 [0.5]	50 [0.5]	12	35.4 ± 9.3
6		200 [0.5]	100 [1.0]	28	54.6 ± 12.3
7		280 [0.6]	50 [0.5]	10	32.9 ± 8.1
8		200 [0.4]	50 [0.5]	17	48.9 ± 8.6
9		200 [0.4]	100 [1.0]	25	69.3 ± 15.2
10		280 [0.5]	50 [0.5]	9	33.1 ± 9.3
11		200 [0.3]	50 [0.5]	13	21.3 ± 5.3
12		200 [0.3]	100 [1.0]	22	18.5 ± 4.5

a) Used methanol and 25 wt. % ammonia were 5.0 ml and 2.0 ml, respectively.

b) Yield was based on PFAF and CaCO<sub>3</sub>

c) Determined by dynamic light scattering (DLS) measurements in methanol

As shown in Scheme 5-1 and Table 5-1, the yields of the composites thus obtained are dependent upon the feed ratios of the acyl fluorides and calcium carbonate nanoparticles employed, increasing with greater feed ratios of calcium carbonate in the calcium carbonate/acyl fluorides. This finding suggests that the higher feed amounts of calcium carbonate are effective for the nanocomposite reactions with the acyl fluorides.

The composites thus obtained were found to provide a good dispersibility in water and traditional organic solvents such as methanol, 2-propanol (IPA), tetrahydrofuran (THF), 1, 2-dichloroethane (DE), and fluorinated aliphatic solvents [1 : 1 mixed solvents (AK-225) of 1, 1-dichloro-2, 2, 3, 3, 3-pentafluoropropane and 1, 3-dichloro-1, 2, 2, 3, 3-pentafluoropropane].

The field emission scanning electron micrographs (FE-SEM) of methanol solutions of these composites (Runs 3, 6, 9 and 12 in Table 5-1) have been measured, and the results are shown in Fig. 5-1.

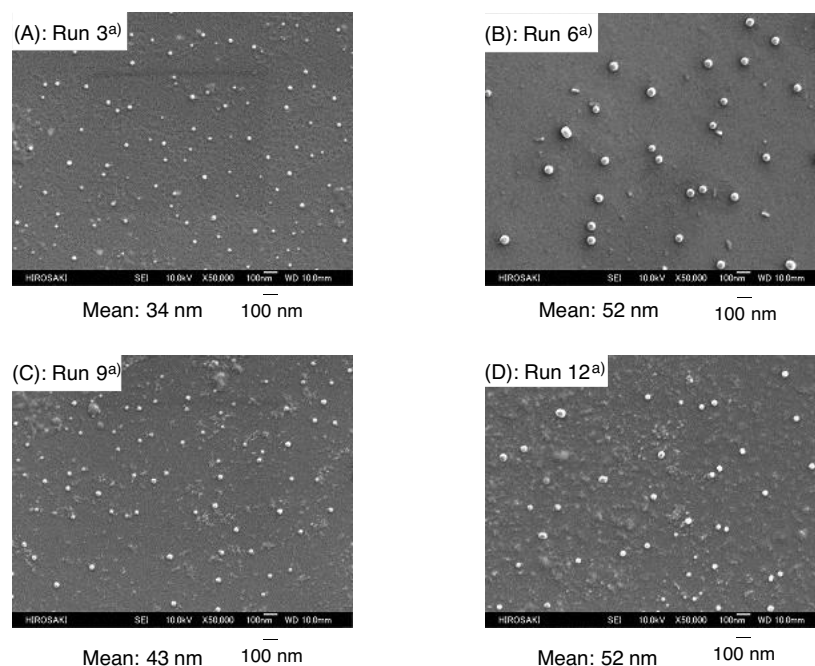


Fig. 5-1 FE-SEM images of well-dispersed methanol solutions of the perfluorocarboxamides/ $\text{CaCO}_3$ / $\text{CaF}_2$  nanocomposites [(A): Run 3; (B) Run 6; (C): Run 9; (D): Run 12]  
a) Each Run No. correspond to that of Table 5-1

As shown in Fig. 5-1, FE-SEM image of each composites shows the formation of very fine nanoparticles with mean diameters of 34 ~ 52 nm. The sizes for the composites (18 ~ 69 nm) determined by the dynamic light scattering (DLS) measurements were almost the same as to those in FE-SEM measurements.

In order to clarify the crystalline structures of the obtained nanocomposites, the XRD

spectra of the nanocomposites in Table 5-1 have been measured. The results are shown in Fig.

5-2.

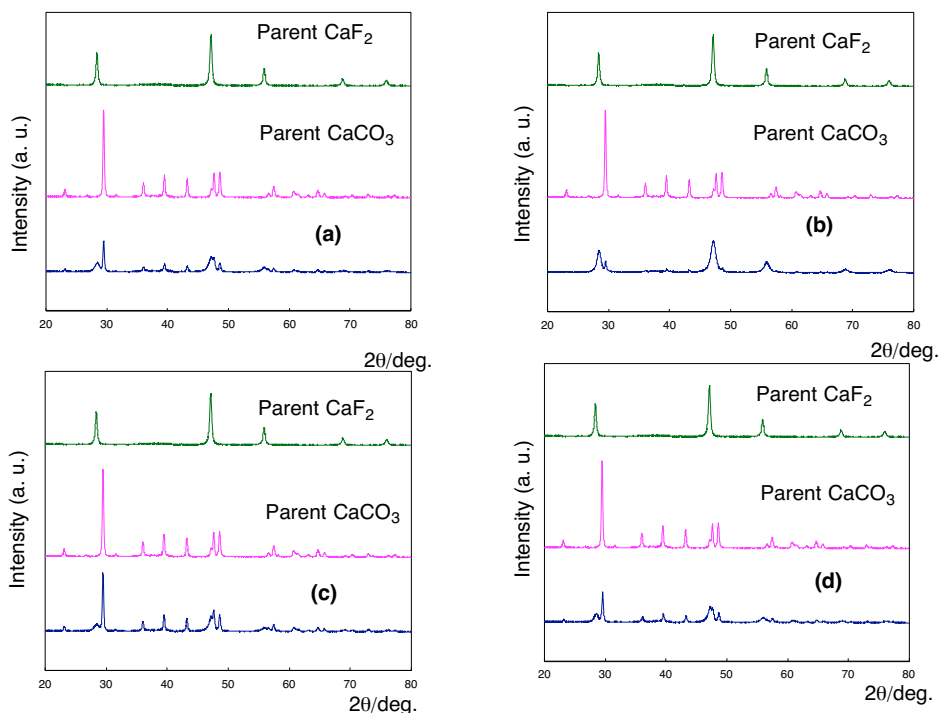


Fig. 5-2 XRD patterns of the perfluorocarboxamides/ $\text{CaCO}_3$ / $\text{CaF}_2$  nanocomposites [(a): Run 2; (b) Run 5; (c): Run 8; (d): Run 11; Each Run No. corresponds to that of Table 5-1]

As shown in Fig. 5-2, the XRD spectra of each nanocomposite were found to afford the characteristic peaks related to not only calcium carbonate but also calcium fluoride. The formation of calcium fluoride is attributed to the reaction of calcium carbonate with hydrogen fluoride, which should be formed during the composite reactions with the acyl fluorides illustrated in Scheme 5-1 and Table 5-1. It was previously reported that the end-capped acyl fluoride groups in tetrafluoroethylene/perfluoropropylvinylether copolymers (PFA

copolymers) are transformed into amide groups through the exposition to ammonia vapors, and ammonium fluoride is also formed during this transformation (see Scheme 5-2).<sup>17)</sup>



Scheme 5-2

In this transformation, the band at  $1884 \text{ cm}^{-1}$  which is assigned to C=O stretching in  $\text{R}_\text{F}\text{C(=O)F}$  groups has been completely disappeared in the FT-IR spectra measurements.<sup>17)</sup> Thus, the present nanocomposite reactions of the perfluoroacyl fluorides with calcium carbonate in the presence of ammonia in methanol illustrated in Scheme 5-1 should afford the corresponding methyl esters  $[\text{R}_\text{F}\text{-C(=O)OMe}]$  and hydrogen fluoride, and successively give the perfluorocarboxamides  $[\text{R}_\text{F}\text{-C(=O)NH}_2]$  and ammonium fluoride through the reaction with ammonia. The produced hydrogen fluoride and ammonium fluoride react with calcium carbonate to produce calcium fluoride illustrated in Fig. 2.

In fact, ATR-FTIR spectra of the modified glass surface treated with fluorinated nanocomposites (Run 11 in Table 5-1) shows the amide band around at  $1708 \text{ cm}^{-1}$  with the complete disappearance of the C=O band at  $1880 \text{ cm}^{-1}$  related to the parent acyl fluoride: PF-DBAPF (see Fig. 5-3).

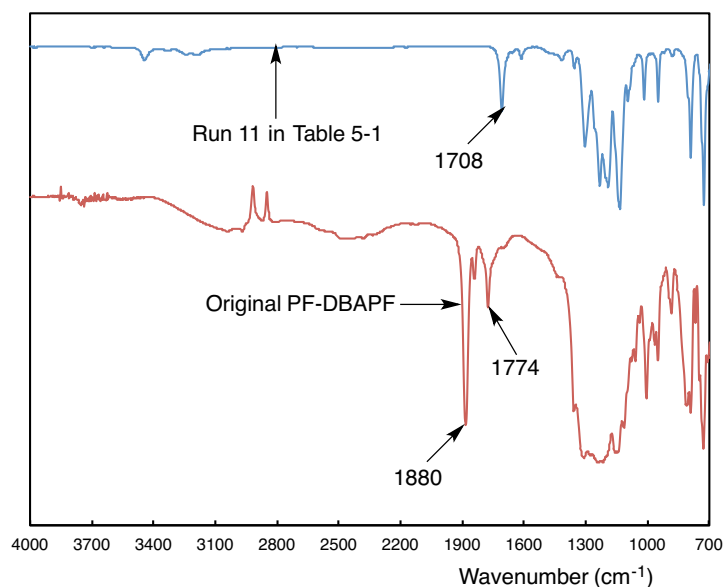


Fig. 5-3 ATR-FTIR spectra of modified glass surface treated with the perfluorocarboxamides/ $\text{CaCO}_3$ / $\text{CaF}_2$  nanocomposites (Run 11 in Table 5-1)

### 5.3.2. Preparation of modified glass treated with perfluorocarboxamides/calcium carbonate/calcium fluoride nanocomposites

The modified glasses treated with the present perfluorocarboxamides/ $\text{CaCO}_3$ / $\text{CaF}_2$  nanocomposites in Table 5-1 have been prepared to verify the surface active characteristic of the corresponding composites. The contact angles of dodecane and water for each modified glass surface were measured by depositing a droplet of dodecane or water (2  $\mu\text{l}$ ) on the modified glass surfaces. These results are shown in Table 5-2.

Table 5-2 Contact angles of water and dodecane on the modified glasses treated with the perfluorocarboxamides/  
CaCO<sub>3</sub>/CaF<sub>2</sub> nanocomposites<sup>a)</sup>

Run <sup>a)</sup>	Feed ratio (g/g) [mol/mol]: CaCO <sub>3</sub> /R <sub>F</sub> C(=O)F <sup>b)</sup>	Contact angle (degree)							
		dodecane	water						
			time						
			0 min	5 min	10 min	15 min	20 min	25 min	30 min
1	0.17 [0.71]	72	23	0 <sup>c)</sup>	-	-	-	-	-
2	0.25 [1.00]	44	19	0 <sup>c)</sup>	-	-	-	-	-
3	0.50 [2.00]	60	52	0 <sup>c)</sup>	-	-	-	-	-
4	0.17 [0.71]	22	120	0 <sup>c)</sup>	-	-	-	-	-
5	0.25 [1.00]	18	15	0 <sup>c)</sup>	-	-	-	-	-
6	0.50 [2.00]	38	141	0 <sup>c)</sup>	-	-	-	-	-
7	0.17 [0.83]	96	141	0 <sup>c)</sup>	-	-	-	-	-
8	0.25 [1.25]	117	150	0 <sup>c)</sup>	-	-	-	-	-
9	0.50 [2.50]	126	180 <sup>c)</sup>	-	-	-	-	-	-
10	0.17 [1.00]	112	141	0 <sup>c)</sup>	-	-	-	-	-
11	0.25 [1.67]	106	145	0 <sup>c)</sup>	-	-	-	-	-
12	0.50 [3.33]	104	180 <sup>c)</sup>	-	-	-	-	-	-
Non-treated glass		0	50	50	48	44	43	39	35

(a) Each Run No. corresponds to that of Table 5-1

(b) See each feed ratio in Table 5-1

(c) A time dependence was not observed over 30 min

As shown in Table 5-2, the modified glass surface treated with the fluorinated nanocomposites: Runs 1 ~ 6 in Table 5-1 can exhibit a good oleophobicity (18 ~ 72°) on the modified surface. Especially, the effective decrease of water contact angle values can be observed from 15 ~ 120° to 0° over only 5 min to provide a superhydrophilicity on each modified surface. The smooth flip-flop motion between the hydrophobic fluoroalkyl moieties and the hydrophilic amido segments in the nanocomposites would afford the creation of the superhydrophilic surface at the interface with water. On the other hand, the fluorinated nanocomposites (Runs 7, 8, 10 and 11) possessing not cyclic but linear perfluoroalkyl moieties can provide not only superhydrophilic but also superoleophobic characteristics on the

modified surfaces. Because, water contact angle values can decrease successively from 141 ~ 150° to 0° over 5 min and dodecane contact angle values are 96 ~ 117°, indicating that linear perfluoroalkyl moieties in the nanocomposites are likely to be arranged more regularly on the modified surface, compared with that of the cyclic perfluoroalkyl ones to afford the roughness surface. Such roughness structure should afford the superoleophobic characteristic on the modified surfaces. In addition, the fluorinated nanocomposites possessing the linear perfluoroalkyl moieties (Runs 9 and 12 in Table 5-1), which were prepared under the higher feed ratio [0.50 g/g (2.5 and 3.33 mol/mol)] of calcium carbonate, can exhibit a superamphiphobic characteristic imparted by the linear perfluoroalkyl moieties in the composites on the modified surface.

In order to clarify the formation of such superoleophobic-superhydrophilic and superamphiphobic surfaces, the surface roughness of the modified glasses treated with the fluorinated nanocomposites (Runs 8, 9, 11 and 12 in Table 5-2) was studied by FE-SEM and dynamic force microscopy (DFM) measurements. These results are shown in Figs. 5-4 and 5-5.



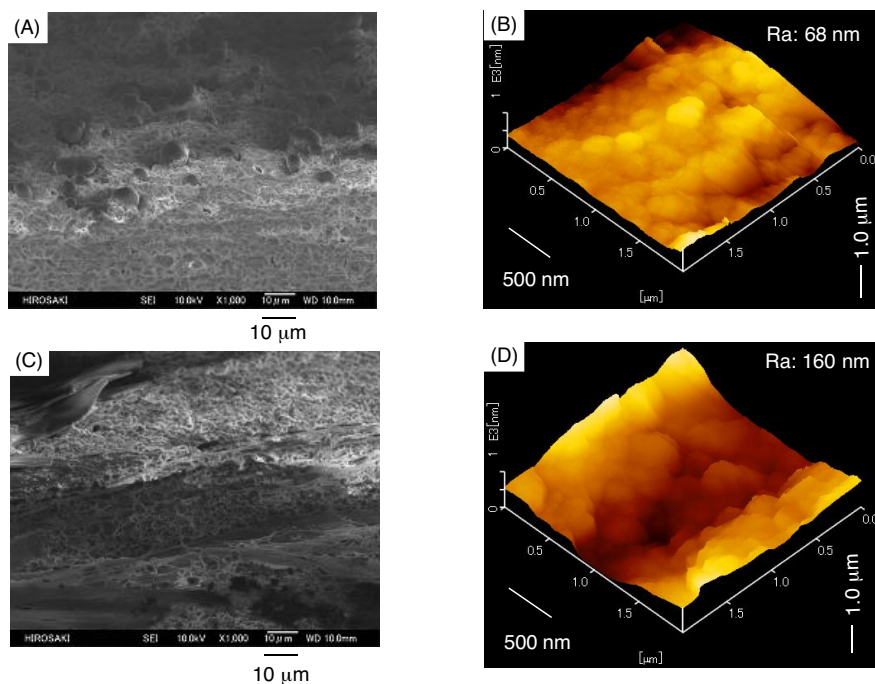


Fig. 5-4 FE-SEM (Field emission scanning electron microscopy) images (A and C) and DFM (dynamic force microscopy) topographic images (B and D) of the modified glass surfaces treated with the fluorinated nanocomposites [(A) and (B) correspond to Run 8 in Table 5-2, and (C) and (D) correspond to Run 9 in Table 5-2, respectively]

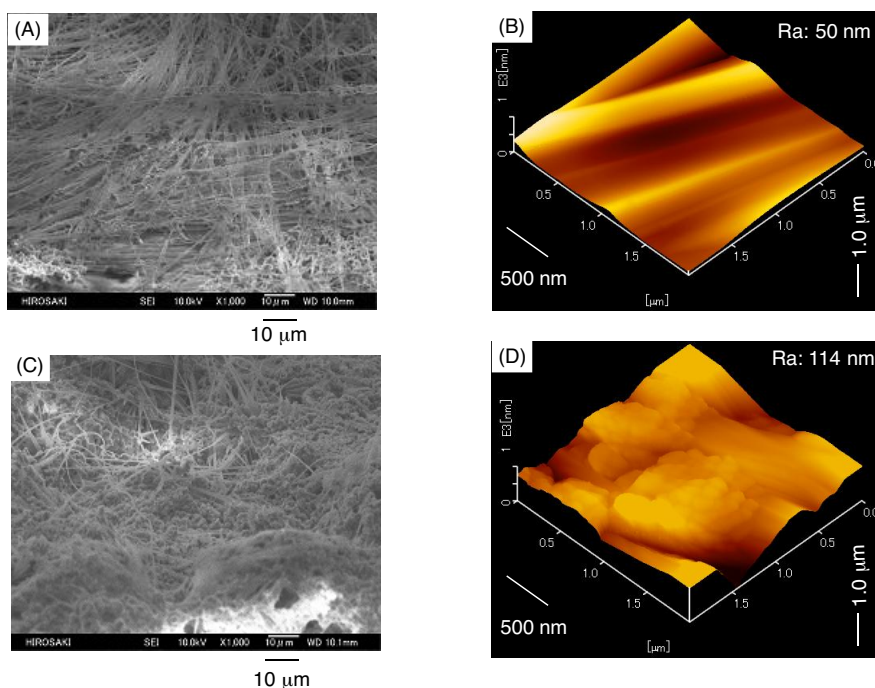


Fig. 5-5 FE-SEM (Field emission scanning electron microscopy) images (A and C) and DFM (dynamic force microscopy) topographic images (B and D) of the modified glass surfaces treated with the fluorinated nanocomposites [(A) and (B) correspond to Run 11 in Table 5-2, and (C) and (D) correspond to Run 12 in Table 5-2, respectively]

The architecture of the roughness surface on each modified surface can be observed by FE-SEM measurements. Especially, FE-SEM images show that the fluorinated nanocomposites can form the fiber-like assemblies on the modified surface. This finding would be due to the synergistic interaction between the fluorophilic-fluorophilic interaction of the relatively longer perfluorobutyl units and the intermolecular hydrogen bonding interaction of the amido units in the composites. The topographical images of the fluorinated nanocomposites can also provide a roughness surface, and the roughness averages (Ra) derived from the modified surface possessing the superoleophobic-superhydrophilic and superamphiphobic characteristics are 50 ~ 68 nm and 114 ~ 160 nm, respectively. Higher roughness average values (Ra: 160 nm and 114 nm) were observed in the superamphiphobic surface: Figs. 5-4-(D) and 5-5-(D), respectively. Thus, such higher roughness average values are effective to create the superamphiphobic surface. In this way, the creation of controlled modified surface between the superamphiphobic and superoleophobic-superhydrophilic characteristics have been succeeded by controlling the feed ratios of the acyl fluorides and  $\text{CaCO}_3$  for the preparation of the fluorinated nanocomposites illustrated in Runs 7 ~ 12 in Table 5-1.

### **5.3.3. Application of the perfluorocarboxamides/calcium carbonate/calcium fluoride nanocomposites to the membrane materials for liquid-liquid separation**

Considerable effort has been recently devoted to the creation of superhydrophilic surface, due to its high potential applications in a wide variety of fields such as coating technology including self-cleaning coatings, textile industry, and separation membranes, and much interest has been focused on the randomly fluoroalkylated acrylate copolymers in these fields.<sup>18, 19)</sup> However, there are some difficulties with removing the oil stain on the traditional superhydrophilic or hydrophilic surface due to their easy adhesion of the oils.<sup>20)</sup> Therefore, the creation of the superhydrophilic coatings possessing a superoleophobic property would enable the modified polyester (PET) surface to afford the antiadhesion ability. Thus, not only the modified PET fabric swatch but also the modified filter paper has been prepared by using the fluorinated nanocomposites (Run 11 in Table 5-1) under the similar dipping technique to that of the glass illustrated in Run 11 in Table 5-2. These results are shown in Table 5-3.

Table 5-3 Contact angles of dodecane and water on modified PET fabric and filter paper treated with the fluorinated nanocomposites (Run 11 in Table 5-1)

		Contact angle (degree)						
		dodecane	water					
			time					
		0 min	5 min	10 min	15 min	20 min	25 min	30 min
PET fabric	105	0 <sup>a)</sup>	-	-	-	-	-	-
Filter paper	106	51	0 <sup>a)</sup>	-	-	-	-	-
Original PET fabric	0	113	0 <sup>a)</sup>	-	-	-	-	-
Original filter paper	0	0 <sup>a)</sup>	-	-	-	-	-	-

a) A time dependence was not observed over 30 min

As shown in Table 5-3, dodecane and water contact angle values are 105 ~ 106° and 0° (modified filter paper surface shows the time dependence for water contact angle to afford 0° over 5 min), respectively, although the parent PET fabric and filter paper afford no oleophobicity (dodecane contact angle value: 0°). Thus, it was demonstrated that the modified PET fabric swatch and modified filter paper can exhibit a superoleophobic-superhydrophilic characteristic as well as that of the modified glass surface illustrated in Table 5-2. Such superoleophobic-superhydrophilic characteristic should enable the application of the modified PET fabric swatch and the modified filter paper to the oil-water separation membranes. In fact, the separation of oil (dodecane) and water (red-colored water with Rhodamine B) has been studied by the use of modified fabric swatch as the liquid-liquid separation membrane, and the results are illustrated in Fig. 5-6.

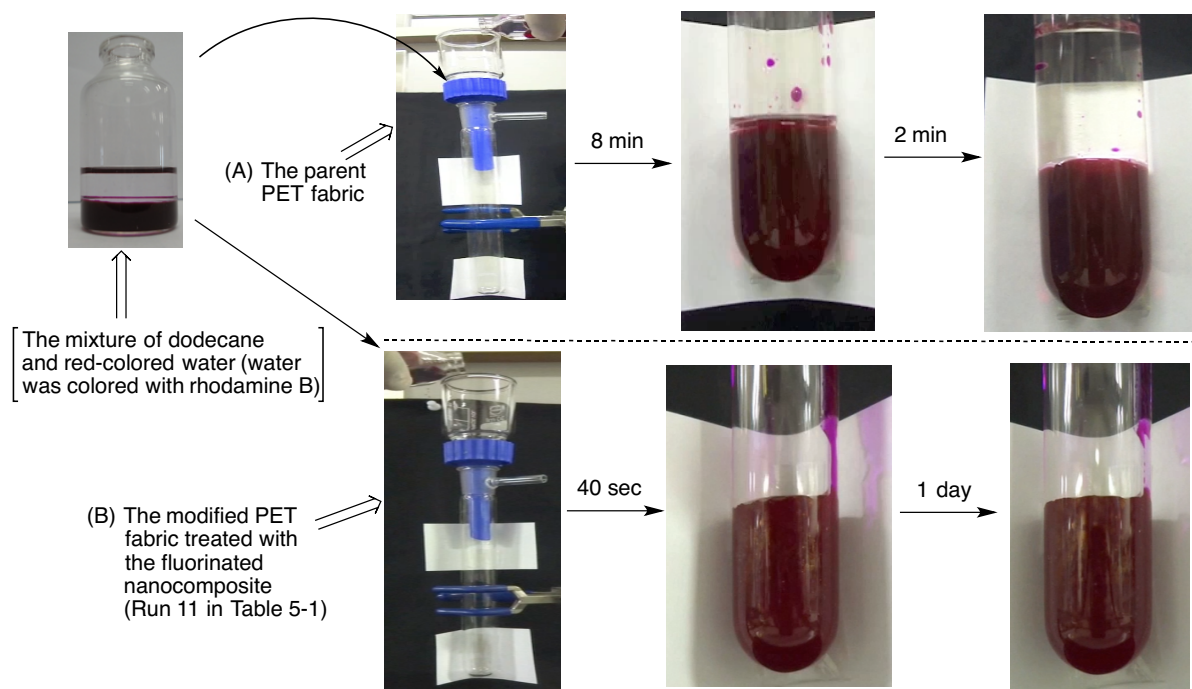


Fig. 5-6 Separation of oil (dodecane)/water (red-colored with rhodamine B) by using the parent PET fabric swatch (A) and the modified PET fabric swatch treated with the fluorinated nanocomposite (Run 11 in Table 5-1) under atmospheric conditions

Fig. 5-6-(B) shows that the modified PET fabric is effective for the separation of oil/water under atmospheric conditions, and the red-colored water can be smoothly isolated due to its superhydrophilic-superoleophobic characteristic. The contamination of oil into aqueous phase was not observed in 1 day. On the other hand, the mixture of oil and water was failed to separate by the use of the non-treated original PET fabric swatch under similar conditions (see Fig. 5-6-(A)). The mixture of oil (dodecane) and water (red-colored water with Rhodamine B) has been also succeeded in separating by using the modified filter paper under the similar technique.

Furthermore, not only the mixture of oil and water but also the oil (dodecane)-in-water

(O/W) emulsion, which was stabilized by SDS (sodium dodecyl sulfate), were tried to separate by the use of the modified filter paper treated with the fluorinated nanocomposites (see Table 5-3), and the results are shown in Fig. 5-7.

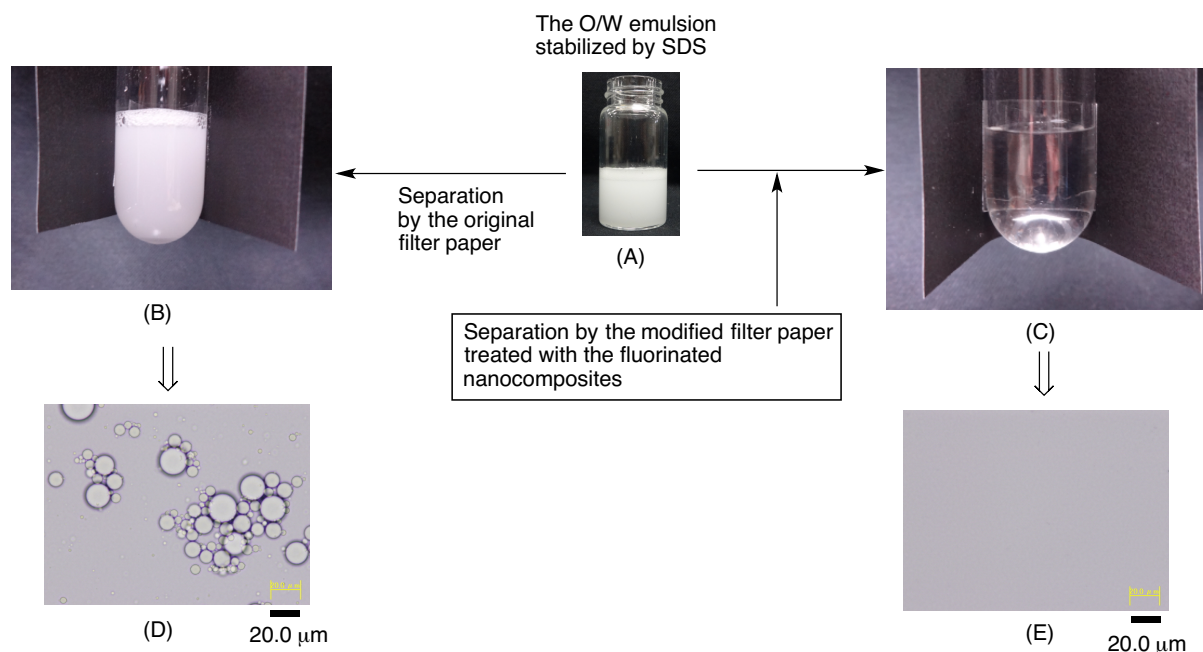


Fig. 5-7 Photography of the O/W emulsion stabilized by SDS (mixture of dodecane and water): (A). the O/W emulsion after the separation by the original filter paper: (B), the O/W emulsion after the separation by the modified filter paper treated with the fluorinated nanocomposites (Run 11 in Table 5-1): (C), and optical microscopy of each separated O/W emulsion [(D) and (E)]

Fig. 5-7 shows that the fluorinated nanocomposites are effective for the separation of the fresh SDS (300 mg)-stabilized oil (dodecane: 0.15 ml)-in-water (5 ml) emulsion under reduced pressure to isolate the transparent water. Optical micrograph also showed that the oil droplet cannot be detected at all in the isolated water (Fig. 5-7-E), although the oil droplet can be easily detected in the parent O/W emulsion (Fig. 5-7-D).

As mentioned above, the facile creation of the modified surface possessing the controlled wettability between the superoleophobic-superhydrophilic and superamphiphobic characteristics has been succeeded by controlling the feed ratios of the acyl fluorides and  $\text{CaCO}_3$  in the nanocomposite reactions illustrated in Scheme 5-1 and Table 5-1. Thus, the mixture of the fluorocarbon and hydrocarbon was tried to separate by making the best use of this superamphiphobic characteristic. The modified filter paper possessing a superamphiphobic characteristic (dodecane and water contact angle values on this modified filter paper are  $105^\circ$  and  $180^\circ$ , respectively) treated with the fluorinated nanocomposites (Run 12 in Table 5-1) was applied to the separation of the mixture of fluorocarbon (*1H*-tridecafluorohexane) and hydrocarbon [dodecane: colored blue with organic dye (see Fig. 5-8).] The results are shown in Fig. 5-8.

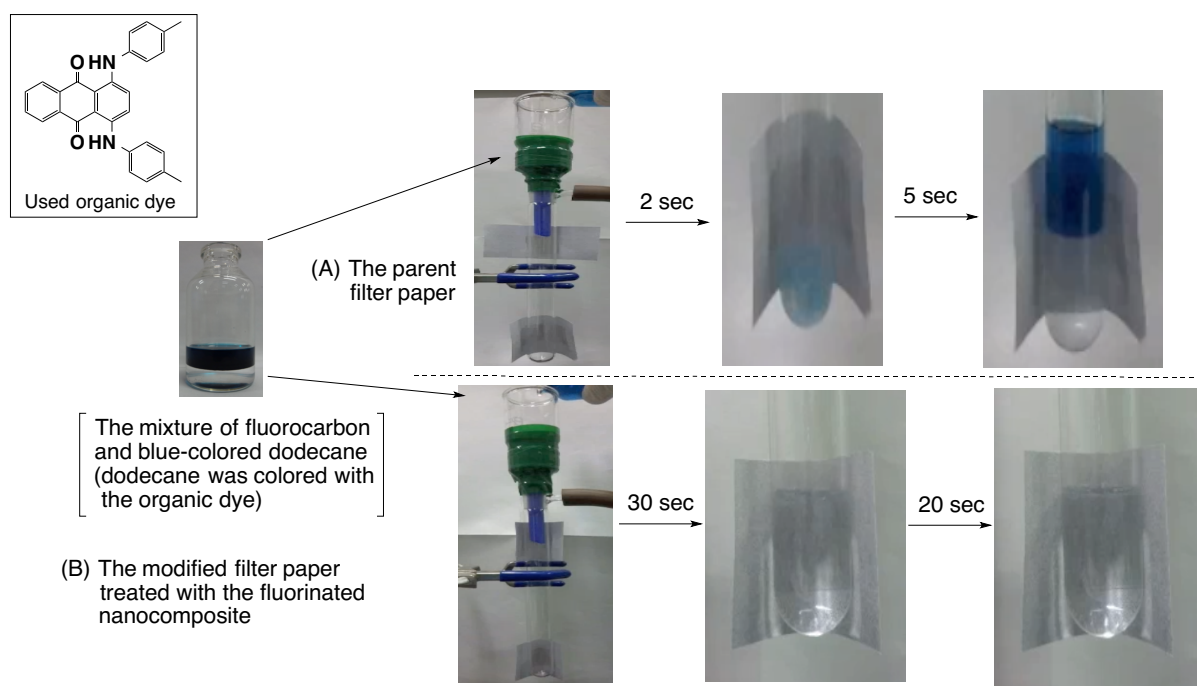


Fig. 5-8 Separation of fluorocarbon (1H-tridecafluorohexane)/dodecane (blue-colored with organic dye) by using the parent filter paper: (A) and the modified filter paper treated with the fluorinated nanocomposite: (B) (Run 12 in Table 5-1) under reduced pressure conditions

As shown in Fig. 5-8, the original filter paper has no ability for the separation of the mixture of 1H-tridecafluorohexane and blue-colored dodecane; however, the smooth separation of this mixture was observed under reduced pressure. This finding is due to the amphiphobic characteristic on the modified filter paper surface, and fluorocarbon such as 1H-tridecafluorohexane should possess an effective fluorophilic-fluorophilic interaction between the fluorocarbon and the perfluorobutyl units in the nanocomposites to cause a smooth separation of the fluorocarbon.



## 5.4. Conclusion

A variety of perfluorocarboxamides/ $\text{CaCO}_3$ / $\text{CaF}_2$  nanocomposites were prepared by the composite reactions of the corresponding acyl fluorides and  $\text{CaCO}_3$  nanoparticles under alkaline conditions. ATR-FTIR and XRD measurements show that the perfluorocarboxamides and calcium fluoride in the nanocomposites would be obtained through the nanocomposite reactions. These nanocomposites thus obtained were applied to the surface modification of glass. The nanocomposites possessing cyclic perfluoroalkyl units such as perfluoro-1-piperidinyl and perfluoromorpholino units were found to afford a good oleophobic characteristic with a superhydrophilicity on the modified glass surfaces. On the other hand, the controlled wettability between a superamphiphobic and a superoleophobic-superhydrophilic characteristics on the modified glass surfaces was observed by controlling the feed ratios of the acyl fluorides and  $\text{CaCO}_3$  nanoparticles for the preparation of the nanocomposites possessing the linear perfluoroalkyl units. The modified PET fabric swatch and filter paper treated with the fluorinated nanocomposites possessing a superoleophobic-superhydrophilic characteristic were applied to the separation membranes for the effective separation of not only the mixture of oil (dodecane) and water but also the oil (dodecane)-in-water emulsion-stabilized by sodium dodecyl sulfate. In addition, the fluorinated nanocomposites

possessing a superamphiphobic characteristic enabled the modified filter paper treated with these nanocomposites to separate the mixture of fluorocarbon and hydrocarbon. Hitherto, there are some reports on the separation of oil and water by the use of a superoleophobic-superhydrophilic characteristic derived from the fluoroalkyl end-capped vinyltrimethoxysilane oligomer/calcium silicide nanocomposites <sup>21)</sup>, the fluoroalkyl end-capped vinyltrimethoxysilane oligomer/talc composites-encapsulated cross-linked polystyrene <sup>22)</sup>, and the perfluoropolyether dicarboxylic acid/silica nanocomposites. <sup>23)</sup> However, we believe that this is the first example for the application of the separation membranes for the separations of oil/water and fluorocarbon/hydrocarbon by the use of the controlled wettability between the superamphiphobic and superoleophobic-superhydrophilic characteristics. Therefore, the present nanocomposites are expected to be applicable as the novel fluorinated functional material for the separation of the mixtures of oil/water and fluorocarbon/hydrocarbon.

## References

- 1) B. Ameduri and B. Boutevin, "*Well-Architected Fluoropolymers: Synthesis: Properties and Applications*", Elsevier, Amsterdam (2004).
- 2) H. Fukaya, M. Nishida, E. Hayashi, Y. Hayakawa, T. Abe, N. Nose, T. Shimizu, and M. Tatemoto, *J. Fluorine Chem.*, **101**, 117 (2000).
- 3) C. Tonelli and V. Tortelli, *J. Fluorine Chem.*, **101**, 117 (2000).
- 4) J. F. Harris Jr, *J. Org. Chem.*, **30**, 2182 (1965).
- 5) H. Sawada, *Chem. Rev.*, **96**, 1779 (1996).
- 6) H. Sawada, *Prog. Polym. Sci.*, **32**, 509 (2007).
- 7) H. Sawada, *Polym. J.*, **39**, 637 (2007).
- 8) H. Sawada and M. Nakayama, *J. Chem. Soc., Chem. Commun.*, 677 (1991).
- 9) H. Sawada, T. Suzuki, H. Takashima, and K. Takishita, *Colloid Polym. Sci.*, **286** 1569 (2008).
- 10) H. Sawada, Y. Shikauchi, H. Kakehi, Y. Katoh, and M. Miura, *Colloid Polym. Sci.*, **285**, 499 (2007).
- 11) H. Sawada, *Polym. Chem.*, **3**, 46 (2012).
- 12) H. Sawada, M. Kikuchi, and M. Nishida, *J. Polym. Sci., Part A: Polym. Chem.*, **49**, 1070

(2011).

- 13) H. Sawada, T. Tashima, Y. Nishiyama, M. Kikuchi, Y. Goto, G. Kostov, and B. Ameduri, *Macromolecules*, **44**, 1114 (2011).
- 14) T. Saito, H. Kakehi, Y. Kato, M. Miura, N. Isu, and H. Sawada, *Polym. Adv. Technol.*, **24**, 532 (2013).
- 15) G. D. Blue, J. W. Green, R. G. Bautista, and J. L. Margrave, *J. Phys. Chem.*, **67**, 877 (1963).
- 16) M. Sansotera, C. Gambarotti, A. Famulari, A. Baggioli, R. Soave, F. Venturini, S. V. Meille, I. Wlassics, and W. Navarrini, *Tetrahedron*, **79**, 5298 (2014).
- 17) M. Pianca, E. Barchiesi, G. Esposto, and S. Radice, *J. Fluorine Chem.*, **95**, 71 (1999).
- 18) Q. An, W. Xu, L. Hao, and L. Huang, *J. Appl. Polym. Sci.*, **127**, 1519 (2013).
- 19) Y. Furukawa and M. Kotera, *J. Appl. Polym. Sci.*, **87**, 1085 (2003).
- 20) K. Liu, Y. Tian, and L. Jiang, *Prog. Mater. Sci.*, **58**, 503 (2013).
- 21) T. Saito, Y. Tsushima, and H. Sawada, *Colloid Polym. Sci.*, **293**, 65 (2015).
- 22) Y. Oikawa, T. Saito, S. Yamada, M. Sugiya, and H. Sawada, *ACS Appl. Mater. Interfaces*, **7**, 13782 (2015).
- 23) E. Sumino, T. Saito, T. Noguchi, and H. Sawada, *Polym. Adv. Technol.*, **26**, 345 (2015).

## Conclusions

The results obtained from this study are summarized as follows.

1. Calcium chloride reacted with sodium carbonate in the presence of a variety of fluoroalkyl end-capped oligomers such as fluoroalkyl end-capped acrylic acid oligomer  $[R_F-(ACA)_n-R_F]$ , 2-methacryloyloxyethanesulfonic acid oligomer  $[R_F-(MES)_n-R_F]$ , *N,N*-dimethylacrylamide oligomer  $[R_F-(DMAA)_n-R_F]$  and acryloylmorpholine oligomers  $[R_F-(ACMO)_n-R_F]$  to afford the corresponding fluorinated oligomers/calcium carbonate composites. Each fluorinated oligomer/calcium carbonate composite thus obtained is nanometer size-controlled very fine particles (25 ~ 114 nm) possessing a good dispersibility and stability in a variety of solvents including water. Thermal stability of these fluorinated calcium carbonate nanocomposites was studied by thermogravimetric analyses measurements. Fluorinated oligomers, in which the theoretical oligomer content in the composites is 19 %, were able to give no weight loss corresponding to the content of oligomer in each case even after calcination at 800 °C. On the other hand, a slight weight loss corresponding to the contents of oligomers in the composites after calcination at 800 °C was observed in  $R_F-(MES)_n-R_F/$ ,  $R_F-(DMAA)_n-R_F/$  and  $R_F-(ACMO)_n-R_F/$ calcium carbonate nanocomposites, in

which the theoretical contents of the oligomers were 36 ~ 53 %, although  $R_F-(ACA)_n-R_F$ /calcium carbonate nanocomposites gave a clear weight loss corresponding to the contents of oligomer under similar conditions. Fluorinated oligomers/calcium carbonate nanocomposites possessing no weight loss at 800 °C were applied to the surface modification of poly(methyl methacrylate) [PMMA] to exhibit a good oleophobicity imparted by fluorines on the surfaces. Interestingly, these fluorinated calcium carbonate nanocomposites after calcination at 800 °C were found to exhibit the similar oleophobic characteristic on the modified PMMA surfaces as well as that of the nanocomposites before calcination.

2. Calcium chloride reacted with potassium fluoride in the presence of low molecular weight aromatic compounds (*ArH*) such as bisphenol AF, bisphenol A, bisphenol F, biphenyl, and 1-(2-naphthyl)ethanol under alkaline conditions to afford new calcium fluoride/*ArH* composites. Dynamic light scattering and field emission scanning electron micrographs measurements show that these calcium fluoride/*ArH* composites are nanometer size-controlled fine particles and have a good dispersibility and stability in water, tetrahydrofuran, 1,2-dichloroethane, methanol, dimethyl sulfoxide, *N, N*-dimethylformamide, and 2-propanol. Interestingly, aromatic compounds possessing acidic hydroxyl groups in the calcium fluoride nanocomposites were found to exhibit a nonflammable characteristic even after calcination at

800 °C, although the corresponding aromatic compounds possessing neither acidic hydroxyl groups nor hydroxyl groups in the nanocomposites exhibited a usual flammable characteristic under similar conditions. In contrast, calcium fluoride/*ArH* nanocomposites, which were prepared under no catalytic conditions, afforded a clear weight loss corresponding to the contents of *ArH* in the composites to exhibit a usual flammable characteristic.

3. A variety of fluorinated aliphatic alcohols such as 1*H*, 1*H*, 2*H*, 2*H*-nonafluoro-1-hexanol (FA-4), 1*H*, 1*H*, 2*H*, 2*H*-tridecafluoro-1-*n*-octanol (FA-6), 1*H*, 1*H*, 2*H*, 2*H*-heptadecafluoro-1-decanol (FA-8), 1*H*, 1*H*, 2*H*, 2*H*, 6*H*, 6*H*-nonadecafluoro-1-undecanol (DTFA), 2, 3, 3, 3-tetrafluoro-2-[1, 1, 2, 3, 3, 3-hexafluoro-2-(heptafluoropropoxy) propoxy]-1-propanol (PO-3-OH) and 2, 4, 4, 5, 7, 7, 8, 10, 10, 11, 13, 13, 14, 16, 16, 17, 17, 18, 18, 18-icosafluoro-2, 5, 8, 11, 14-pentakis(trifluoromethyl)-3, 6, 9, 12, 15-pentaoxaoctadecane-1-ol (PO-6-OH) were applied to the reaction with calcium chloride under alkaline conditions. In these fluorinated alcohols, only the DTFA can react with calcium chloride under alkaline conditions to provide the corresponding fluorinated alcohol/calcium fluoride nanocomposites. This reactivity is due to the relatively higher acidity of the inside methylene unit in the DTFA, of whose acidic protons should react with the neighboring fluorides and successively with calcium chloride under alkaline conditions to afford the

DTFA/calcium fluoride nanocomposites. Interestingly, the DTFA/CaF<sub>2</sub> nanocomposites were found to exhibit no weight loss characteristic even after calcination at 800 °C. More interestingly, the DTFA/CaF<sub>2</sub> nanocomposites after calcination at 800 °C are applicable to the surface modification of poly(methyl methacrylate) [PMMA] to exhibit both good oleophobicity and lower refractive indices imparted by longer fluoroalkyl units in the composites on the modified PMMA film surfaces, as well as those of before calcination of the DTFA/CaF<sub>2</sub> nanocomposites.

4. Fluoroalkyl end-capped vinyltrimethoxysilane oligomer/calcium silicide nanocomposites [R<sub>F</sub>-(VM-SiO<sub>2</sub>)<sub>n</sub>-R<sub>F</sub>/CaSi<sub>2</sub>] were prepared by the sol-gel reactions of the corresponding fluorinated oligomer [R<sub>F</sub>-(VM)<sub>n</sub>-R<sub>F</sub>] with calcium silicide particles under alkaline conditions. These nanocomposites thus obtained can exhibit a good dispersibility and stability in traditional organic solvents such as methanol, tetrahydrofuran (THF), *N,N*-dimethylformamide (DMF), and fluorinated aliphatic solvents (1:1 mixed solvents (AK-225) of 1,1-dichloro-2,2,3,3,3-pentafluoropropane and 1,3-dichloro-1,2,2,3,3-pentafluoropropane). Methanol sol solutions of R<sub>F</sub>-(VM-SiO<sub>2</sub>)<sub>n</sub>-R<sub>F</sub>/CaSi<sub>2</sub> nanocomposites were applied to the surface modification of glass through the dipping technique. R<sub>F</sub>-(VM-SiO<sub>2</sub>)<sub>n</sub>-R<sub>F</sub>/CaSi<sub>2</sub> nanocomposites, in which the contents of CaSi<sub>2</sub> are 1 ~ 8 %, can give the superhydrophobic



and highly oleophobic characteristics on the modified glass surfaces. In contrast,  $R_F-(VM-SiO_2)_n-R_F/CaSi_2$  nanocomposites, in which the contents of  $CaSi_2$  are 67 ~ 88 %, enabled the modified surfaces to give the both superoleophobic and superhydrophilic characteristics. In this way, the switching behavior between the superhydrophobic and superhydrophilic surfaces with the highly oleophobic characteristic can be easily observed by controlling the contents of  $CaSi_2$  in the fluorinated nanocomposites. In addition,  $R_F-(VM-SiO_2)_n-R_F/CaSi_2$  nanocomposites were found to give the calcium fluoride as the pyrolytic product through the calcination of these nanocomposites at 800 °C, indicating that the present composites have high potential for the development to the new environmental cyclical type-fluorine recycle system.

5. A variety of perfluoroacyl fluorides (PFAFs) such as perfluoro-3-(1-piperidiny)propionyl fluoride (PF-PPF), perfluoro-2-methyl-3-morpholinopropionyl fluoride (PF-MMPF), perfluoro-3-di-*n*-propylaminopropionyl fluoride (PF-DPAPF) and perfluoro-3-di-*n*-butylaminopropionyl fluoride (PF-DBAPF) were applied to the nanocomposite reactions with calcium carbonate nanoparticles under alkaline conditions to afford the corresponding perfluorocarboxamides/calcium carbonate/calcium fluoride

nanocomposites. The modified glass surfaces treated with the fluorinated nanocomposites, which were prepared by using PF-PPF and PF-MMPF, afforded an oleophobic-superhydrophilic characteristic. The fluorinated nanocomposites, of whose each preparative feed ratio of PF-DPAPF (or PF-DBAPF) and  $\text{CaCO}_3$  is 0.50 (g/g) [2.50 (mol/mol)], can provide a superamphiphobic characteristic on the modified surfaces; however, the lower feed ratios: 0.25 ~ 0.17 (g/g) [1.25 ~ 0.83 (mol/mol)] of the acyl fluorides based on  $\text{CaCO}_3$  can afford a superoleophobic-superhydrophilic characteristic on the modified surfaces. The similar wettability was observed on the modified filter paper and polyethylene terephthalate (PET) fabric surfaces by using the fluorinated nanocomposites, which were prepared with PF-DBAPF. Interestingly, these modified filter paper and PET fabric swatch were applied to the separation membranes for not only the mixture of oil and water but also the oil-in-water emulsion. The modified filter paper treated with the fluorinated nanocomposites possessing a superamphiphobic characteristic were also applied to the separation membrane for the mixture of fluorocarbon and hydrocarbon.

## **Publications**

- 1) T. Saito, M. Nishida, H. Fukaya, H. Kakehi, Y. Kato, M. Miura, N. Isu, and H. Sawada, "Low Molecular Weight Aromatic Compounds Possessing Nonflammable and Flammable Characteristics in Calcium Fluoride Nanocomposite Matrices after Calcination at 800 °C", *Colloid Polym. Sci.*, **291**, 945 ~ 953 (2013).
- 2) T. Saito, H. Kakehi, Y. Kato, M. Miura, N. Isu, and H. Sawada, "Fluoroalkyl End-capped Oligomers Possessing Nonflammable Characteristic in Calcium Carbonate Nanocomposites", *Polym. Adv. Technol.*, **24**, 532 ~ 540 (2013).
- 3) T. Saito, Y. Tsushima, and H. Sawada, "Facile Creation of Superoleophobic and Superhydrophilic Surface by Using Fluoroalkyl End-capped Vinyltrimethoxysilane Oligomer/Calcium Silicide Nanocomposites – Development of These Nanocomposites to Environmental Cyclical Type-Fluorine Recycle Through Formation of Calcium Fluoride", *Colloid Polym. Sci.*, **293**, 65 ~ 73 (2015).

4) T. Saito, S. Yamazaki, Y. Tsushima, K. Sato, and H. Sawada, "Reaction of Fluorinated Aliphatic Alcohols with Calcium Chloride: Formation of the Fluorinated Alcohol/Calcium Fluoride Nanocomposites – Thermal Stability and Application to the Surface Modification of These Nanocomposites", *J. Coat. Technol. Res.*, in press.

5) T. Saito, Y. Tsushima, T. Honda, T. Kamiya, M. Fujita, and H. Sawada, "Facile Creation of Modified Surface Possessing the Controlled Wettability between Superamphiphobicity and Superoleophobic-Superhydrophilic Characteristics by Using Perfluorocarboxamides/Calcium Carbonate/Calcium Fluoride Nanocomposites: Application to the Separation of Oil and Water", *J. Composites Mater.*, in press.

(not described in this thesis)

6) S. Guo, T. Ogasawara, T. Saito, H. Kakehi, Y. Kato, M. Miura, N. Isu, and H. Sawada, "Preparation and Photocatalytic Activity of Fluoroalkyl End-capped Vinyltrimethoxysilane Oligomer/Anatase Titanium Oxide Nanocomposite-encapsulated Low Molecular Weight Aromatic Compounds", *Colloid Polym. Sci.*, **291**, 2947 ~ 2957 (2013).

- 7) E. Sumino, S. Ise, T. Saito, M. Nishida, T. Noguchi, and H. Sawada, "Preparation and Properties of Fluorinated Carboxylic Acid/Silica Nanocomposite-encapsulated Low Molecular Weight Compounds", *Colloid Polym. Sci.*, **292**, 369 ~ 379 (2014).
- 8) H. Sawada, Y. Oikawa, Y. Matsuki, and T. Saito, "UV-resistance of Encapsulated Low Molecular Weight Aromatic Compounds in Fluoroalkyl End-capped Trimethoxysilane Oligomer/Silica Nanocomposites", *Polym. Adv. Technol.*, **25**, 388 ~ 395 (2014).
- 9) S. Guo, S. Soma, K. Okuno, T. Saito, T. Nakagawa, K. Sato, and H. Sawada, "Preparation and Properties of Fluorinated Aliphatic Alcohols/Silica Nanocomposites – Application to the Encapsulation of Anatase Titanium Oxide Nanoparticles into These Composite Cores", *Composites Part B*, **70**, 80 ~ 91 (2015).
- 10) E. Sumino, T. Saito, T. Noguchi, and H. Sawada, "Facile Creation of Superoleophobic and Superhydrophilic Surface by Using Perfluoropolyether Dicarboxylic Acid/Silica Nanocomposites", *Polym. Adv. Technol.*, **26**, 345 ~ 352 (2015).

11) Y. Oikawa, T. Saito, S. Yamada, M. Sugiya, and H. Sawada, "Preparation and Surface Property of Fluoroalkyl End-capped Vinyltrimethoxysilane Oligomer/Talc Composite-encapsulated Organic Compounds: Application for the Separation of Oil and Water", *ACS Appl. Mater. Interfaces*, **7**, 13782 ~ 13793 (2015).

12) Y. Oikawa, T. Saito, S. Idomukai, T. Tanaka, M. Nishida, and H. Sawada, "Preparation of Magnesium Carbonate Nanoparticles Encapsulated by Nanocomposite Material Derived from Fluoroalkyl End-capped Vinyltrimethoxysilane Oligomer – Application to the Surface Modification of Glass and Poly(Methyl Methacrylate)", *J. Fluorine Chem.*, **177**, 70 ~ 79 (2015).

## **Acknowledgements**

The author would like to express his sincerest gratitude to Professor Hideo Sawada for his inspired supervision and valuable discussions.